



TALLINN UNIVERSITY OF TECHNOLOGY
SCHOOL OF ENGINEERING
Department of Mechanical and Industrial Engineering

HIGHER-ORDER SHEAR DEFORMATION THEORY FOR COUPLED BEAM METHOD

KÕRGEMAT JÄRKU LÕIKE DEFORMATSIOONI TEOO- RIA SEOTUD TALADE MEETODI JAOKS

MASTER'S THESIS

Student: Mikk-Markus Imala

Student code: 176497MATM

Supervisor: Hendrik Naar, Associate Professor

AUTORIDEKLARATSIOON

Olen koostanud lõputöö iseseisvalt.

Lõputöö alusel ei ole varem kutse- või teaduskraadi või inseneridiplomit taotletud.

Kõik töö koostamisel kasutatud teiste autorite tööd, olulised seisukohad, kirjandusallikatest ja mujalt pärinevad andmed on viidatud.

25 Mai 2020

Autor: Mikk-Markus Imala

Töö vastab magistritööle esitatud nõuetele

25 Mai 2020

Juhendaja: Hendrik Naar

Kaitsmisele lubatud

".....".....201... .

Kaitsmiskomisjoni esimees

/ nimi ja allkiri /

Lihtlitsents lõputöö reprodutseerimiseks ja lõputöö üldsusele kättesaadavaks tegemiseks¹

Mina, Mikk-Markus Imala (sünnikuupäev: 22.04.1995)

1. Annan Tallinna Tehnikaülikoolile tasuta loa (lihtlitsentsi) enda loodud teose Kõrgemat järku lõike deformatsiooni teooria seotud talade meetodi jaoks,

mille juhendaja on Hendrik Naar.

1.1 reprodutseerimiseks lõputöö säilitamise ja elektroonse avaldamise eesmärgil, sh Tallinna Tehnikaülikooli raamatukogu digikogusse lisamise eesmärgil kuni autoriõiguse kehtivuse tähtaja lõppemiseni;

1.2 üldsusele kättesaadavaks tegemiseks Tallinna Tehnikaülikooli veebikeskkonna kaudu, sealhulgas Tallinna Tehnikaülikooli raamatukogu digikogu kaudu kuni autoriõiguse kehtivuse tähtaja lõppemiseni.

2. Olen teadlik, et käesoleva lihtlitsentsi punktis 1 nimetatud õigused jäävad alles ka autorile.

3. Kinnitan, et lihtlitsentsi andmisega ei rikuta teiste isikute intellektuaalomandi ega isikuandmete kaitse seadusest ning muudest õigusaktidest tulenevaid õigusi.

¹*Lihtlitsents ei kehti juurdepääsupiirangu kehtivuse ajal, välja arvatud ülikooli õigus lõputööd reprodutseerida üksnes säilitamise eesmärgil.*

Mikk-Markus Imala

25.05.2020

Mehaanika ja tööstustehnika instituut
LÕPUTÖÖ ÜLESANNE

Üliõpilane: Mikk-Markus Imala, 176497MATM (nimi, üliõpilaskood)
Õppekava, peeriala: MATM02/15 Tootearendus ja tootmistehnika (kood ja nimetus)
Juhendaja(d): dotsent, Hendrik Naar, +372 53425269
Konsultant: Heikki Remes, professor, Aalto Ülikool, heikki.remes@aalto.fi

Lõputöö teema:

(eesti keeles) Kõrgemat järku lõike deformatsiooni teooria seotud talade meetodi jaoks
(inglise keeles) Higher-order shear deformation theory for coupled beam method

Lõputöö põhieesmärgid:

1. Talaelemendi defineerimine kasutades selleks valitud vabadusastmeid.
2. Kihilise talateooria väljatöötamine, defineerides siduvuselemendid talaelementide sidumiseks.
3. Talateooria analüütiliste tulemuste valideerimine lõplike elementide meetodi abil.

Lõputöö etapid ja ajakava:

Nr	Ülesande kirjeldus	Tähtaeg
1.	Kirjanduse ülevaade ning talateooria defineerimine	01.04.2020
2.	Talateooria analüütilise lahenduse arvutuskoodi defineerimine	01.05.2020
3.	Analüütiliste tulemuste valideerimine ning lõputöö viimistlus	25.05.2020

Töö keel: Inglise keel **Lõputöö esitamise tähtaeg:** 25 Mai 2020a

Üliõpilane: Mikk-Markus Imala 25 Mai 2020a

Juhendaja: Hendrik Naar 25 Mai 2020a

Konsultant: Heikki Remes 25 Mai 2020a

Programmijuht: "....." Mai 2020a

Author		
Mikk-Markus Imala		
Title of thesis		
Higher-order shear deformation theory for coupled beam method		
Master programme	Mechanical Engineering	Code EA7oLT
Thesis supervisor	Hendrik Naar	
Thesis advisor(s)	Heikki Remes, Aalto University	
Date	Number of pages	Language
25.05.2020	94	English

Abstract

Today, more and more cruise ships are built every year. As the market expands, so change the requirements from new-build vessels. Typically, this means the increase in ships gross tonnage, which requires an increase in dimensions, or more complex structures due to the desired design. Despite the requirements set by the industry, the ship's internal and external structures must provide a safe voyage for passenger and the crew. In standard ship design practice, initial strength evaluation is performed with a small amount of structural detail, for which there are numerous different methods.

This thesis introduces a new shear deformation theory designed for accurate assessment of global displacements and stresses. The theory utilises a beam element with 6 variables defined in each beam element node: deflection, rotation of cross-section, displacement due to shear and axial forces and shear deformation in beam element bottom surface and displacement due to shear and axial forces and shear deformation in beam element top surface. Approximations are presented so that variables could be described over the length and width of the beam elements. Coupling of beam elements in the global matrix has been presented for the holistic behaviour of the beam theory.

The thesis provides a comparative analysis between higher-order shear deformation theory calculations and FEM results performed with NX Nastran on two structures, first of which is a simple box structure and second is a nonuniform beam model, where three layers of beams are of different length.

The analysis shows a very good coincidence between analytically calculated displacements and stresses and FEM results for the box struct and between displacements for the nonhomogeneous structure and FEM results. In nonhomogeneous beam element configuration, the theory proved to lack the capability of assessing peak stress values and showed deficiencies in describing vertical stress distribution. Based on the results, the theory needs additional research to be done in terms of defining boundary conditions and element coupling to provide better results in the case of more complex structures.

Keywords higher-order shear deformation theory, ship's global strength, Coupled Beam method, finite element method, master's thesis

Autor

Mikk-Markus Imala

Lõputöö teema

Kõrgemat järku lõike deformatsiooniga teooria seotud talade meetodi jaoks

Õppekava Tootearendus ja Tootmistehnika**Õppekava kood** EA70LT

Lõputöö juhendaja Hendrik Naar

Lõputöö lisajuhendaja Heikki Remes, Aalto Ülikool

Kuupeäv 25.05.2020**Lehekülgede arv** 94**Keel** Inglise

Abstrakt

Tänapäeva kasvavas majanduses tõuseb iga aastaga uute ehitatavate kruisilaevade hulk. Majandusvaldkonna laienemisega muutuvad ka nõuded laevadele. Tüüpiliselt tähendab see laevade kogumahtuvuse kasvu, mille võimaldab dimensioonide suurendamine või keerulisema struktuuri rakendamist, et saavutada soovitud disain ja konstruktsiooni originaalsus. Laevade sise- ja väliskonstruktsioon peavad suutma tagada reisijate ja meeskonnaliikmete ohutu reisimise hoolimata valdkonna nõuetest disainile. Mitmeid meetodeid on loodud, et pakkuda esmast hinnangut laevakonstruktsiooni tugevusele, seejuures nõudmata üksikdetailideni viimistletud struktuuri disaini.

Käesolev lõputöö esitleb kõrgemat järku lõike deformatsiooni teooriat, mis võimaldab täpsemat siirete ja pingete hinnangut võrreldes klassikalise talateooriaga. Teooria defineerib uut tüüpi talaelemendi, mille igas sõlmes on defineeritud 6 vabadusastet: läbipaine, ristlõike pööre, lõikest ja pikijõust tingitud siire ja lõike deformatsioon talaelemendi alumisel pinnal ning lõikest ja pikijõust tingitud siire ja lõike deformatsioon talaelemendi ülemisel pinnal. Läbipainde ja pikisiirde hindamiseks vabalt valitud ristlõikes ning kõrgusel on kasutatud kolmanda ja esimese astme polünoomidena aproksimeeritud kujufunktsioone. Teooria hõlilisiliseks rakendamiseks globaalses mudelis on defineeritud siduvuselement ning elementide sidumisskeem.

Lõputöös on esitatud võrdlusanalüüs kõrgemat järku lõike deformatsiooniga teooria ning lõplike elementide meetodi (LEM) kohta, mis käsitleb kahte lihtsat talamudelit. Esimeseks mudeliks on ühtlase talaelementide paigutusega kaststruktuur ning teiseks on ebäühtlase talaelementide paigutusega mudel.

Analüüsi tulemused näitavad väga head kokkulangevust siirete ja pingete tulemuste osas kaststruktuuri puhul. Ebäühtlase paigutusega mudeli puhul ei ole teooria võimeline suure kokkulangevusega hindama maksimaalseid pingeväärtusi piirkondades, kus ebäühtlasest paigutusest tingitud lokaalsed mõjud. Lisaks sellele esines erinevusi vertikaalses pingejao- tuses. Tulemustele põhinedes vajab esitatud teooria edasist tööd rajatingimuste defineerimisel ning elementide sidumisega, et saavutada paremaid tulemusi keerulistes struktuurides.

Keywords kõrgemat järku lõike deformatsiooniga teooria, laeva globaaltugevus, seotud talade meetod, lõplike elementide meetod, magistritöö

Preface

This thesis was carried out as a cooperation between Aalto University and Tallinn University of Technology.

I would like to thank Tallinn University of Technology for funding this thesis as a part of the project: Numerical simulation of the FSI for the dynamic loads and response of ships. My gratitude goes out for Kristjan Tabri for his help during the studies abroad and his help in organising the funding for this thesis.

I would like to express my deep gratitude to Hendrik Naar for his time and effort to guide me on this topic and future encouragement to take this topic even further.

I wish to thank Professor Heikki Remes for his advisory during the thesis process and forthcomingness during these difficult times.

Exceptional gratitude to Aalto University School of Engineering for all the great moments and many friends I had the chance to meet during the studies.

I would like to express my gratitude for my employer MEC Insenerilahendused OÜ for being supportive of my absence and providing the tools necessary for completing this thesis.

Finally, I would like to thank my lovely Hanna-Liisa for supporting me during this process and my family for believing in me every step on the way.

Tallinn 25.05.2020

Mikk-Markus Imala

Contents

Abstract.....	iv
Abstrakt.....	v
Preface	vi
Contents	vii
List of Figures	ix
List of Tables	xi
List of Abbreviations	xii
List of symbols.....	xiii
1 Introduction.....	1
1.1 Background and motivation	1
1.2 Aim of the thesis	2
1.3 Scope of the work.....	3
2 State of the art	4
2.1 Global Loads on ships	4
2.1.1 Load classification	4
2.1.2 Internal loads acting on rigid hull girder	5
2.2 Research on evaluating hull and superstructure interaction.....	8
2.3 Coupled beam method [1].....	9
2.3.1 Method description	9
2.3.2 Equilibrium equations.....	10
2.3.3 Coupling equations	12
2.3.4 Relations between deformations and displacements	15
2.3.5 Differential equations to be solved	16
2.3.6 Comparison of coupled beam method to FEM.....	17
2.4 Hyperbolic shear deformation theory.....	18
2.4.1 Development of shear deformation theories	18
2.4.2 Overview of hyperbolic shear deformation theory by Ghugal and Sharma [27]	
3 Higher-order shear deformation theory	23
3.1 Definition of variables.....	23
3.2 Definition of the displacement field.....	24

3.3	Expression of potential energy	28
3.4	Coupling of elements	31
3.4.1	Single-layer beam model	31
3.4.2	Multiple layer beam model	32
3.4.3	Vertical coupling of beam elements	34
4	Case studies.....	42
4.1	Comparative calculation of refined shear deformation theory and FE-modelling	42
4.1.1	Models used for comparative analysis.....	42
4.1.2	Cantilever beam under uniform distributed load	42
4.1.3	Results and analysis	43
4.2	Higher-order shear deformation theory comparative calculations.....	43
4.2.1	Models used for analysis.....	43
4.2.2	Loading	45
4.2.3	Calculation cases.....	46
5	Higher-order shear deformation theory calculation results and discussion.....	47
5.1	Case A results.....	47
5.2	Case B results.....	50
6	Further work on the topic.....	54
7	Conclusions.....	55
8	Kokkuvõte (conclusions in Estonian).....	59
	Appendix A.....	63
	Appendix B.....	67
	Appendix C.....	69
	Appendix D.....	70
	Bibliography	74

List of Figures

Figure 1-1 Cross-section examples of a typical modern passenger ship	2
Figure 2-1 Hull sagging and hogging	5
Figure 2-2 Definition of ship fixed coordinate system and ship motions [3]	6
Figure 2-3 Definition of a ship section	7
Figure 2-4 Typical loading, ultimate shear force and the ultimate bending moment [4]	7
Figure 2-5 The basic concept of dividing ship hull girder into beams	10
Figure 2-6 Types of coupling between beams	10
Figure 2-7 Beam segment i with internal forces and external load	11
Figure 2-8 Shear coupling in adjacent beams	14
Figure 2-9 Vertical coupling in adjacent beams	15
Figure 2-10 Dimensions for box structure with no openings [1]	17
Figure 2-11 Distribution of normal stress in the box structure at $x = L/2$ cross-section [1]	18
Figure 3-1 Beam in the Cartesian coordinate system	23
Figure 3-2 Degrees of freedom for a beam segment	23
Figure 3-3 Axial displacement approximation	24
Figure 3-4 Vertical displacement approximation	26
Figure 3-5 Beam element coupling in single layer beam model	31
Figure 3-6 Global stiffness matrix scheme	32
Figure 3-7 Global external force vector scheme	32
Figure 3-8 Uniform beam model with element coupling and element blocks	33
Figure 3-9 Beam model with structural discontinuity, element coupling and element blocks	33
Figure 3-10 Global stiffness matrix scheme without vertical coupling for multiple layer beam model	34
Figure 3-11 Vertically coupled beam dimensions	35
Figure 3-12 Beam coupling with the assigned variable θ_1^m	36
Figure 3-13 Beam coupling with the assigned variable $u_{top,1}^m$	37
Figure 3-14 Beam coupling with the assigned variable θ_1^n	37
Figure 3-15 Beam coupling with the assigned variable $u_{bot,1}^n$	38
Figure 3-16 Beam coupling with the assigned variable w_1^m	39

Figure 3-17 Beam coupling with the assigned variable w_1^n	40
Figure 3-18 Vertical coupling scheme	41
Figure 4-1 Case A FE plate model.....	44
Figure 4-2 Case B FE plate model.....	44
Figure 4-3 Case A HOSDT model.....	45
Figure 4-4 Case B HOSDT model.....	45
Figure 4-5 Distributed loading curve.....	46
Figure 4-6 Calculation cross-section for beam models	46
Figure 5-1 Case A deflection comparison	47
Figure 5-2 Case A axial displacement comparison	48
Figure 5-3 Case A normal stress comparison	49
Figure 5-4 Case A shear stress comparison	49
Figure 5-5 Case B deflection comparison.....	50
Figure 5-6 Case B axial displacement comparison.....	51
Figure 5-7 Case B normal stress comparison	52
Figure 5-8 Case B shear stress comparison	53
Figure 7-1 Vertical normal stress distribution in case A beam model [28].....	56
Figure 7-2 Vertical normal stress distribution in case B beam model [28]	57
Figure 7-3 Case A normal stress distribution	57
Figure 7-4 Case B normal stress distribution.....	57
Figure 0-1 Axial displacement and shear deformation comparison for cross-section 1.....	70
Figure 0-2 Axial displacement and shear deformation comparison for cross-section 2.....	70
Figure 0-4 Axial displacement and shear deformation comparison for cross-section 3.....	71
Figure 0-3 Axial displacement and shear deformation comparison for cross-section 4.....	71
Figure 0-5 Axial displacement and shear deformation comparison for cross-section 5.....	71
Figure 0-6 Axial displacement and shear deformation comparison for cross-section 6.....	72
Figure 0-7 Axial displacement and shear deformation comparison for cross-section 7.....	72
Figure 0-8 Axial displacement and shear deformation comparison for cross-section 8.....	72
Figure 0-9 Axial displacement and shear deformation comparison for cross-section 9.....	73
Figure 0-10 Axial displacement and shear deformation comparison for cross-section 10..	73

List of Tables

Table 2-1 Load classification according to time variability and strength analysis performed	4
Table 0-1 Cross-sections used for comparative analysis	69

List of Abbreviations

3D	Three-dimensional
CB	Coupled beam
FE	Finite element
FEM	Finite element method
ISUM	Idealised structural unit method
HOSDT	Higher-order shear deformation theory
LEM	Lõplike elementide meetod

List of symbols

A_0	[-]	Hyperbolic shear deformation theory constant
A_{ii}	[mm ²]	Cross-sectional area of beam i
A_{ii}^S	[mm ²]	Effective cross-sectional area in shear of beam i
A_l	[m ²]	Cross-sectional area of under waterline at coordinate x
B_0	[-]	Hyperbolic shear deformation theory constant
C_0	[-]	Hyperbolic shear deformation theory constant
$C_1 - C_6$	[-]	Constants of integration
C_i	[-]	Coupling stiffness matrix component
C_{ij}	[mm]	Coupling distance for beam i attached to beam j
F_{el}	[-]	Beam element external loading vector
F_i	[N]	The external force applied on node i
H_{ij}	[mm]	Effective height of coupling shear member between beam i and j
I_{ii}	[mm ⁴]	Moment of inertia of cross-sectional area of beam i
I_y	[mm ⁴]	Moment of inertia of a beam cross-section
K_c	[-]	Vertical coupling matrix
K_{el}	[-]	Beam element stiffness matrix
K_{gl}	[-]	The global stiffness matrix for beam stiffness without coupling components
K_{ij}	[N/mm ²]	Vertical elongation stiffness of coupling between beams i and j
$K_{m,n}^i$	[-]	The global stiffness matrix for beam block i with m rows and n columns
M_i	[N*mm]	Bending moment in beam i
M_i	[N*mm]	The external moment applied on node i
M_l	[N*m]	Bending moment on hull cross-section at coordinate x
M_y	[N/mm]	Bending moment at a beam cross-section

N_i	[N]	Axial force in beam i
N_x	[N]	Axial force at a beam cross-section
Q_i	[N]	Shear force in beam i
Q_l	[N]	Shear force on hull cross-section at coordinate x
Q_z	[N]	Shear force at a beam cross-section
S_y	[mm ³]	First moment of area
T_{ij}	[N/mm ²]	...
X_{ii}	[mm ³]	First moment of cross-sectional area of beam i
$a_{1,1}, a_{2,1}$	[mm]	Alternative nomenclature for higher-order shear deformation variables
$a_{3,1}, a_{4,1}$	[-]	Alternative nomenclature for higher-order shear deformation variables
b_1, b_3	[mm]	Alternative nomenclature for higher-order shear deformation variables
b_2, b_4	[-]	Alternative nomenclature for higher-order shear deformation variables
d_{ik}	[mm]	Coupling distance between beam i reference line and beam k top surface
e_{ij}	[mm]	Coupling distance between beam i reference line and beam j bottom surface
f_m^i	[-]	External load vector for beam i , node m
$k_{c_{m,n}}^i$	[-]	6x6 coupling stiffness matrix quadrant for coupling element i , where m and n define the described quadrant
$k_1 - k_{20}$	[-]	Stiffness matrix variational multipliers
$k_{m,n}^i$	[-]	6x6 stiffness matrix quadrant for beam element i , where m and n define the described quadrant
k_u	[N/mm]	Spring axial stiffness in vertical coupling
k_w	[N/mm]	Spring vertical stiffness in vertical coupling
m_l	[kg/m]	Mass distribution over the ship hull
n_{nodes_i}	[-]	Number of nodes for beam block i
p_0	[N/mm]	Distributed vertical force amplitude

p_{ij}	[N/mm]	Vertical distributed coupling force between beam i and j
p_z	[N/mm]	Distributed vertical force
q_i	[N/mm]	External distributed load for beam i
q_l	[N/m]	Net loading per unit length over the ship hull
s_{bot}	[N/mm]	Distributed shear force on the bottom surface of a beam
s_{ij}	[N/mm]	Horizontal distributed coupling force between beam i and j
s_{top}	[N/mm]	Distributed shear force on the top surface of a beam
u_0	[mm]	Axial displacement due to universal axial force
$u_{bot,i}$	[mm]	Displacement due to shear on the bottom surface in node i
u_i	[mm]	Axial displacement of beam i
u_i	[mm]	Axial displacement in node i
$u_{top,i}$	[mm]	Displacement due to shear on the top surface in node i
v_i	[mm]	Total deflection of beam i
v_i^M	[mm]	Deflection of beam i due to bending deformation
v_i^Q	[mm]	Deflection of beam i due to shear deformation
w_i	[mm]	Transversal displacement of a beam in node i
$x_{l,i}$	[m]	Coordinate x for hull loading and buoyancy calculations
z_r	[mm]	Height of the reference line from beam bottom surface
h	[mm]	Depth of a beam
A	[-]	Third-degree polynomial constant
B	[-]	Third-degree polynomial constant
C	[-]	Third-degree polynomial constant
D	[-]	Third-degree polynomial constant
E	[MPa]	Young's modulus
G	[MPa]	Shear modulus
L	[mm]	Length of a beam
b	[mm]	Width of a beam
$f(x, z)$	[mm]	A function describing axial displacement due to shear between vertical layers of a beam
g	[N/kg]	Gravitational constant
$p(x)$	[N/mm]	Distributed vertical force function

q	[N/mm]	Transverse load intensity acting on a beam surface
s	[mm]	Web thickness of a beam
t	[mm]	Flange thickness of a beam
u	[mm]	Axial displacement of a beam
w	[mm]	Transversal displacement of a beam
x	[mm]	Local axial coordinate for a beam
y	[mm]	Local width coordinate for a beam
z	[mm]	Local vertical coordinate for a beam
$\gamma_{bot,i}$	[-]	Shear deformation on beam bottom surface in node i
$\gamma_{top,i}$	[-]	Shear deformation on beam top surface in node i
γ_{xz}	[-]	Shear strain of a beam
δ^u	[mm]	Relative axial displacement
δ^v	[mm]	Relative deflection
ε_x	[-]	Normal strain of a beam
θ_i	[-]	Rotation in node i
ν	[-]	Poisson's ratio
$\xi_1, \xi_2, \xi_3, \xi_4$	[-]	Third-degree polynomial constant
ρ_l	[kg/m ³]	Density of water around ship hull
σ_x	[MPa]	Normal stress of a beam
τ_{xy}	[MPa]	Shear stress of a beam
$\psi_1, \psi_2, \psi_3, \psi_4$	[-]	Third-degree polynomial constant
ϕ_1, ϕ_2	[-]	Linear weight function constants
Π	[J]	Potential energy for a closed system
α	[-]	Hyperbolic shear deformation theory variable
β	[mm ⁻²]	Hyperbolic shear deformation theory variable
λ	[mm]	Hyperbolic shear deformation theory variable

1 Introduction

1.1 Background and motivation

Today, more and more cruise ships are built every year. As the market expands, so change the requirements from new-build vessels. Typically, this means the increase in ships gross tonnage, which requires an increase in dimensions, or more complex structures due to the desired design. Multi-story atriums, large concert halls, and indoor pools are just a few examples of what design challenges engineers face. Despite the requirements set by the industry, ship's internal structures, together with the hull, must provide safe voyage for passenger and the crew.

Typical passenger ship consists of the hull and superstructure, separated with the main deck and lifeboat recess, see Figure 1-1. The structures are supported by longitudinal and transversal bulkheads together with pillar lines throughout the height of the ship.

Recent trends have been introducing large openings in side shell and bulkheads, which changes the typical transfer of shear stresses to a more complex problem. In a case where complicated design is desired, Classification Society regulations for ship structural dimensioning do not provide sufficient coverage. Here arises the necessity for checking global strength in early design stages. Today, the most widely used method for solving passenger ship response to loads acting on the ship is a three-dimensional (3D) finite element method (FEM) as it provides most life-like results. However, it is unreasonably time-consuming in most cases. Therefore, engineers use more straightforward and simplified methods.

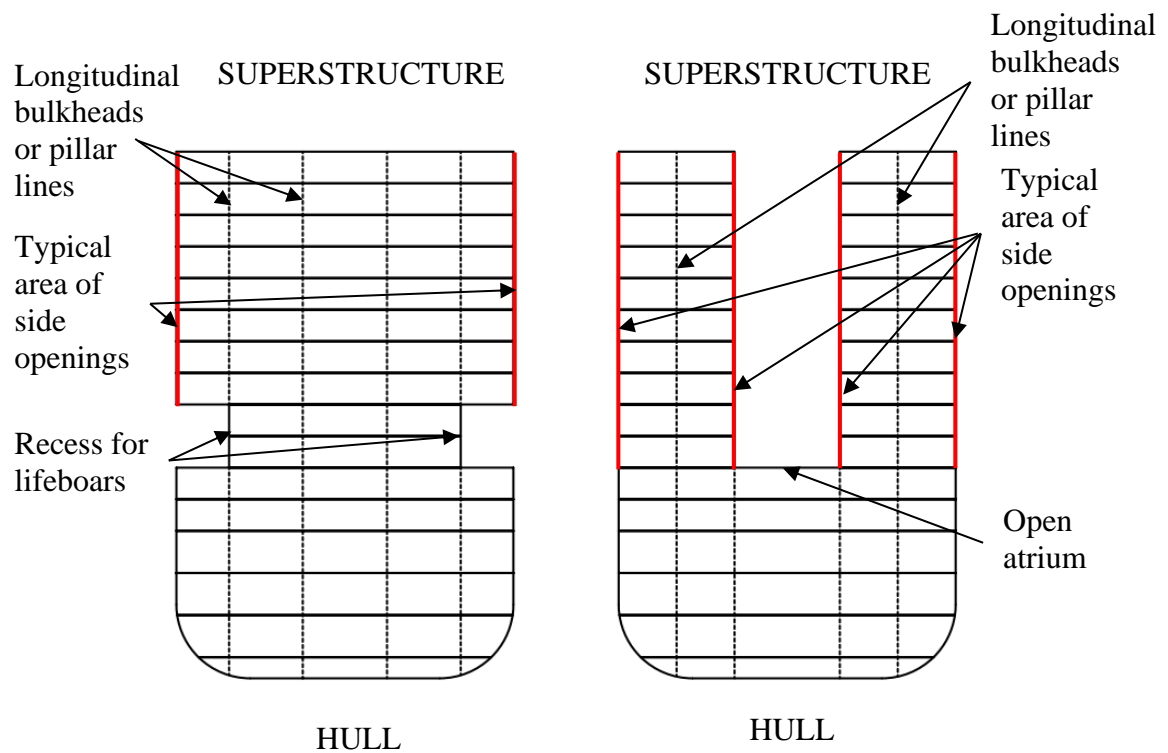


Figure 1-1 Cross-section examples of a typical modern passenger ship

One simplified method is the coupled beam theory, presented by Naar et al [1]. Coupled beam (CB) was created to evaluate hull girder response using beam elements to represent ship structures with the preliminary design. These beam elements were coupled together using distributed spring elements to transfer normal and shear forces between the beam elements. In this thesis, further development of vertical stress transfer is investigated, as the formerly mentioned CB theory lacked the capability of generating a continuous normal and shear stress distribution curve over the height of the ship analyses, see chapter 2.3.6. This thesis is written to explore a different way of defining a beam element and coupling element to assess stresses and displacements over the whole vertical span as a continuous function.

1.2 Aim of the thesis

This thesis aims to present an effective analytical solution for a new higher-order shear deformation beam theory, which would consider normal and shear stress distribution within

the beam cross-section as a continuous function to provide more accurate results applying the general CB method.

To accomplish this goal, research objectives were defined:

- O1: Generating a single element stiffness matrix by approximating the axial displacement field and deformations in the beam cross-section with an arbitrary reference line. Approximations are validated by comparing analytical results coincidence with a single beam FE-model.
- O2: Adjusting single layer beam model to multi-layered beam model by defining coupling of vertically adjacent elements.
- O3: Comparison of an analytical solution for a coupled simple beam model to plate element FE-models.

Objectives mentioned above generate the following research questions:

- Q1: How can axial displacement within the cross-section be defined in reference to a non-specific axis using the defined variables.
- Q2: How to express and solve the differential equations to define a stiffness matrix to a beam element with the defined variables?
- Q3: How to achieve coupling between vertically adjacent beam elements?
- Q3: Is the new higher-order shear deformation theory applicable when comparing to FEM results?

1.3 Scope of the work

In this thesis, the author performed analytical calculations using primarily Mathcad performing analytical calculations and Microsoft Excel for data analysis. FEM calculations used in comparative analyses were performed using FEMAP 2019.1 Academic software with NX Nastran. The performed analyses are limited by the level of detail of FE-models that are reasonable to create for this thesis as well as the necessary level of detail to assess the quality of developed beam theory. As the analytical solution provides extensive data for a single beam element, complicated models were unable to be used in this thesis due to time and computing power restrictions.

2 State of the art

2.1 Global Loads on ships

2.1.1 Load classification

For ships strength analysis, it is essential to understand the loads induced to the ship hull and structural members. In general, the specificity of the loads used for design is dependant on the stage in which the ship is currently in terms of structural details. Even though loads can be classified into four groups according to the structure level these are acting on as follows:

- hull girder,
- hull module,
- principal member,
- local,

the global strength analysis performed during early-stage design only focuses on two former groups. These loads can be considered as globally acting loads [2].

Loads are additionally classified by their time variability: static, slowly varying and rapidly varying. Depending on the type of loading, static or dynamic strength analysis is carried out to estimate ship response. See Table 2-1 for typical loads and structural analysis performed

Table 2-1 Load classification according to time variability and strength analysis performed

Time variation	Loading type	Strength analysis performed
Static	Stillwater loads Drydocking loads Thermal loads	Static
Slowly varying	Wave-induced hydrodynamic pressure Liquid cargo sloshing Green water on deck Wave slapping Inertia loads Launching, berthing loads Ice-breaking loads	Static (Quasi-static)
Rapidly varying	Slamming Forced vibration Springing, whipping	Dynamic

In essence, slowly varying loads need a quasi-static strength analysis. However, as even the shortest loading periods are significantly longer than the natural frequencies of the structure, slowly varying loads can be considered within the context of static analysis with only small loss of accuracy. In contrast, rapidly varying loads need dynamic analysis for sufficient accuracy [2].

2.1.2 Internal loads acting on rigid hull girder

In global strength analysis, internal forces and moments acting on a hull are estimated, while the ship is operating in waves. These are mainly induced by ships mass distribution over the length of the ship and the interaction between hull and waves. In still water mass forces consists of the distributed ship weight. Interaction between the hull and waves is described as buoyancy forces in the form of hydrostatic pressure [3].

When waves are present, ship mass is subject to accelerations. As a result, the inertia component is added. In addition to inertia, hull and water interactions become more complicated as radiation, Froude-Krylov and diffraction forces are introduced [3].

Sagging is the state in which wave crests are located in the bow and stern and the hull girder is compressed in the top deck. The sagging increases with hull features such as a large bow flare and a flat stern bottom, which increase vertical slamming forces. Hogging is the state where a wave crest is located in the midship and the ship is compressed at the bottom [3].

Figure 2-1 presents the deformation shapes for sagging and hogging.

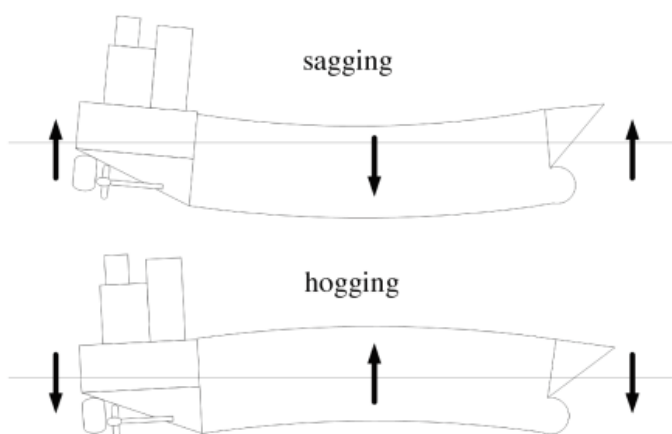


Figure 2-1 Hull sagging and hogging

Hull bending moment and shear force is assessed using a linear approach for which a typical body-specific coordinate system is defined with assigned ship motions, see Figure 2-2.

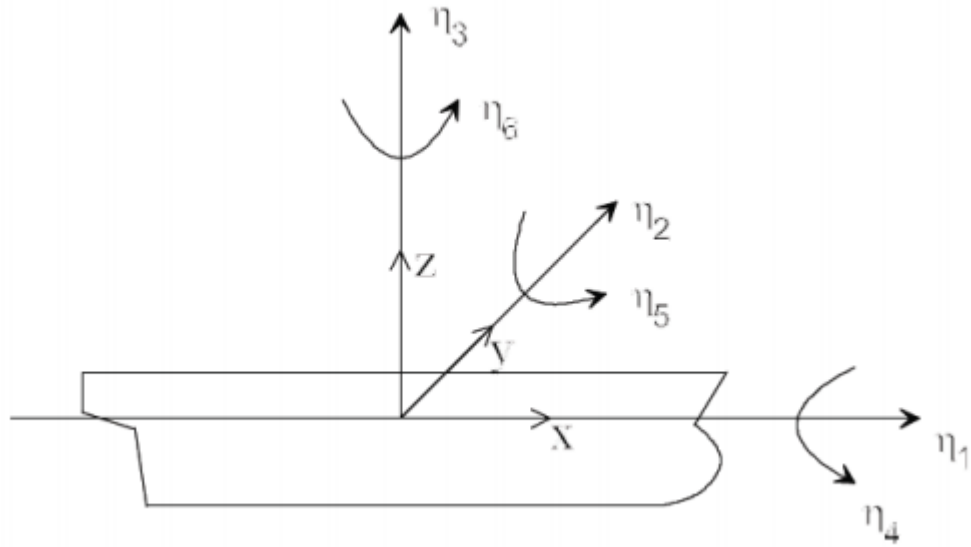


Figure 2-2 Definition of ship fixed coordinate system and ship motions [3]

Assessment of ultimate bending moment and shear force requires the definition of net loading per unit length $q_l(x)$ on ship cross-section. To do so, initial weight distribution $m_l(x)g$ and buoyancy distribution $\rho_l g A_l(x)$ must be defined, where $A_l(x)$ is the cross-sectional area under waterline at coordinate x .

Weight distribution is typically estimated roughly by factoring in primary and secondary structural elements such as shell, deck and bulkhead plating, floors, transversal, longitudinal girders and stringers as well as dimensioning of main equipment and placing their respective mass elements along the length of the ship as precisely as possible [4]. Structural elements at the earliest stage are typically dimensioned according to Classification Society rules. For example, Det Norske Veritas sets the standards for hull principles in Part 3 Ch 1 [5].

Buoyancy distribution is estimated by defining the hull shape and draft at still water condition. Equilibrium is achieved at the draft, where the total buoyancy of the hull section Under waterline opposes the total weight of the ship. In the state of global equilibrium, the difference of local weight component and buoyancy component creates vertical shear force, which can be positive, negative or even equal to 0 depending on the coordinate [4].

By defining a section of the ship dx_i , see Figure 2-3 , distributed load in that section becomes

$$q_l(x_i) = -m_l(x_{l,i})g + \rho_l g A_l(x_{l,i}). \quad (1)$$

By integrating distributed load over the length $dx_{l,i}$ shear force becomes

$$Q_l(x_{l,i}) = \int q_l(x_{l,i})dx_{l,i} = \int_{x_{l,i}^0}^{x_{l,i}^1} q_l(x_{l,i})dx_{l,i}. \quad (2)$$

By integrating shear force over the length dx_i , the bending moment becomes

$$\begin{aligned} M_l(x_{l,i}) &= \int Q_l(x_{l,i})dx_{l,i} = \int \int q_l(x_{l,i})dx_{l,i} dx_{l,i} \\ &= \int_{x_{l,i}^0}^{x_{l,i}^1} \int_{x_{l,i}^0}^{x_{l,i}^1} q_l(x_{l,i})dx_{l,i} dx_{l,i}. \end{aligned} \quad (3)$$

Example of net loading, ultimate shear stress and extreme bending moment curves are presented in Figure 2-4.

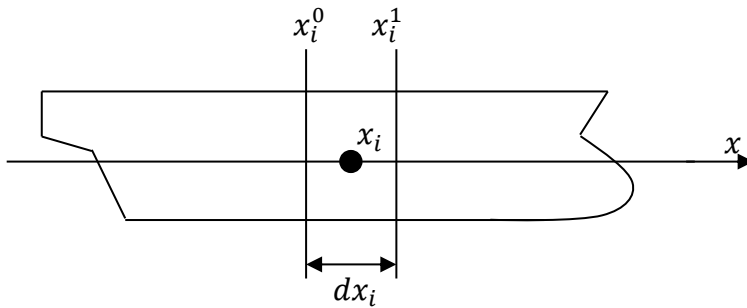


Figure 2-3 Definition of a ship section

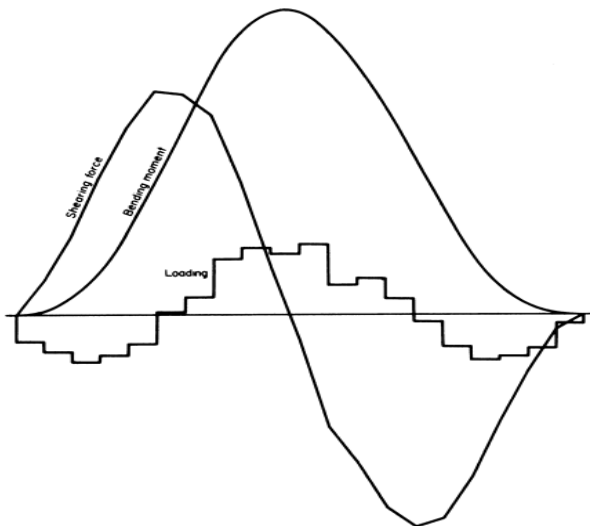


Figure 2-4 Typical loading, ultimate shear force and the ultimate bending moment [4]

2.2 Research on evaluating hull and superstructure interaction

Methods using beam theory to describe hull and superstructure interactions were first introduced by Crawford et al. [6] by considering longitudinal shear force and vertical force in a two-beam system. A similar approach was introduced by Bleich et al. [7], where the computation of stresses in prismatic beams in a vertically coupled two-beam system is presented. Terazawa and Yagi [8] further developed two-beam theory by introducing shear lag phenomena

Further development of Bleich's method was presented by Naar et al [1] introducing the Coupled Beam method, where shear and vertical coupling between beams is defined to evaluate multi-deck passenger ships. The coupled beam theory is described in length in Chapter 2.3. Romanoff et al [9] investigated hull and superstructure interaction in optimised passenger ships. The research showed that simplified two-dimensional section models are not adequate for the assessing load-carrying mechanism of the hull girder. Andri and Ani [10] researched the vertical stress distributions in the hull girder considering effects caused by side shell openings. Bending efficiencies of superstructure decks of aluminium alloy superstructure have been researched by Chen [11].

With the development of software, FEM calculations are more widely used to describe hull and superstructure interaction. The performed calculations are used to verify analytical methods as well as perform entire analyses if the ship can be modelled with sufficient time and detail. Zhiyong et al [12] provided a modification to Bureau Veritas, 2019 PART - B analytical calculation for stress in the vertical direction. A correction factor of bending efficiency is presented for various superstructure width and length to provide more accurate coincidence to FEM results. 3D FE models of various types of ships are researched in Zanic et al [13], Andric [14] etc. Zou [15] performed FEM analysis for typical inland passenger ship and compared vertical stress distribution values to rule values of Bureau Veritas (NR 217, 2011). Fricke and Gerlach [16] presented a method of evaluating the contribution of large openings on shear stiffness, which was validated with FEM.

In addition to beam theory approach, Crawford [17] and Fransman [18] provided an alternative approach using plane stress theory which allows the inclusion of shear lag phenomenon.

2.3 Coupled beam method [1]

This sub-chapter presents the principles of the coupled beam theory [1] and discusses its deficiencies, which the higher-order shear deformation theory presented in this thesis aims to resolve.

2.3.1 Method description

Coupled beam method was proposed by Naar et al. [1]. In the research, the author described the longitudinal bending response of a modern passenger ship with a long, multi-deck superstructure and a recess on the main deck. The ship's girder was described as a prismatic beam with constant cross-section. The model consisted of longitudinal beams each describing a section of a deck plate with connecting side shell or longitudinal bulkheads with stiffeners and girders. Vertical and horizontal coupling of beams is created with spring elements. All beam elements had axial and bending stiffness dependent on the ship structural section it represented.

The basic concept of dividing ship hull girder into beams using the CB method is shown in Figure 2-5. Two separate types of coupling were defined. The first method uses only vertical coupling, which is used for simple cross-section without longitudinal bulkheads. The second method uses both vertical and horizontal coupling to obtain more accurate results, see Figure 2-6.

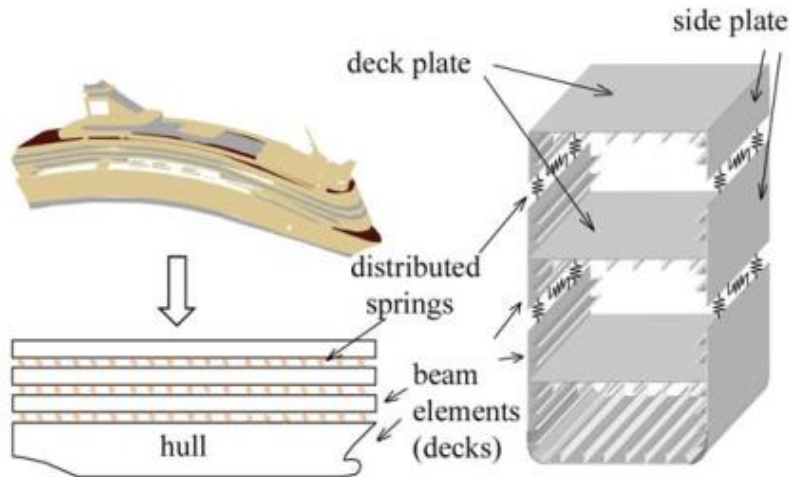


Figure 2-5 The basic concept of dividing ship hull girder into beams [1]

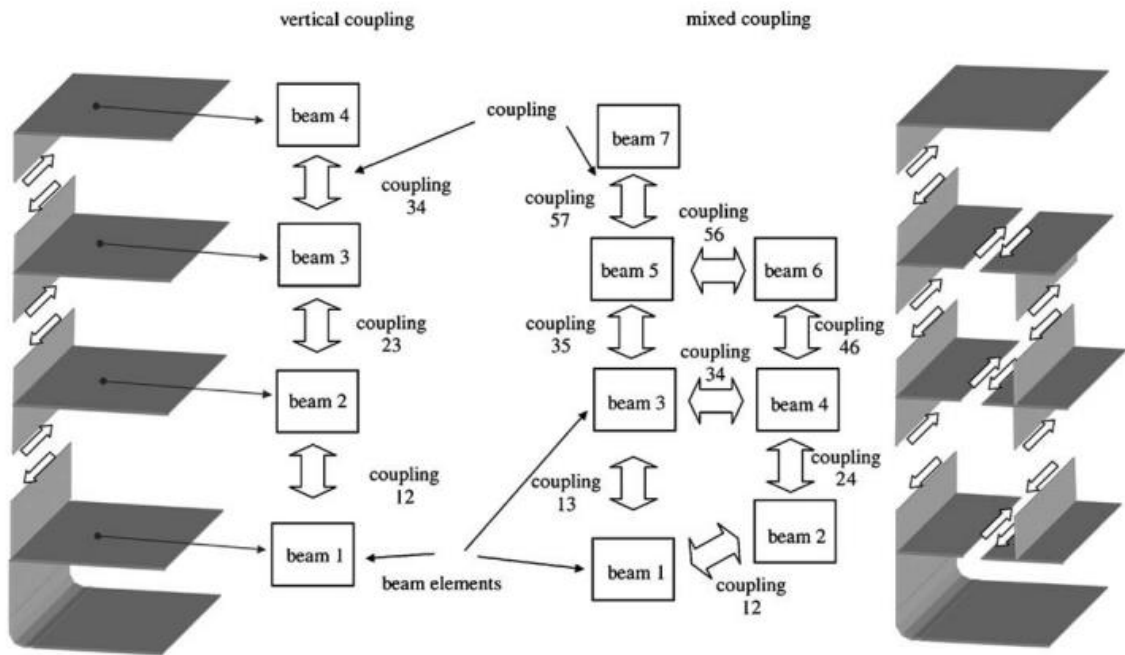


Figure 2-6 Types of coupling between beams [1]

2.3.2 Equilibrium equations

A beam segment to which internal forces, coupling forces and external load is presented. Basic beam theory defines two active internal forces and bending moment: axial force N_i ,

shear force Q_i and bending moment M_i . Coupling forces are applied on the surfaces of the beam segment: vertical distributed force p_{ij} and longitudinal shear force s_{ij} . Subscripts i and j are used to describe beam i with its adjacent beam j . External loads such as wave pressure, loads induced by weights acting upon ship structures are described using distributed vertical force q_i . Symbols e_{ij}, d_{ik} describe the distance from beam top and bottom surfaces to the reference line, where j denotes the lower adjacent beam segment, and k denotes the upper adjacent beam segment. The described beam segment is presented in Figure 2-7.

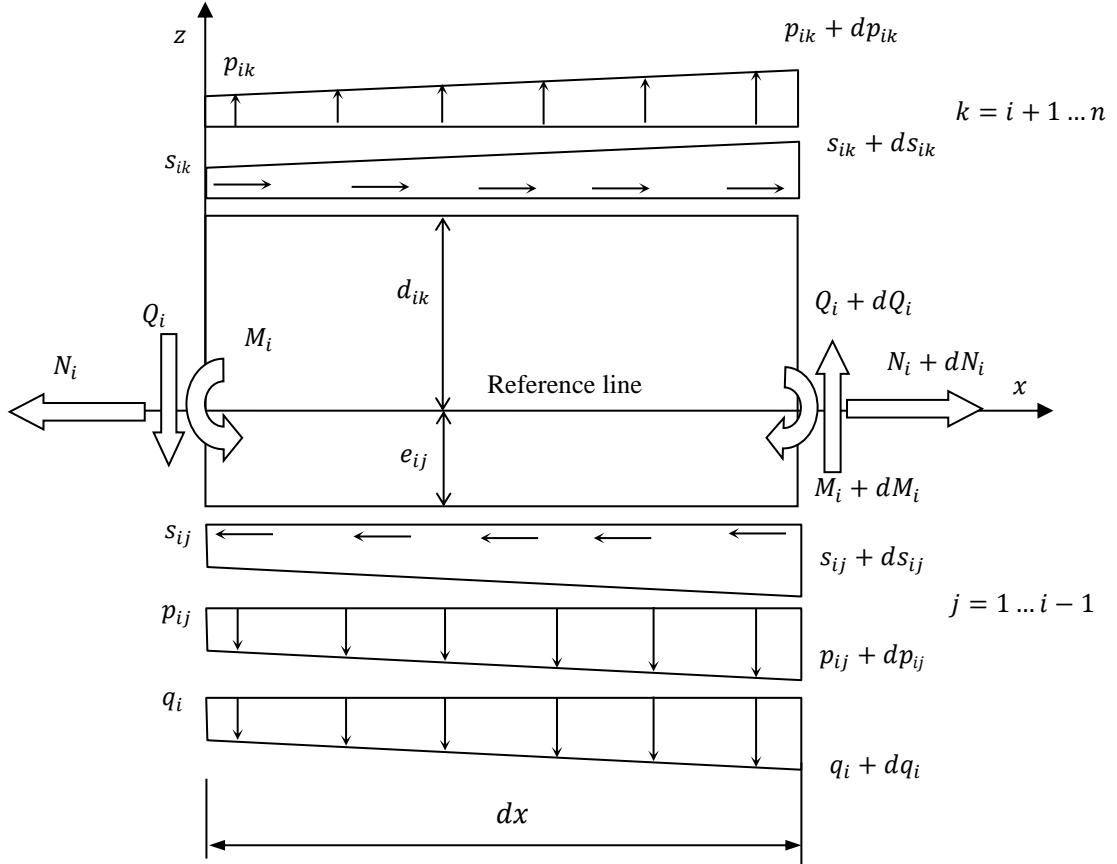


Figure 2-7 Beam segment i with internal forces and external load

Equilibrium equation for beam i with n couplings are defined as:

$$N_i + dN_i - N_i + (s_{ik} + ds_{ik})dx - (s_{ij} + ds_{ij})dx = 0 \quad (4)$$

$$Q_i + dQ_i - Q_i + (p_{ik} + dp_{ik})dx - (p_{ij} + dp_{ij})dx - (q_i + dq_i)dx = 0 \quad (5)$$

$$M_i + dM_i - M_i - Q_i dx + \left(\frac{p_{ik} dx^2}{2} + \frac{dp_{ik} dx^2}{6} \right) - \left(\frac{p_{ij} dx^2}{2} + \frac{dp_{ij} dx^2}{6} \right) - \left(\frac{q_i dx^2}{2} + \frac{dq_i dx^2}{6} \right) = 0 \quad (6)$$

After assuming that $dx; ds_{ik}; ds_{ij}; dp_{ik}; dp_{ij}; dq_i \rightarrow 0$ equations are reorganised.

The equilibrium equation for axial forces:

$$\frac{\partial N_i}{\partial x} + \sum_{j=1}^n s_{ij} = 0, \quad (7)$$

where the external load vector does equal 0 and distributed axial coupling force s_{ij} is described in matrix form such that

$$s_{ij} = \begin{cases} s_{ij} & \text{if } j > i, \\ 0 & \text{if } j = i, \\ -s_{ji} & \text{if } j < i. \end{cases} \quad (8)$$

The equilibrium equation vertical forces:

$$\frac{\partial Q_i}{\partial x} + \sum_{j=1}^n p_{ij} = q_i, \quad (9)$$

where q_i is the external distributed load vector and distributed vertical coupling force p_{ij} is described in matrix form such that

$$p_{ij} = \begin{cases} p_{ij} & \text{if } j > i, \\ 0 & \text{if } j = i, \\ -p_{ji} & \text{if } j < i. \end{cases} \quad (10)$$

The equilibrium equation of moments around y-axis:

$$\frac{\partial^2 M_i}{\partial x^2} + \sum_{j=1}^n p_{ij} + \frac{\partial}{\partial x} \left(\sum_{j=1}^n C_{ij} s_{ij} \right) = q_i. \quad (11)$$

Distance from the reference line is described with matrix C :

$$C_{ij} = \begin{cases} d_{ij} & \text{if } j > i, \\ 0 & \text{if } j = i, \\ -e_{ij} & \text{if } j < i. \end{cases} \quad (12)$$

2.3.3 Coupling equations

Interaction of adjacent beams is described by coupling equations. These equations are used to approximate distributed internal vertical and axial forces. Shear forces can be visualized

with a shear element, see Figure 2-8. Displacement discontinuity δ_{ij}^u causes shear force between the beams. These forces can be evaluated by signing the shear element stiffness T_{ij} , which is dependant on the effective area of the element and the effective height H_{ij} . As the reference lines correspond with deck levels, the effective height equals to deck height. As the shear force is constant over the length dx , horizontal springs are used to apply this force on the beam segment surfaces.

Shear force is approximated for horizontal coupling as:

$$s_{ij}(x) = T_{ij}(x)\delta_{ij}^u(x). \quad (13)$$

Using axial displacement u and vertical deflection due to bending v^M , displacement discontinuity can be described as

$$\delta_{ij}^u = u_j + e_{ji} \frac{\partial v_j^M}{\partial x} - u_i + d_{ij} \frac{\partial v_i^M}{\partial x}. \quad (14)$$

By substitution, equation (13) can be written as

$$s_{ij} = T_{ij} \left(u_j - C_{ji} \frac{\partial v_j^M}{\partial x} - u_i + C_{ij} \frac{\partial v_i^M}{\partial x} \right). \quad (15)$$

The shear element stiffness matrix is

$$T_{ij} = \begin{cases} T_{ij} & \text{if } j \neq i, \\ 0 & \text{if } j = i. \end{cases} \quad (16)$$

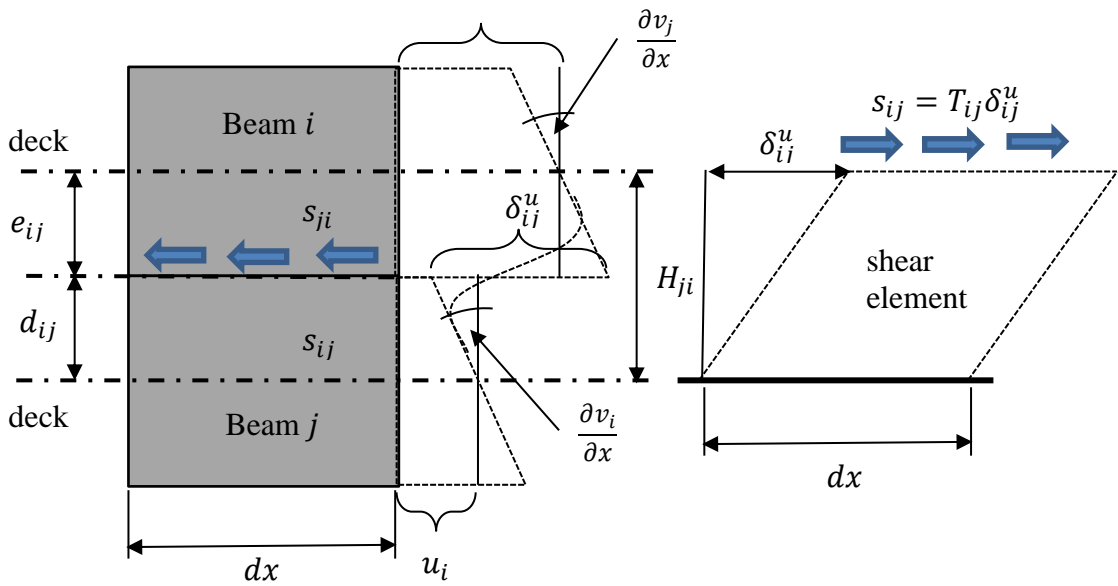


Figure 2-8 Shear coupling in adjacent beams

Shear forces are similarly calculated in the case of mixed coupling, where the model has also been divided into beam segments in the transversal direction. In these situations shear element is located in the ships horizontal plane, thus changing effective height from deck height to transversal distance of adjacent longitudinal members such as side shell and longitudinal bulkheads.

Secondly, the vertical coupling is described, which occurs when vertically adjacent beams have different bending shape. Coupling forces become greater in situations, where structures are not sufficiently supported. Less supported pillars and long bulkhead spacing results in higher vertical forces in supporting side shell or bulkheads. In CB method vertical loads are modelled with vertical springs, which have been assigned vertical coupling stiffness K_{ij} . Elongation element visualizes relative deflection δ_{ij}^v in adjacent beams, see Figure 2-9.

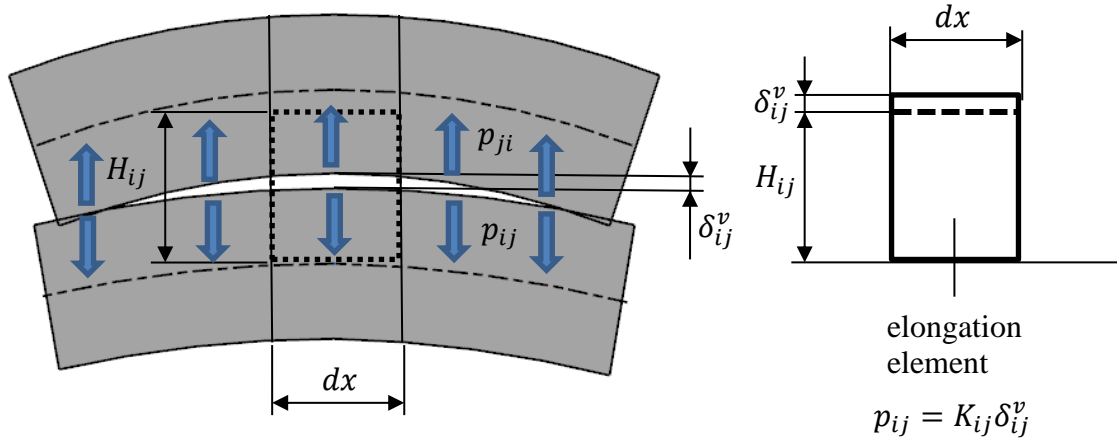


Figure 2-9 Vertical coupling in adjacent beams

Vertical coupling force is dependant on the coupling stiffness and discontinuity of vertical deflection, thus it is described as

$$p_{ij}(x) = K_{ij}(x)\delta_{ij}^v(x) \quad (17)$$

where vertical displacement discontinuity is

$$\delta_{ij}^v(x) = v_j(x) - v_i(x). \quad (18)$$

Vertical stiffness in matrix form is given as

$$K_{ij} = \begin{cases} K_{ij} & \text{if } j \neq i, \\ 0 & \text{if } j = i. \end{cases} \quad (19)$$

Further estimation of coupling stiffnesses T_{ij} and K_{ij} based on the characteristics of the beam segment can be seen in Naar [1].

2.3.4 Relations between deformations and displacements

The coupled beam method utilises beam theory to describe relations between internal forces and displacements assuming that the material follows Hooke's law.

Axial force and bending moment are described as:

$$N_i = EA_{ii} * \frac{\partial u_i}{\partial x} - EX_{ii} * \frac{\partial^2 v_i^M}{\partial x^2} \quad (20)$$

$$M_i = -EI_{ii} * \frac{\partial^2 v_i^M}{\partial x^2} + EX_{ii} * \frac{\partial u_i}{\partial x} \quad (21)$$

where A_{ii} is the cross-sectional area of the beam, I_{ii} is the moment of inertia of the cross-section and X_{ii} is the First moment of the cross-sectional area in reference to the neutral axis. The relation between shear force and deflection due to shear is given as:

$$Q_i = GA_{ii}^S * \frac{\partial v_i^Q}{\partial x} \quad (22)$$

where A_{ii}^S is the effective area of the cross-section in shear.

2.3.5 Differential equations to be solved

Based on Chapter 2.3.2 equilibrium equations (7), (9) and (11) are to be solved:

$$\left\{ \begin{array}{l} \frac{\partial N_i}{\partial x} + \sum_{j=1}^n s_{ij} = 0, \\ \frac{\partial Q_i}{\partial x} + \sum_{j=1}^n p_{ij} = q_i, \\ \frac{\partial^2 M_i}{\partial x^2} + \sum_{j=1}^n p_{ij} + \frac{\partial}{\partial x} \left(\sum_{j=1}^n C_{ij} s_{ij} \right) = q_i \end{array} \right. \quad (23)$$

By substituting internal components with constitutive equations (20), (21) and (22) and replacing partial derivative with full derivative as the axial coordinate is the only variable for displacements, equations to be solved are:

$$\left\{ \begin{array}{l} \frac{d}{dx} \left(EA_{ii} \frac{\partial u_i}{\partial x} - EX_{ii} \frac{\partial^2 v_i^M}{\partial x^2} \right) = - \sum_{j=1}^n s_{ij}, \\ \frac{d}{dx} \left(GA_{ii}^S \frac{\partial v_i^Q}{\partial x} \right) = q_i - \sum_{j=1}^n p_{ij}, \\ \frac{d^2}{dx^2} \left(-EI_{ii} \frac{\partial^2 v_i^M}{\partial x^2} + EX_{ii} \frac{\partial u_i}{\partial x} \right) = q_i - \sum_{j=1}^n p_{ij} - \frac{d}{dx} \left(\sum_{j=1}^n C_{ij} s_{ij} \right). \end{array} \right. \quad (24)$$

Differential equations are solved for variables u_i , v_i^M and v_i^Q .

2.3.6 Comparison of coupled beam method to FEM

By analysing the research result presented by Naar et al. [1], deficits of the CB can be observed.

First, results for a simple box structure is described, for which the dimensions are shown in Figure 2-10. The structure was simply supported and was subjected to sinusoidal vertical distributed loading. Normal stress vertical distribution curve is presented in Figure 2-11. It can be seen that normal stress calculated using the CB method in the marked sections are not continuous. This suggests a noncontinuous axial displacement field over the height of the structure. In the CB method, when using shear coupling, axial displacements are coupled at the reference line and away from that is dependant on axial displacement due to bending. Noncontinuous axial displacement field results on noncontinuous axial and shear deformations over the vertical span and thus resulting in an inaccurate assessment of stresses.

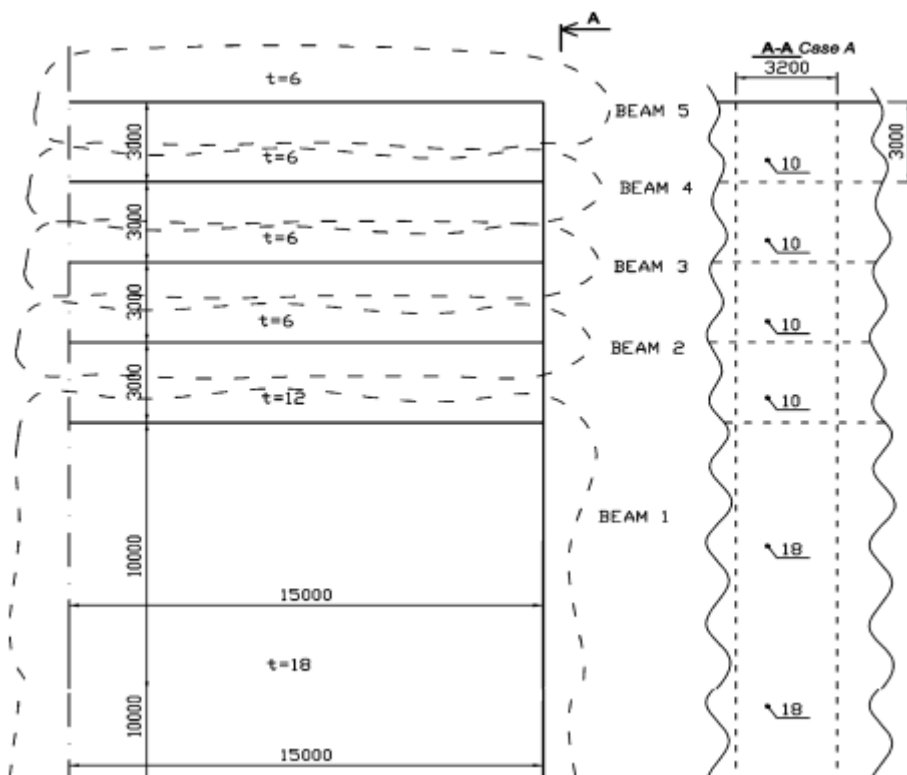


Figure 2-10 Dimensions for box structure with no openings [1]

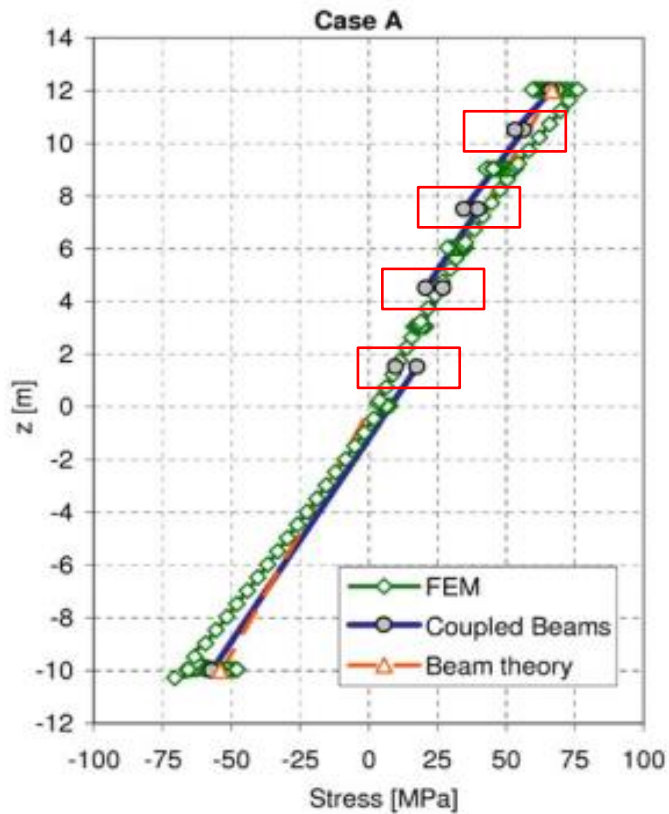


Figure 2-11 Distribution of normal stress in the box structure at $x = L/2$ cross-section [1]

2.4 Hyperbolic shear deformation theory

2.4.1 Development of shear deformation theories

In most classical beam theory application Euler-Bernoulli beam theory is used. This theory assumes that the transverse normal of a cross-section remains in the direction of the neutral axis of the beam. Euler-Bernoulli beam theory is only applicable in the case of slender beams, which are described by the aspect ratio of a beam. This assumption, however, negates the effects of shear deformation resulting in underestimation of deflections and overestimation of natural frequencies in thick beams.

Timoshenko et al [19] introduced the effects of shear deformations for beam displacements. The theory is now widely known as Timoshenko beam theory or first-order shear deformation theory. The theory requires the use of correctional factors as the shear deformation distribution is considered to be constant through the beam cross-section.

Since then, many shear deformation theories have been developed to more accurately describe displacements without the use of correctional factors. Levinson [20], Bickford [21], Rehfield and Murthy [22], Krishna Murty et al.[23], Bhimaraddi and Chandrashekhara [24] and Baluch et al. [25] presented parabolic shear deformation theories, which used a higher variation of axial displacement in terms of thickness coordinate, thus allowed omitting previously used correctional factors as these satisfied shear stress-free boundary conditions on the top and bottom surface.

Ghugal and Sharma [26] presented a variationally consistent hyperbolic shear deformation theory for thick beams. This theory provided a general bending solution for thick rectangular beams in various loading and boundary conditions. A refined theory is presented in Ghugal and Sharma [27]. This theory is reviewed more in-depth in chapter 2.4.2. and a comparative calculation with analytical results and FEM results on various cross-sections are presented in Appendix D . The formulation of the displacement field in the theory is considered during the research to define shear deformation and displacement due to shear and axial forces in the top and bottom surfaces.

2.4.2 Overview of hyperbolic shear deformation theory by Ghugal and Sharma [27]

Principle of virtual work is used for the formulation of differential equations and boundary conditions, based on the assumed displacement field. The beam occupies the region:

$$0 \leq x \leq L;$$

$$-b/2 \leq y \leq b/2;$$

$$-h/2 \leq z \leq h/2,$$

where x, y, z are Cartesian system coordinates. L is the length of the beam, b is the width and h is the depth of the beam. Transverse load intensity $q(x)$ is used to induce bending in the beam.

Several assumptions are made in the hyperbolic shear deformation theory such as:

1. The axial displacement is made up of two parts:
 - a. Axial displacement due to bending:
 - b. Axial displacement due to shear deformation, which is estimated with a hyperbolic function of thickness coordinate
2. Axial displacement is such that the resultant axial stress σ_x acting over the cross-section results in only bending moment and not as a force in the x-direction.
3. The transverse displacement w is assumed to be a function of longitudinal coordinate x .
4. The displacements are considered to be small compared to the total depth of the beam
5. The body forces are ignored in the analysis, which can be taken into account by adding them as external forces.
6. One-dimensional constitutive equations are used.
7. Only transverse load is applied to the beam.

The displacement field in the hyperbolic shear deformation theory is given as:

$$u(x, z) = -z * \frac{dw(x)}{dx} + \left[z * \cosh\left(\frac{1}{2}\right) - h * \sinh\left(\frac{z}{h}\right) \right] \phi(x), \quad (25)$$

$$w(x, z) = w(x). \quad (26)$$

Axial displacement u and transverse displacement w are considered from the beam center-line in x and z directions respectively, variable t denotes time. Shear stress distribution through the thickness of the beam is used for definition of the hyperbolic function. $\phi(x)$ is an unknown function associated with the rotation of the cross-section due to shear with respect to beam neutral axis and is to be determined.

Normal strain and shear strain are defined as:

$$\varepsilon_x = \frac{\partial u}{\partial x} = -z * \frac{d^2w}{dx^2} + \left[z * \cosh\left(\frac{1}{2}\right) - h * \sinh\left(\frac{z}{h}\right) \right] \frac{d\phi}{dx}, \quad (27)$$

$$\gamma_{xz} = \frac{\partial u}{\partial z} + \frac{dw}{dx} = \left[\cosh\left(\frac{1}{2}\right) - \cosh\left(\frac{z}{h}\right) \right] \phi(x). \quad (28)$$

Stresses are given by:

$$\sigma_x = E\varepsilon_x, \quad \tau_{xy} = G\gamma_{xz}, \quad (29)$$

where E and G are Young's modulus and shear modulus, respectively.

Using equations (27)-(29) and a dynamic version of the principle of virtual work governing differential equations and boundary conditions for the beam under consideration are obtained. The principle of virtual work is given as:

$$b \int_0^L \int_{-\frac{h}{2}}^{\frac{h}{2}} (\sigma_x \delta \varepsilon_x + \tau_{xz} \delta \gamma_{xz}) dz dx - \int_0^L q \delta w dx = 0, \quad (30)$$

where the symbol δ denotes the variational operator. By using applying Green's theorem in equation (30) the governing differential equations are obtained

$$EI_y \frac{d^4 w}{dx^4} - EI_y A_0 \frac{d^3 \phi}{dx^3} = q(x), \quad (31)$$

$$EI_y A_0 * \frac{d^3 w}{dx^3} - EI_y B_0 * \frac{d^2 \phi}{dx^2} + GAC_0 \phi = 0, \quad (32)$$

where A_0, B_0 and C_0 are constants given as:

$$A_0 = \cosh\left(\frac{1}{2}\right) - 12 * \left[\cosh\left(\frac{1}{2}\right) - 2 * \sinh\left(\frac{1}{2}\right) \right], \quad (33)$$

$$B_0 = \cosh^2\left(\frac{1}{2}\right) + 6 * [\sinh(1) - 1] - 24 * \cosh\left(\frac{1}{2}\right) * \left[\cosh\left(\frac{1}{2}\right) - 2 * \sinh\left(\frac{1}{2}\right) \right], \quad (34)$$

$$C_0 = \cosh^2\left(\frac{1}{2}\right) + \left(\frac{1}{2}\right) [\sinh(1) + 1] - 4 * \cosh\left(\frac{1}{2}\right) * \sinh\left(\frac{1}{2}\right) \quad (35)$$

Boundary conditions for equations (31) and (32) are obtained as follows:

$$\text{Either } EI_y * \frac{d^3 w}{dx^3} - EI_y A_0 * \frac{d^2 \phi}{dx^2} = 0 \quad \text{or } w \text{ is prescribed.}$$

$$\text{Either } EI_y * \frac{d^2 w}{dx^2} - EI_y A_0 * \frac{d \phi}{dx} = 0 \quad \text{or } \frac{dw}{dx} \text{ is prescribed.}$$

$$\text{Either } EI_y A_0 * \frac{d^2 w}{dx^2} - EI_y B_0 * \frac{d \phi}{dx} = 0 \quad \text{or } \phi \text{ is prescribed.}$$

After integration, rearrangement and application of boundary conditions, first governing equation (31) can be written as:

$$\frac{d^3 w}{dx^3} - A_0 * \frac{d^2 \phi}{dx^2} = \frac{Q(x)}{EI_y} \quad (36)$$

where generalized shear force $Q(x)$ is given by:

$$Q_z(x) = \int q dx + C_1. \quad (37)$$

After rearrangement, the second governing equation (32) can be written as:

$$\frac{d^3 w}{dx^3} - \frac{A_0}{B_0} * \frac{d^2 \phi}{dx^2} + \beta \phi = 0 \quad (38)$$

where

$$\beta = \frac{GAC_0}{EI_y A_0}. \quad (39)$$

A single differential equation in terms of cross-sectional rotation ϕ can be written by combining governing equations (36) and (38):

$$\frac{d^2\phi}{dx^2} - \lambda^2\phi = \frac{Q_z(x)}{\alpha EI_y} \quad (40)$$

where

$$\alpha = \frac{B_0}{A_0} - A_0, \quad (41)$$

$$\lambda^2 = \frac{\beta}{\alpha}. \quad (42)$$

The general solution for equation (40) is given by:

$$\phi(x) = C_2 \cosh(\lambda x) + C_3 \sinh(\lambda x) - \frac{Q_z(x)}{\beta EI_y}. \quad (43)$$

The general solution for transverse displacement w is obtained by replacing equation (43) into governing equation (38) and integrating thrice over the length of the beam. The general solution is:

$$\begin{aligned} EIw(x) = & \int \int \int \int q dx dx dx dx + \frac{C_1 x^3}{6} + \frac{A_0 EI_y}{\lambda} [C_2 \sinh(\lambda x) \\ & + C_3 \cosh(\lambda x) + C_4 \frac{x^2}{2} + C_5 x + C_6 \end{aligned} \quad (44)$$

where $C_1 - C_6$ are the constants of integration.

An illustrative calculation example for a cantilever beam using the refined shear deformation theory for flexure of beams is presented in chapter 4.1.

The refined shear deformation theory is a well-designed tool to assess thick beams with simple cross-sections however, it has several deficits. First, the theory allows only the use of external vertical loading as the equations describing deformations and displacements only define vertically applied loading. Secondly, the theory is only applicable for rectangular cross-sections, which in many cases is not feasible. This limits the practical applications of the theory when dealing with more complicated structures such as a ship. Thirdly, the theory is not applicable for the evaluation of openings as it is not capable of assessing nonhomogeneous structures.

3 Higher-order shear deformation theory

3.1 Definition of variables

A higher-order shear deformation theory (HOSDT) is derived for a beam in the Cartesian coordinate system, where the x -axis is aligned with beam axial direction and the z -axis is aligned with beam cross-section vertical direction, see Figure 3-1.

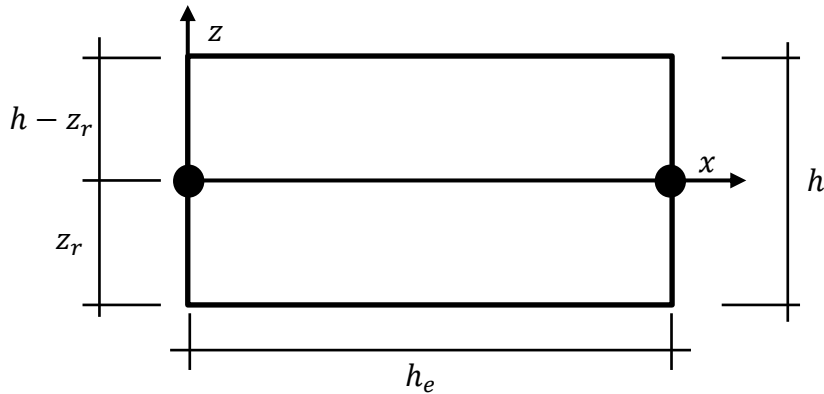


Figure 3-1 Beam in the Cartesian coordinate system

Degrees of freedom are defined at beam end nodes as presented in Figure 3-2.

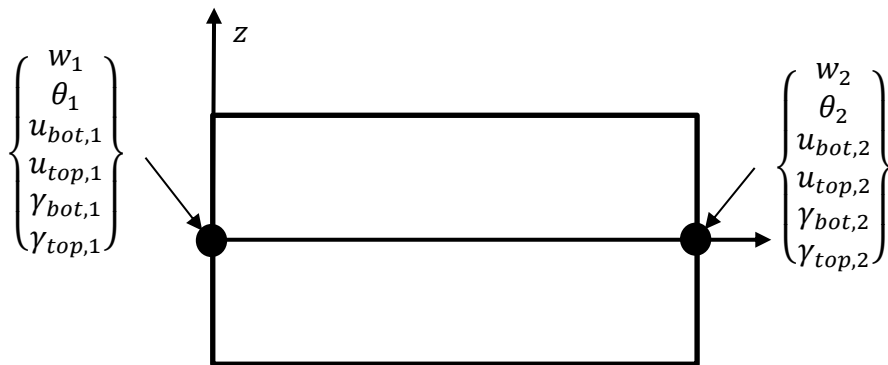


Figure 3-2 Degrees of freedom for a beam segment

Degrees of freedom in beam nodes are as follows:

- w_i – deflection at the beam reference line in node i ,
- θ_i – rotation of the beam cross-section measured at reference line in node i ,
- $u_{bot,i}$ – axial displacement in the bottom layer in node i ,
- $u_{top,i}$ – axial displacement in the top layer in node i ,
- $\gamma_{bot,i}$ – shear deformation in the bottom layer in node i ,
- $\gamma_{top,i}$ – shear deformation in the top layer in node i .

3.2 Definition of the displacement field

Beam axial displacement field is expressed as:

$$u(x, z) = -(z) * \frac{\partial w(x)}{\partial x} + f(x, z), \quad (45)$$

where the first member denotes axial displacement due to bending, and the second member is a function describing displacement due to shear and axial forces in a beam cross-section.

Axial deformation is expressed as:

$$\varepsilon_x = \frac{\partial u(x, z)}{\partial x} = -(z) * \frac{\partial^2 w}{\partial x^2} + \frac{\partial f(x, z)}{\partial x} \quad (46)$$

Shear deformation is expressed as:

$$\gamma_{xz} = \frac{\partial u(x, z)}{\partial z} + \frac{\partial w}{\partial x} = -\frac{\partial w}{\partial x} + \frac{\partial f(x, z)}{\partial z} + \frac{\partial w}{\partial x} = \frac{\partial f(x, z)}{\partial z} \quad (47)$$

The function expressing displacement due to shear and axial forces is assumed to follow a 3-order polynomial in the vertical direction and thus is expressed as:

$$f(x, z) = A(x)z^3 + B(x)z^2 + C(x)z + D(x) \quad (48)$$

By expressing axial displacement and shear deformation in the top surface and bottom surface, see Figure 3-3, displacement function equations are

$$\begin{cases} f(x, -z_r) = u_{bot} \\ f(x, h - z_r) = u_{top} \\ \frac{\partial f}{\partial z}(x, -z_r) = \gamma_{bot} \\ \frac{\partial f}{\partial z}(x, h - z_r) = \gamma_{top} \end{cases} \quad (49)$$

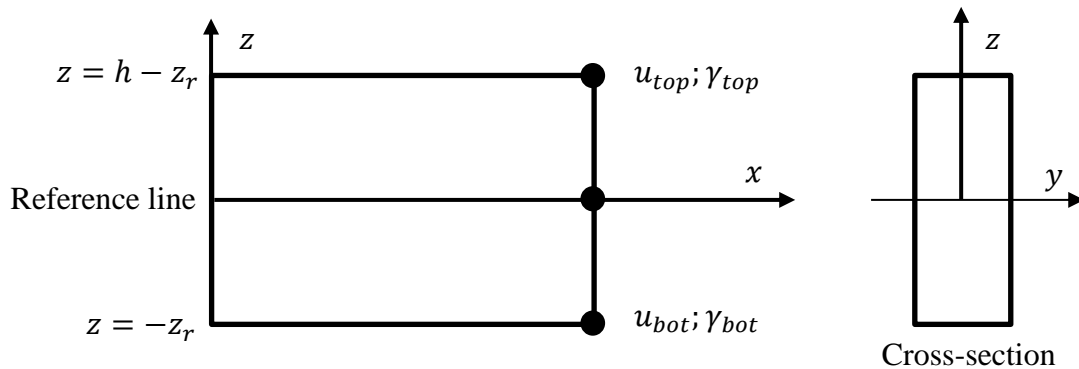


Figure 3-3 Axial displacement approximation

Polynomial equations are:

$$\begin{cases} A(-z_r)^3 + Bz_r^2 + C(-z_r) + D = u_{bot} \\ A(h - z_r)^3 + B(h - z_r)^2 + C(h - z_r) + D = u_{top} \\ 3A(-z_r)^2 + 2B(-z_r) + C = \gamma_{bot} \\ 3A(h - z_r)^2 + 2B(h - z_r) + C = \gamma_{top} \end{cases} \quad (50)$$

Matrix form:

$$\begin{bmatrix} (-z_r)^3 & (z_r)^2 & -z_r & 1 \\ (h - z_r)^3 & (h - z_r)^2 & h - z_r & 1 \\ 3z_r^2 & 2(-z_r) & 1 & 0 \\ 3(h - z_r)^2 & 2(h - z_r) & 1 & 0 \end{bmatrix} \begin{Bmatrix} A \\ B \\ C \\ D \end{Bmatrix} = \begin{Bmatrix} u_{bot} \\ u_{top} \\ \gamma_{bot} \\ \gamma_{top} \end{Bmatrix} \quad (51)$$

By combining polynomial equations and finding constants A, B, C, D , polynomial equation can be written as:

$$f(x, z) = \psi_1(z)u_{bot} + \psi_2(z)u_{top} + \psi_3(z)\gamma_{bot} + \psi_4(z)\gamma_{top}, \quad (52)$$

where

$$\psi_1(z) = \frac{(h + 2z + 2z_r)(z - h + z_r)^2}{h^3}, \quad (53)$$

$$\psi_2(z) = \frac{(z + z_r)^2(3h - 2z - 2z_r)}{h^3}, \quad (54)$$

$$\psi_3(z) = \frac{(z + z_r)(z - h + z_r)^2}{h^2}, \quad (55)$$

$$\psi_4(z) = \frac{(z + z_r)^2(z - h + z_r)}{h^2}. \quad (56)$$

An arbitrary cross-section between beam end nodes can be described by defining linear weight functions to node variables:

$$\phi_1 = \left(1 - \frac{x}{h_e}\right); \phi_2 = \frac{x}{h_e} \quad (57)$$

which define variables in arbitrary cross-section as:

$$u_{bot} = \left(1 - \frac{x}{h_e}\right) * u_{bot,1} + \frac{x}{h_e} * u_{bot,2}, \quad (58)$$

$$u_{top} = \left(1 - \frac{x}{h_e}\right) * u_{top,1} + \frac{x}{h_e} * u_{top,2}, \quad (59)$$

$$\gamma_{bot} = \left(1 - \frac{x}{h_e}\right) * \gamma_{bot,1} + \frac{x}{h_e} * \gamma_{bot,2}, \quad (60)$$

$$\gamma_{top} = \left(1 - \frac{x}{h_e}\right) * \gamma_{top,1} + \frac{x}{h_e} * \gamma_{top,2}. \quad (61)$$

By replacing equations (58), (59), (60) and (61) into equation (52) shear displacement function becomes:

$$f(x, z) = \psi_1 \phi_1 * u_{bot}^1 + \psi_1 \phi_2 * u_{bot}^2 + \psi_2 \phi_1 * u_{top}^1 + \psi_2 \phi_2 * u_{top}^2 + \psi_3 \phi_1 * \gamma_{bot}^1 + \psi_3 \phi_2 * \gamma_{bot}^2 + \psi_4 \phi_1 * \gamma_{top}^1 + \psi_4 \phi_2 * \gamma_{top}^2 \quad (62)$$

Function $f(x, z)$ can be alternatively represented as:

$$f(x, z) = \sum_{i=1}^4 \psi_i(z) * \phi_1(x) * a_{i,1} + \sum_{j=1}^4 \psi_j(z) * \phi_2(x) * a_{j,2} \quad (63)$$

where

$$\begin{Bmatrix} a_{1,1} \\ a_{2,1} \\ a_{3,1} \\ a_{4,1} \end{Bmatrix} = \begin{Bmatrix} u_{bot,1} \\ u_{top,1} \\ \gamma_{bot,1} \\ \gamma_{top,1} \end{Bmatrix}; \begin{Bmatrix} a_{1,2} \\ a_{2,2} \\ a_{3,2} \\ a_{4,2} \end{Bmatrix} = \begin{Bmatrix} u_{bot,2} \\ u_{top,2} \\ \gamma_{bot,2} \\ \gamma_{top,2} \end{Bmatrix}. \quad (64)$$

The deflection function is assumed to follow a 3-order polynomial in axial direction and thus is expressed as:

$$w(x) = A(x)x^3 + B(x)x^2 + C(x)x + D(x). \quad (65)$$

By expressing deflection and rotation of cross-section at the reference line for both element nodes, see Figure 3-4, displacement function equations are

$$\begin{cases} w(0) = w_1 \\ w(h_e) = w_2 \\ \frac{\partial w}{\partial x}(0) = \theta_1 \\ \frac{\partial w}{\partial x}(h_e) = \theta_2 \end{cases} \quad (66)$$

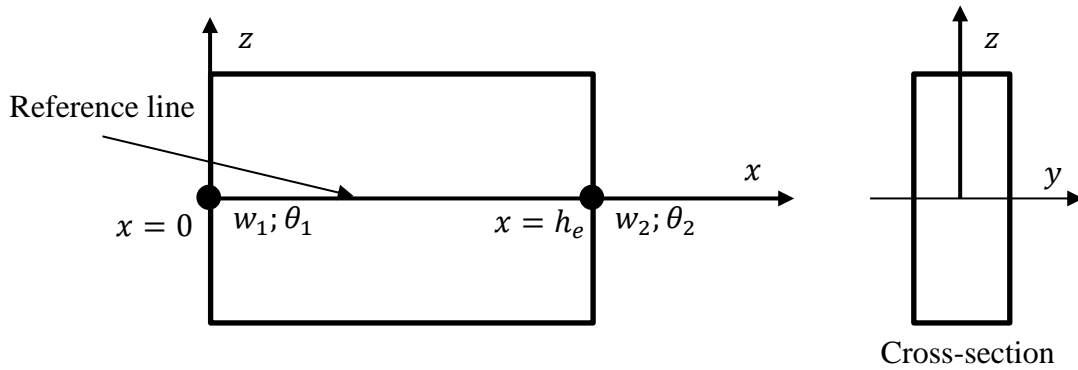


Figure 3-4 Vertical displacement approximation

Polynomial equations are:

$$\begin{cases} A * 0^3 + B * 0^2 + C * 0 + D = w_1 \\ A(h_e)^3 + B(h_e)^2 + C(h_e) + D = w_2 \\ 3A(0)^2 + 2B(0) + C = \theta_1 \\ 3A(h_e)^2 + 2B(h_e) + C = \theta_2 \end{cases} \quad (67)$$

Matrix form:

$$\begin{bmatrix} 0 & 0 & 0 & 1 \\ (h_e)^3 & (h_e)^2 & h_e & 1 \\ 0 & 0 & 1 & 0 \\ 3(h_e)^2 & 2(h_e) & 1 & 0 \end{bmatrix} \begin{Bmatrix} A \\ B \\ C \\ D \end{Bmatrix} = \begin{Bmatrix} w_1 \\ w_2 \\ \theta_1 \\ \theta_2 \end{Bmatrix} \quad (68)$$

By combining polynomial equations and finding constants A, B, C, D , polynomial equation, which describes deflection in a random cross-section can be written as:

$$w(x) = \xi_1(x)w_1 + \xi_2(x)\theta_1 + \xi_3(x)w_2 + \xi_4(x)\theta_2 \quad (69)$$

where

$$\xi_1(x) = \left(\frac{2x^3}{h_e^3} - \frac{3x^2}{h_e^2} + 1 \right) \quad (70)$$

$$\xi_2(x) = \left(x - \frac{2x^2}{h_e} + \frac{x^3}{h_e^2} \right) \quad (71)$$

$$\xi_3(x) = \left(\frac{3x^2}{h_e^2} - \frac{2x^3}{h_e^3} \right) \quad (72)$$

$$\xi_4(x) = \left(\frac{x^3}{h_e^2} - \frac{x^2}{h_e} \right) \quad (73)$$

Equation (69) can alternatively be presented as:

$$w(x) = \sum_{k=1}^4 \xi_k * b_k \quad (74)$$

where

$$\begin{Bmatrix} b_1 \\ b_2 \\ b_3 \\ b_4 \end{Bmatrix} = \begin{Bmatrix} w_1 \\ \theta_1 \\ w_2 \\ \theta_2 \end{Bmatrix} \quad (75)$$

By replacing equation (63) and (74) into equations (46) and (47), axial and shear deformations become:

$$\begin{aligned} \varepsilon_x = & -z * \sum_{k=1}^4 \frac{\partial^2 \xi_k}{\partial x^2} * b_k + \sum_{i=1}^4 \psi_i(z) * \frac{\partial \phi_1(x)}{\partial x} * a_{i,1} \\ & + \sum_{j=1}^4 \psi_j(z) * \frac{\partial \phi_2(x)}{\partial x} * a_{j,2} \end{aligned} \quad (76)$$

$$\gamma_{xz} = \sum_{i=1}^4 \frac{\partial \psi_i(z)}{\partial z} * \phi_1(x) * a_{i,1} + \sum_{j=1}^4 \frac{\partial \psi_j(z)}{\partial z} * \phi_2(x) * a_{j,2} \quad (77)$$

3.3 Expression of potential energy

Principle of minimum energy states that in a closed system, where external parameters are constant, the potential energy will reach its minimum when the difference between the internal energy and the work done by external forces reaches a minimum value. In the case of beam bending, an external force is applied at the beam surface as distributed force and internal energy is expressed with vertical and axial displacement. The potential energy equation for a beam system is written as:

$$\begin{aligned} \Pi = & \frac{1}{2} \int_0^L \int_A (\sigma_x \varepsilon_x + \tau_{xz} \gamma_{xz}) dA dx - \int_0^L p_z w(x) dx - \int_0^L s_{bot} f(x, z) dx \\ & - \int_0^L s_{top} f(x, z) dx - \int_0^L s_{bot} z_r dw(x) dx \\ & + \int_0^L s_{top} (h - z_r) dw(x) dx = 0 \end{aligned} \quad (78)$$

By assuming that the material follows Hooke's law and by replacing equations (76) and (77) into equation (78), the potential energy equation is given as:

$$\begin{aligned} \Pi = & \frac{1}{2} \int_0^L \int_A (E \varepsilon_x^2 + G \gamma_{xz}^2) dA dx - \int_0^L p_z w(x) dx = \\ & \frac{1}{2} \int_0^L \int_A \left(E \left(-z \sum_{k=1}^4 \frac{\partial^2 \xi_k}{\partial x^2} b_k + \sum_{i=1}^4 \psi_i(z) \frac{\partial \phi_1(x)}{\partial x} a_{i,1} + \right. \right. \\ & \left. \left. \sum_{j=1}^4 \psi_j(z) \frac{\partial \phi_2(x)}{\partial x} a_{j,2} \right)^2 + G \left(\sum_{i=1}^4 \frac{\partial \psi_i(z)}{\partial z} \phi_1(x) a_{i,1} + \right. \right. \end{aligned} \quad (79)$$

$$\sum_{j=1}^4 \left(\frac{\partial \psi_j(z)}{\partial z} a_{j,2} \right)^2 \Big) dA dx - \int_0^L p_z w(x) dx - \int_0^L s_{bot} f(x, z) dx -$$

$$\int_0^L s_{top} f(x, z) dx - \int_0^L s_{bot} z_r dw(x) dx + \int_0^L s_{top} (h - z_r) dw(x) dx = 0$$

The potential energy minimum is described by defining of the partial derivative of the potential energy equation for each variable as is presented in Appendix A . Variable multipliers are alternatively presented in Appendix B with symbols used in the stiffness matrix. By combining equations (105) to (116) potential energy minimum is given in matrix form as:

$$\partial \Pi = K_{el} * \begin{pmatrix} w_1 \\ \theta_1 \\ u_{bot,1} \\ u_{top,1} \\ \gamma_{bot,1} \\ \gamma_{top,1} \\ w_2 \\ \theta_2 \\ u_{bot,2} \\ u_{top,2} \\ \gamma_{top,2} \\ \gamma_{top,2} \end{pmatrix} - F_{el} = 0 \quad (80)$$

where

$$K_{el} = \int_0^L \int_A \begin{pmatrix} Ek_1 k_1 & Ek_1 k_2 & Ek_1 k_3 & Ek_1 k_4 \\ Ek_2 k_1 & Ek_2 k_2 & Ek_2 k_3 & Ek_2 k_4 \\ Ek_3 k_1 & Ek_3 k_2 & Ek_3 k_3 + Gk_{13} k_{13} & Ek_3 k_4 + Gk_{13} k_{14} \\ Ek_4 k_1 & Ek_4 k_2 & Ek_4 k_3 + Gk_{14} k_{13} & Ek_4 k_4 + Gk_{14} k_{14} \\ Ek_5 k_1 & Ek_5 k_2 & Ek_5 k_3 + Gk_{15} k_{13} & Ek_5 k_4 + Gk_{15} k_{14} \\ Ek_6 k_1 & Ek_6 k_2 & Ek_6 k_3 + Gk_{16} k_{13} & Ek_6 k_4 + Gk_{16} k_{14} \\ Ek_7 k_1 & Ek_7 k_2 & Ek_7 k_3 & Ek_7 k_4 \\ Ek_8 k_1 & Ek_8 k_2 & Ek_8 k_3 & Ek_8 k_4 \\ Ek_9 k_1 & Ek_9 k_2 & Ek_9 k_3 + Gk_{17} k_{13} & Ek_9 k_4 + Gk_{17} k_{14} \\ Ek_{10} k_1 & Ek_{10} k_2 & Ek_{10} k_3 + Gk_{18} k_{13} & Ek_{10} k_4 + Gk_{18} k_{14} \\ Ek_{11} k_1 & Ek_{11} k_2 & Ek_{11} k_3 + Gk_{19} k_{13} & Ek_{11} k_4 + Gk_{19} k_{14} \\ Ek_{12} k_1 & Ek_{12} k_2 & Ek_{12} k_3 + Gk_{20} k_{13} & Ek_{12} k_4 + Gk_{20} k_{14} \end{pmatrix} \dots \quad (81)$$

Ek_1k_5	Ek_1k_6	Ek_1k_7	Ek_1k_8	Ek_1k_9	
Ek_2k_5	Ek_2k_6	Ek_2k_7	Ek_2k_8	Ek_2k_9	
$Ek_3k_5 + Gk_{13}k_{15}$	$Ek_3k_6 + Gk_{13}k_{16}$	Ek_3k_7	Ek_3k_8	$Ek_3k_9 + Gk_{13}k_{17}$	
$Ek_4k_5 + Gk_{14}k_{15}$	$Ek_4k_6 + Gk_{14}k_{16}$	Ek_4k_7	Ek_4k_8	$Ek_4k_9 + Gk_{14}k_{17}$	
$Ek_5k_5 + Gk_{15}k_{15}$	$Ek_5k_6 + Gk_{15}k_{16}$	Ek_5k_7	Ek_5k_8	$Ek_5k_9 + Gk_{15}k_{17}$	
$Ek_6k_5 + Gk_{16}k_{15}$	$Ek_6k_6 + Gk_{16}k_{16}$	Ek_6k_7	Ek_6k_8	$Ek_6k_9 + Gk_{16}k_{17}$...
...	Ek_7k_5	Ek_7k_6	Ek_7k_7	Ek_7k_8	Ek_7k_9
	Ek_8k_5	Ek_8k_6	Ek_8k_7	Ek_8k_8	Ek_8k_9
$Ek_9k_5 + Gk_{17}k_{15}$	$Ek_9k_6 + Gk_{17}k_{16}$	Ek_9k_7	Ek_9k_8	$Ek_9k_9 + Gk_{17}k_{17}$	
$Ek_{10}k_5 + Gk_{18}k_{15}$	$Ek_{10}k_6 + Gk_{18}k_{16}$	$Ek_{10}k_7$	$Ek_{10}k_8$	$Ek_{10}k_9 + Gk_{18}k_{17}$	
$Ek_{11}k_5 + Gk_{19}k_{15}$	$Ek_{11}k_6 + Gk_{19}k_{16}$	$Ek_{11}k_7$	$Ek_{11}k_8$	$Ek_{11}k_9 + Gk_{19}k_{17}$	
$Ek_{12}k_5 + Gk_{20}k_{15}$	$Ek_{12}k_6 + Gk_{20}k_{16}$	$Ek_{12}k_7$	$Ek_{12}k_8$	$Ek_{12}k_9 + Gk_{20}k_{17}$	
	Ek_1k_{10}	Ek_1k_{11}	Ek_1k_{12}		
	Ek_2k_{10}	Ek_2k_{11}	Ek_2k_{12}		
$Ek_3k_{10} + Gk_{13}k_{18}$	$Ek_3k_{11} + Gk_{13}k_{19}$	$Ek_3k_{12} + Gk_{13}k_{20}$			
$Ek_4k_{10} + Gk_{14}k_{18}$	$Ek_4k_{11} + Gk_{14}k_{19}$	$Ek_4k_{12} + Gk_{14}k_{20}$			
$Ek_5k_{10} + Gk_{15}k_{18}$	$Ek_5k_{11} + Gk_{15}k_{19}$	$Ek_5k_{12} + Gk_{15}k_{20}$			
$Ek_6k_{10} + Gk_{16}k_{18}$	$Ek_6k_{11} + Gk_{16}k_{19}$	$Ek_6k_{12} + Gk_{16}k_{20}$			
...	Ek_7k_{10}	Ek_7k_{11}	Ek_7k_{12}		
	Ek_8k_{10}	Ek_8k_{11}	Ek_8k_{12}		
$Ek_9k_{10} + Gk_{17}k_{18}$	$Ek_9k_{11} + Gk_{17}k_{19}$	$Ek_9k_{12} + Gk_{17}k_{20}$			
$Ek_{10}k_{10} + Gk_{18}k_{18}$	$Ek_{10}k_{11} + Gk_{18}k_{19}$	$Ek_{10}k_{12} + Gk_{18}k_{20}$			
$Ek_{11}k_{10} + Gk_{19}k_{18}$	$Ek_{11}k_{11} + Gk_{19}k_{19}$	$Ek_{11}k_{12} + Gk_{19}k_{20}$			
$Ek_{12}k_{10} + Gk_{20}k_{18}$	$Ek_{12}k_{11} + Gk_{20}k_{19}$	$Ek_{12}k_{12} + Gk_{20}k_{20}$			

$dAdx,$

$$F_{el} = \int_0^L \left| \begin{array}{c} p_z \xi_1 \\ p_z \xi_2 - s_1 \phi_1(-z_r) - s_2 \phi_1(h - z_r) \\ s_1 \psi_1 \phi_1 + s_2 \psi_1 \phi_1 \\ s_1 \psi_2 \phi_1 + s_2 \psi_2 \phi_1 \\ s_1 \psi_3 \phi_1 + s_2 \psi_3 \phi_1 \\ s_1 \psi_4 \phi_1 + s_2 \psi_4 \phi_1 \\ p_z \xi_3 \\ p_z \xi_4 - s_1 \phi_2(-z_r) - s_2 \phi_2(h - z_r) \\ s_1 \psi_1 \phi_2 + s_2 \psi_1 \phi_2 \\ s_1 \psi_2 \phi_2 + s_2 \psi_2 \phi_2 \\ s_1 \psi_3 \phi_2 + s_2 \psi_3 \phi_2 \\ s_1 \psi_4 \phi_2 + s_2 \psi_4 \phi_2 \end{array} \right| dx. \quad (82)$$

3.4 Coupling of elements

3.4.1 Single-layer beam model

The developed shear deformation can be applied in two separate types of models. First of which involves a beam model, where a single layer of elements is defined. These beam elements are coupled through a shared node at beam element ends. In these shared nodes, all degrees of freedoms are coupled, see Figure 3-5 for a beam model with 3 beam elements and 2 shared nodes. In the figure nodes 2,3 and nodes 4,5 are coupled.

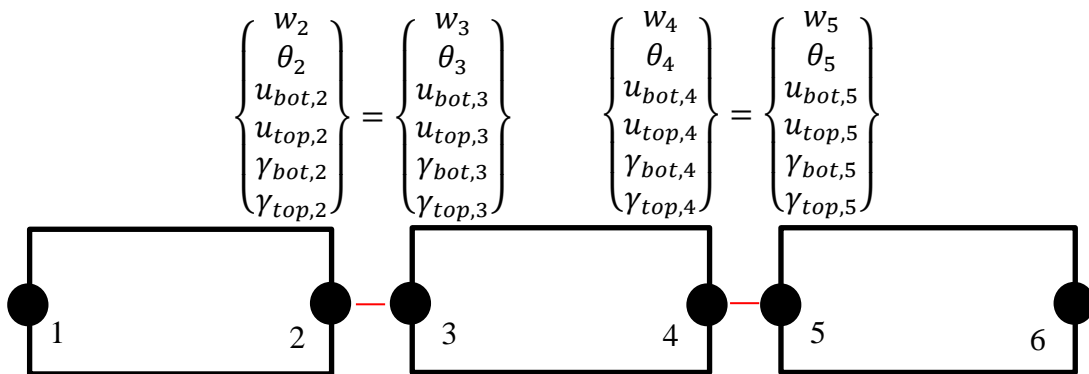


Figure 3-5 Beam element coupling in single layer beam model

Beam model global stiffness matrix is formulated by combining the individual beam element stiffness matrixes. As node coupling is present, adjacent beam element stiffness matrixes are added to the global matrix forming a common part. See Figure 3-6 for global matrix scheme for the beam model depicted in Figure 3-5 where

$k_{n,m}^i$ – 6x6 matrix - beam i stiffness matrix quadrant,

$k_{1,1}^1$	$k_{1,2}^1$	0	0
$k_{2,1}^1$	$k_{2,2}^1 + k_{1,1}^2$	$k_{1,2}^2$	0
0	$k_{2,1}^2$	$k_{2,2}^2 + k_{1,1}^3$	$k_{1,2}^3$
0	0	$k_{2,1}^3$	$k_{2,2}^3$

Figure 3-6 Global stiffness matrix scheme

Global external force vector follows a similar coupling scheme, see Figure 3-7, where external forces acting on coupled nodes are expressed as a common part. f_m^i are forces applied on beam i , node m .

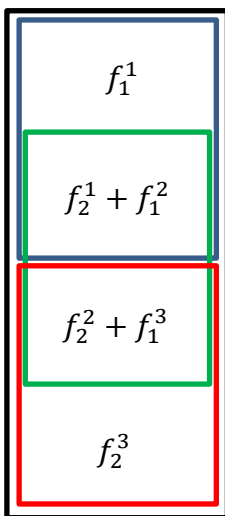


Figure 3-7 Global external force vector scheme

3.4.2 Multiple layer beam model.

In real structures, single layer model has its deficits. For example, structural discontinuities and change in cross-sectional area for beams can not be defined. To evaluate more complex models, multiple layer model is necessary, where geometric parameters can be defined for each layer, discontinuities can be expressed as a nonuniform element configuration.

Figure 3-8 and Figure 3-9 show two types of multiple layer beam models, the former is defined by uniform beam element configuration and the latter is defined by nonuniform beam element configuration.

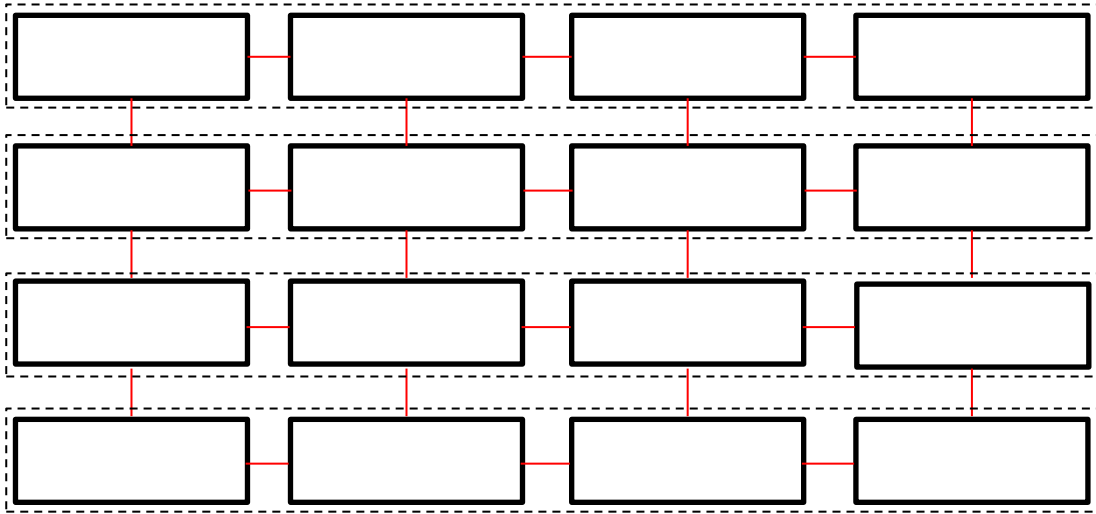


Figure 3-8 Uniform beam model with element coupling and element blocks

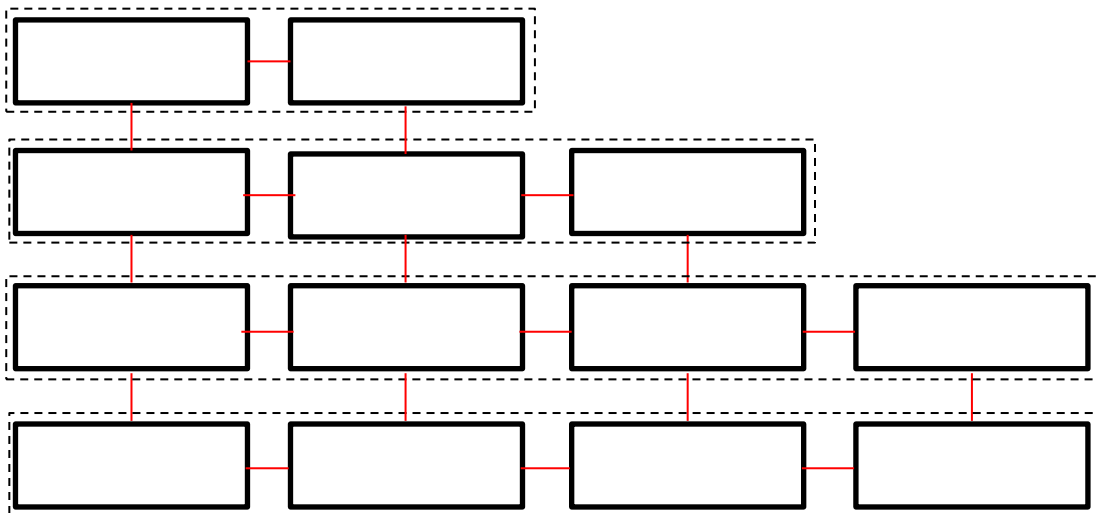


Figure 3-9 Beam model with structural discontinuity, element coupling and element blocks

The primary global stiffness matrix for multiple layer beam model is comprised of individual horizontal beam block stiffness matrixes without vertical coupling. The primary global stiffness matrix follows the scheme shown in Figure 3-10 where,

K_{n_i, m_i}^i – the global stiffness matrix for beam block i ,

$n_i; m_i$ – matrix dimensions.

Matrix dimensions are expressed as

$$n_i = m_i = 6 * n_{nodes_i} \tag{83}$$

where n_{nodes_i} is the number of nodes used to express beam block i .

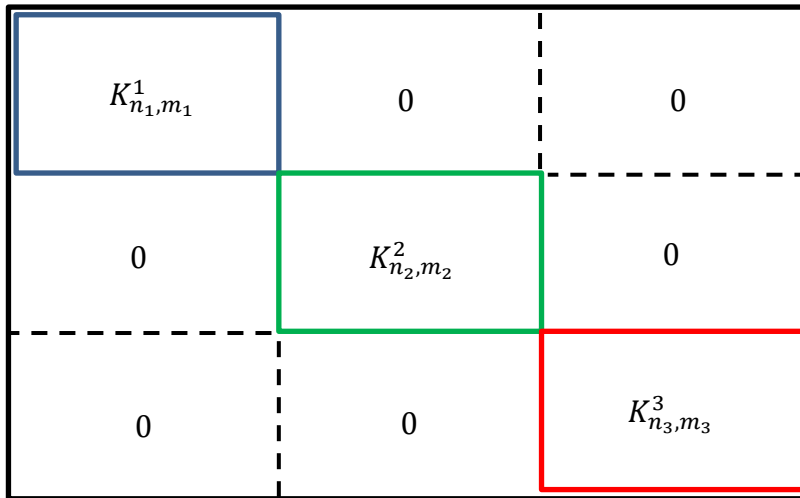


Figure 3-10 Global stiffness matrix scheme without vertical coupling for multiple layer beam model

3.4.3 Vertical coupling of beam elements

In the case of multiple layer beam model, the higher-order shear deformation theory must be able to describe displacements and deformations as continuous throughout the vertical span of the global model. When describing local beam elements, displacements and deformations are defined in a local coordinate system. To keep that definition applicable, the vertical coupling between adjacent elements is introduced by defining a coupling matrix.

Coupling matrix is defined between two vertically adjacent nodes, see Figure 3-11 for vertically coupled beam dimensions.

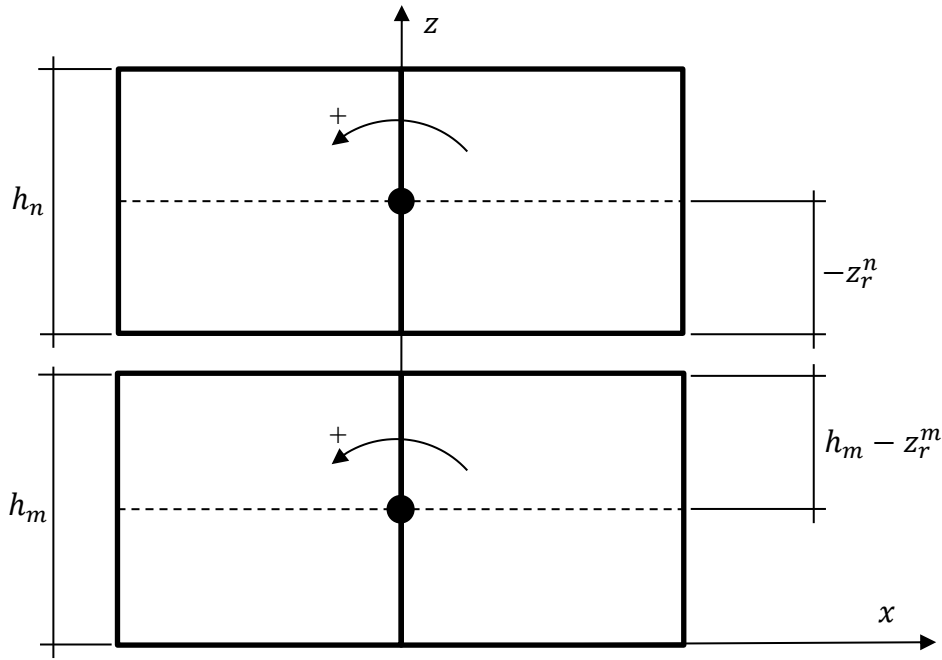


Figure 3-11 Vertically coupled beam dimensions

Total axial displacement is assumed to be continuous over the vertical span of the global model and is described as:

$$u_m(x = 0, z = h_m - z_r^m) = u_n(x = 0, z = -z_r^n) \quad (84)$$

By describing axial displacement in adjacent surfaces using equations (45), (62) and (69) and coordinates described in equation (84), axial displacements for surfaces are:

$$u_m(x = 0, z = h_m - z_{rm}) = -(h_m - z_{rm}) * \theta_1^m + u_{top,1}^m \quad (85)$$

$$u_n(x = 0, z = -z_{rn}) = -(-z_{rn}) * \theta_1^n + u_{bot,1}^n \quad (86)$$

As axial displacement in the described surfaces is only dependant on axial displacement due to shear and rotation of the cross-section, the horizontal coupling can be described in matrix form as:

$$\begin{bmatrix} C_{11} & C_{12} & C_{13} & C_{14} \\ C_{21} & C_{22} & C_{23} & C_{24} \\ C_{31} & C_{32} & C_{33} & C_{34} \\ C_{41} & C_{42} & C_{43} & C_{44} \end{bmatrix} * \begin{Bmatrix} \theta_1^m \\ u_{top,1}^m \\ \theta_1^n \\ u_{bot,1}^n \end{Bmatrix} = \begin{Bmatrix} M_m \\ F_m \\ M_n \\ F_n \end{Bmatrix} \quad (87)$$

Stiffness matrix components are defined by assigning an arbitrary value for one variable, while other variables are 0 and defining internal force and internal moment equations.

Positive force direction aligns with positive x-axis direction while positive rotation direction is defined such that a positive cross-sectional rotation angle would result in positive displacement in the surface according to the equation (85) and (86), see Figure 3-11. Next stiffness matrix components are described:

Positive rotational angle θ_1^m is applied on beam element m , $u_{top,1}^m = u_{bot,1}^n = \theta_1^n = 0$. Beam coupling with the assigned variable is shown in Figure 3-12, where spring element with axial stiffness k_u in beam surface is used to transfer forces between elements.

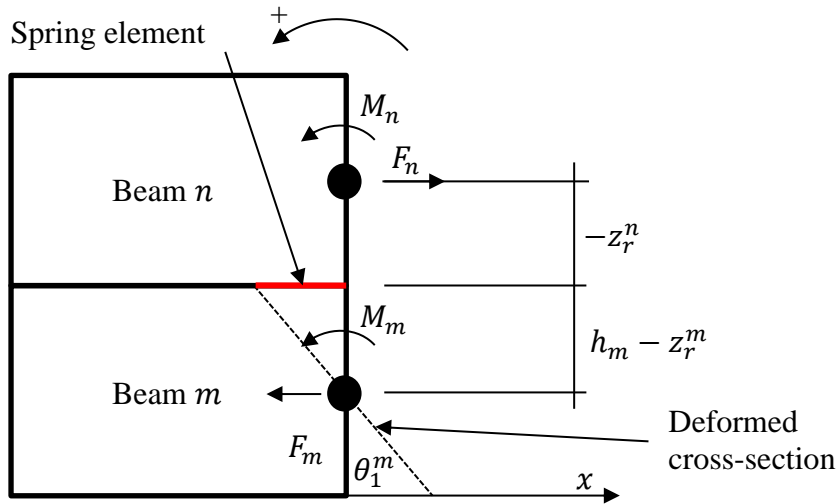


Figure 3-12 Beam coupling with the assigned variable θ_1^m

Internal forces and moments:

$$\begin{aligned}
 M_m &= \theta_1^m * (h^m - z_r^m)^2 k_u \\
 F_m &= \theta_1^m * (h^m - z_r^m)(-k_u) \\
 M_n &= \theta_1^m * (h^m - z_r^m)(-z_r^n)(-k_u) \\
 F_n &= \theta_1^m * (h^m - z_r^m)k_u
 \end{aligned}
 \tag{88}$$

Positive axial displacement $u_{top,1}^m$ is applied on beam element m , $u_{bot,1}^n = \theta_1^m = \theta_1^n = 0$. Beam coupling with the assigned parameter is shown in Figure 3-13.

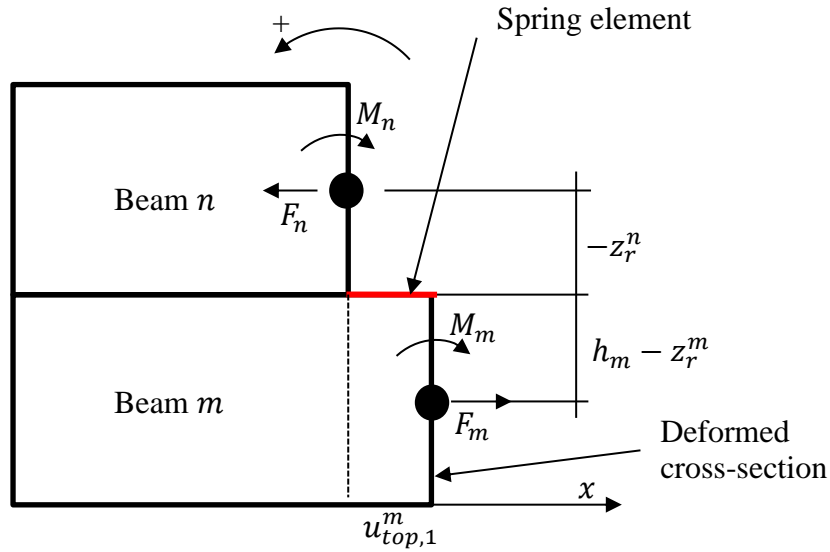


Figure 3-13 Beam coupling with the assigned variable $u_{top,1}^m$

Internal forces and moments:

$$\begin{aligned}
 M_m &= u_{top,1}^m * (h^m - z_r^m)(-k_u) \\
 F_m &= u_{top,1}^m k_u \\
 M_n &= u_{top,1}^m * (-z_r^n)(k_u) \\
 F_n &= u_{top,1}^m (-k_u)
 \end{aligned}
 \tag{89}$$

Positive rotational angle θ_1^n is applied on beam element n , $u_{top,1}^m = u_{bot,1}^n = \theta_1^m = 0$. Beam coupling with the assigned parameter is shown in Figure 3-14.

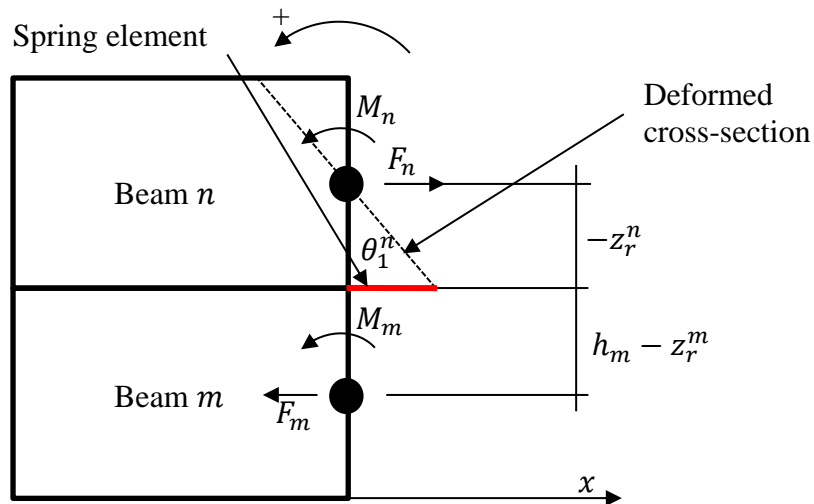


Figure 3-14 Beam coupling with the assigned variable θ_1^n

Internal forces and moments:

$$\begin{aligned}
 M_m &= \theta_1^n (-z_r^n) (h^m - z_r^m) (-k_u) \\
 F_m &= \theta_1^n (-z_r^n) k_u \\
 M_n &= \theta_1^n (-z_r^n)^2 k_u \\
 F_n &= \theta_1^n (-z_r^n) (-k_u)
 \end{aligned} \tag{90}$$

Positive axial displacement $u_{bot,1}^n$ is applied on beam element n, $u_{bot,1}^n = \theta_1^m = \theta_1^n = 0$.

Beam coupling with the assigned parameter is shown in Figure 3-15.

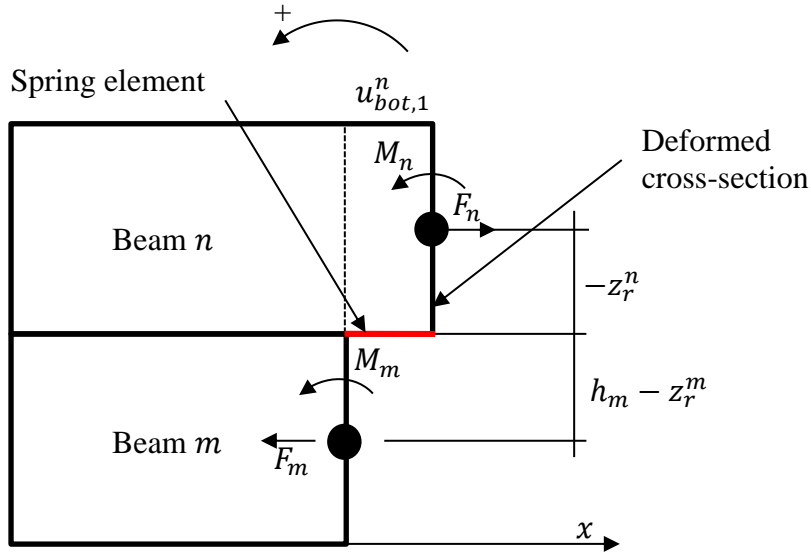


Figure 3-15 Beam coupling with the assigned variable $u_{bot,1}^n$

Internal forces and moments:

$$\begin{aligned}
 M_m &= u_{bot,1}^n (h^m - z_r^m) (k_u) \\
 F_m &= u_{bot,1}^n (-k_u) \\
 M_n &= u_{bot,1}^n (-z_r^n) (-k_u) \\
 F_n &= u_{bot,1}^n (k_u)
 \end{aligned} \tag{91}$$

By replacing equations into the equation, horizontal coupling equations can be written as:

$$\begin{bmatrix}
 (h^m - z_r^m)^2 k_u & (h^m - z_r^m) (-k_u) & (-z_r^n) (h^m - z_r^m) (-k_u) & (h^m - z_r^m) (k_u) \\
 (h^m - z_r^m) (-k_u) & k_u & (-z_r^n) k_u & -k_u \\
 (h^m - z_r^m) z_r^n k_u & -z_r^n k_u & (-z_r^n)^2 k_u & z_r^n k_u \\
 (h^m - z_r^m) k_u & -k_u & z_r^n k_u & k_u
 \end{bmatrix}
 \begin{Bmatrix}
 \theta_1^m \\
 u_{top,1}^m \\
 \theta_1^n \\
 u_{bot,1}^n
 \end{Bmatrix}
 =
 \begin{Bmatrix}
 M_m \\
 F_m \\
 M_n \\
 F_n
 \end{Bmatrix}
 =
 \begin{Bmatrix}
 0 \\
 0 \\
 0 \\
 0
 \end{Bmatrix} \tag{92}$$

Moreover, deflection coupling is defined by assuming equal deflection in vertically coupled beams:

$$w_m(x = 0) = w_n(x = 0) \quad (93)$$

By describing deflection in adjacent beams using equation .. and coordinates described in eq .. deflections for beams are=:

$$w_m(x = 0) = w_1^m \quad (94)$$

$$w_n(x = 0) = w_1^n \quad (95)$$

Deflection coupling can be described in matrix form as:

$$\begin{bmatrix} C_{11} & C_{12} \\ C_{21} & C_{22} \end{bmatrix} * \begin{Bmatrix} w_1^m \\ w_1^n \end{Bmatrix} = \begin{Bmatrix} F_m \\ F_n \end{Bmatrix} \quad (96)$$

Stiffness matrix components are defined with the same method which was applied for axial displacement coupling.

Positive deflection w_1^m is applied on beam element m , deflection in beam element n is assumed to be 0, $w_1^n = 0$. Spring stiffness for deflection coupling is k_w . Beam coupling with the assigned parameter is shown in Figure 3-16.

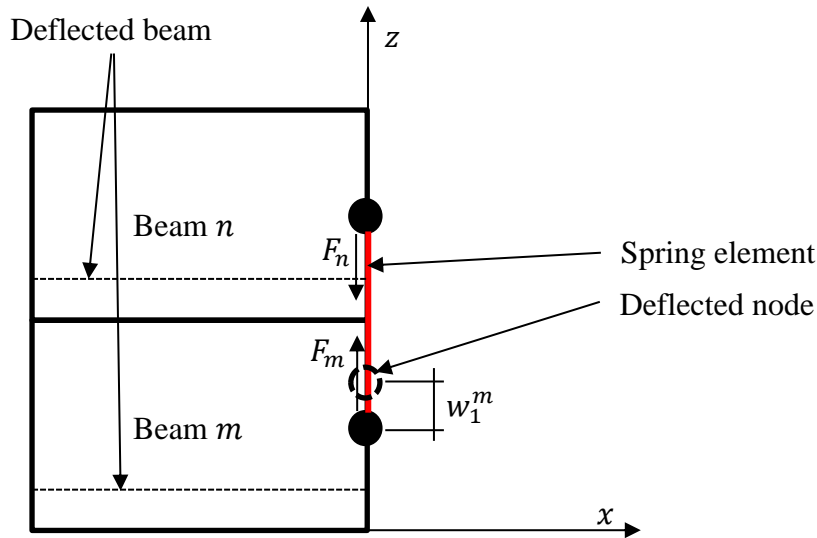


Figure 3-16 Beam coupling with the assigned variable w_1^m

Internal forces and moments:

$$\begin{aligned} F_m &= w_1^m(k_w) \\ F_n &= w_1^m(-k_w) \end{aligned} \quad (97)$$

Positive deflection w_1^n is applied on beam element n , deflection in beam element m is assumed to be 0, $w_1^m = 0$. Beam coupling with the assigned parameter is shown in Figure 3-17.

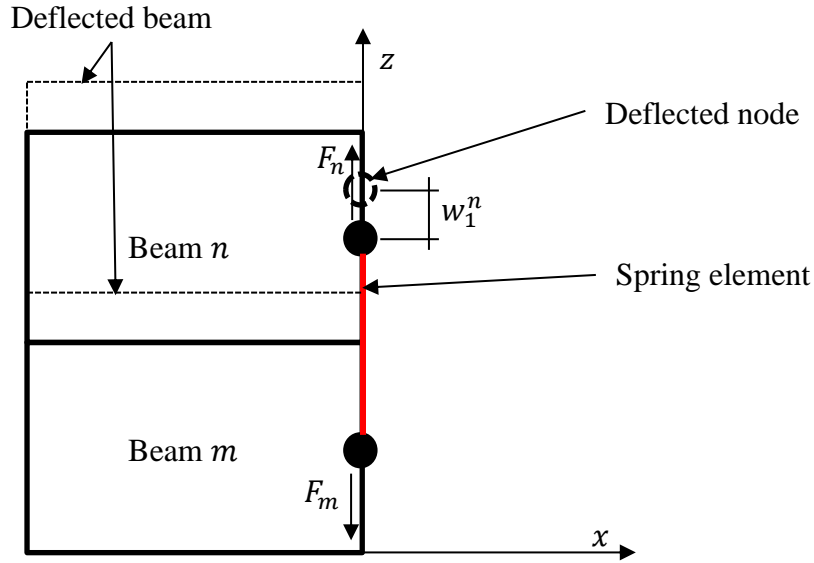


Figure 3-17 Beam coupling with the assigned variable w_1^n

Internal forces and moments:

$$\begin{aligned} F_m &= w_1^n (-k_w) \\ F_n &= w_1^n (k_w) \end{aligned} \quad (98)$$

By replacing equations into the equation, horizontal coupling equations can be written as:

$$\begin{bmatrix} k_w & -k_w \\ -k_w & k_w \end{bmatrix} * \begin{Bmatrix} w_1^m \\ w_1^n \end{Bmatrix} = \begin{Bmatrix} F_m \\ F_n \end{Bmatrix} = \begin{Bmatrix} 0 \\ 0 \end{Bmatrix} \quad (99)$$

Complete coupling matrix is defined using equations... and placing stiffness components in their respective locations. Coupling matrix becomes:

$$K_c = \begin{bmatrix} k_w & 0 & 0 & 0 & 0 & 0 & 0 \\ 0 & (h^m - z_r^m)^2 k_u & 0 & (h^m - z_r^m)(-k_u) & 0 & 0 & 0 \\ 0 & 0 & 0 & 0 & 0 & 0 & 0 \\ 0 & (h^m - z_r^m)(-k_u) & 0 & k_u & 0 & 0 & 0 \\ 0 & 0 & 0 & 0 & 0 & 0 & 0 \\ 0 & 0 & 0 & 0 & 0 & 0 & 0 \\ -k_w & 0 & 0 & 0 & 0 & 0 & 0 \dots \\ 0 & (h^m - z_r^m)z_r^n k_u & 0 & -z_r^n k_u & 0 & 0 & 0 \\ 0 & (h^m - z_r^m)k_u & 0 & -k_u & 0 & 0 & 0 \\ 0 & 0 & 0 & 0 & 0 & 0 & 0 \\ 0 & 0 & 0 & 0 & 0 & 0 & 0 \\ 0 & 0 & 0 & 0 & 0 & 0 & 0 \\ 0 & 0 & 0 & 0 & 0 & 0 & 0 \end{bmatrix} \quad (100)$$

$$\begin{bmatrix}
-k_w & 0 & 0 & 0 & 0 & 0 \\
0 & (z_r^n)(h^m - z_r^m)(k_u) & (h^m - z_r^m)(k_u) & 0 & 0 & 0 \\
0 & 0 & 0 & 0 & 0 & 0 \\
0 & (-z_r^n)k_u & -k_u & 0 & 0 & 0 \\
0 & 0 & 0 & 0 & 0 & 0 \\
\dots & 0 & 0 & 0 & 0 & 0 \\
k_w & 0 & 0 & 0 & 0 & 0 \\
0 & (-z_r^n)^2 k_u & z_r^n k_u & 0 & 0 & 0 \\
0 & z_r^n k_u & k_u & 0 & 0 & 0 \\
0 & 0 & 0 & 0 & 0 & 0 \\
0 & 0 & 0 & 0 & 0 & 0 \\
0 & 0 & 0 & 0 & 0 & 0
\end{bmatrix}$$

Coupling matrix stiffness values k_u, k_w, k_y are arbitrary if the requirement $K_{c_{i,j}} \gg K_{gl_{m,n}}$ is achieved. $K_{c_{i,j}}$ is coupling matrix stiffness component value and $K_{gl_{m,n}}$ is global beam stiffness component value, where the coupling is defined. Coupling scheme example is shown in Figure 3-18 for beam model two vertically coupled elements, where $k_{c_{i,j}}^n$ is coupling matrix 6x6 quadrant for coupled node pair n .

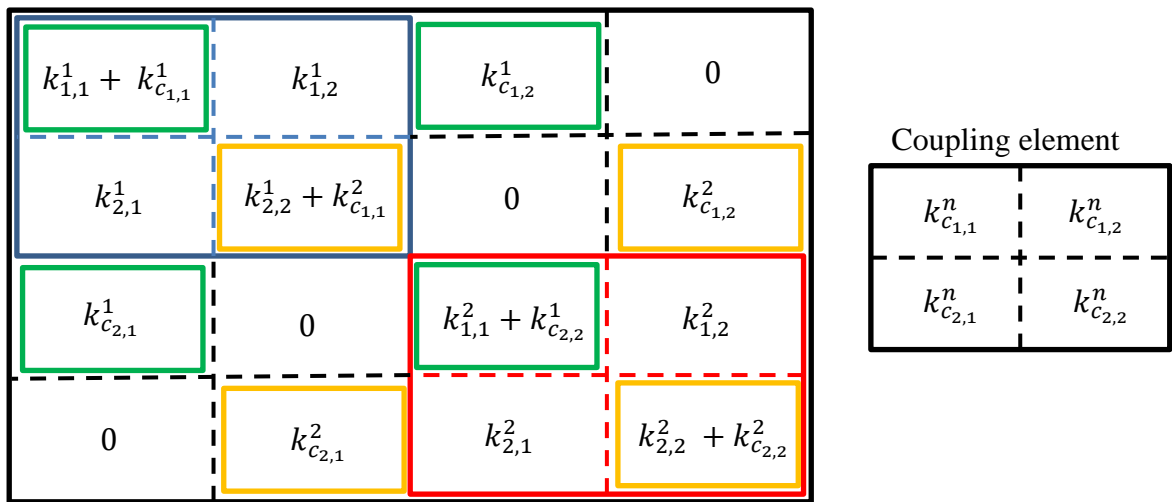


Figure 3-18 Vertical coupling scheme

4 Case studies

4.1 Comparative calculation of refined shear deformation theory and FE-modelling

4.1.1 Models used for comparative analysis

A comparative analysis was carried out by evaluating the analytical axial displacement and shear deformation values of the refined shear deformation theory by Ghugal and Sharma [28] and FE-model. A selection of rectangular beam, I-beam cross-sections and T-beam cross-sections were analysed to illustrate the range of application of the refined shear deformation theory. Cross-sections with dimensions are presented in Appendix C .

4.1.2 Cantilever beam under uniform distributed load

Analytical equations for cantilever beam with uniformly distributed load were provided by Ghugal and Sharma [28], where equations for cross-section rotation function $\phi(x)$, transverse displacement $w(x)$ and first derivative of transverse displacement dw/dx are obtained from general governing equations (38) and (40):

$$\phi(x) = \frac{qL}{\beta EI_y} \left[\frac{\cosh(\lambda x)}{\cosh(\lambda L)} - \frac{\sinh(\lambda L - \lambda x)}{\lambda L \cosh(\lambda L)} - \frac{x}{L} \right], \quad (101)$$

$$w(x) = \frac{qL^4}{24EI_y} \left(\frac{x^4}{L^4} - 4\frac{x}{L} + 3 \right) + \frac{3qL^2}{5GA} \left[1 - \frac{x^2}{L^2} - \frac{2(\sinh(\lambda L) - \sinh(\lambda x))}{\lambda L \cosh(\lambda L)} + \frac{2\cosh(\lambda(L-x))}{(\lambda L)^2 \cosh(\lambda L)} \right], \quad (102)$$

$$\frac{dw(x)}{dx} = \frac{qL^4}{24EI_y} \left(\frac{4x^3}{L^4} - \frac{4}{L} \right) + \frac{3qL^2}{5GA} \left[\frac{2\cosh(\lambda x)}{L \cosh(\lambda L)} - \frac{2x}{L^2} - \frac{2\sinh(\lambda(L-x))}{L^2 \lambda \cosh(\lambda L)} \right] \quad (103)$$

Axial displacement formula is obtained by substituting equation (103) into equation (25).

Shear deformation formula is obtained by substituting equation (103) into equation (28).

4.1.3 Results and analysis

Results of comparative analysis of refined shear deformation theory and FE calculations are described in. Range of cross-sections is described in Appendix C .

Results for a wide range of beam cross-sections show that the refined shear deformation theory is a well-designed tool to assess axial displacement in beams, where the cross-section is symmetrical with respect to the reference line. Shear deformation, however, is only comparable in the beams with prismatic cross-section. For I-beams, the discrepancies between analytical and FE results of shear deformations differentiated greater as the ratio between flange width and web thickness grew.

It is also evident that the refined shear deformation theory is only applicable for assessing beams with a vertically applied load. This suggests that shear strain must equal zero on the top and bottom surface of the beam.

4.2 Higher-order shear deformation theory comparative calculations

Validation of the higher-order shear deformation theory is carried out by comparing the analytical results with a selection of simple beam models. The applicative quality of the theory is explained with several variable comparisons.

4.2.1 Models used for analysis

To illustrate the possible application of the developed higher-order shear theory in ship global strength analysis, simple ship models are used for comparison. Toming et al. [27] introduced three plate models, which emulated a longitudinal ship structure. In this thesis, case A and B from the article are emulated.

Case A model consists of three vertically adjacent plate sections, each with dimensions 60x3 m. FE-model consists of 6000 plate elements with dimensions of 300x300 mm. An elastic foundation is used as boundary conditions. See Figure 4-1 for Case A model.

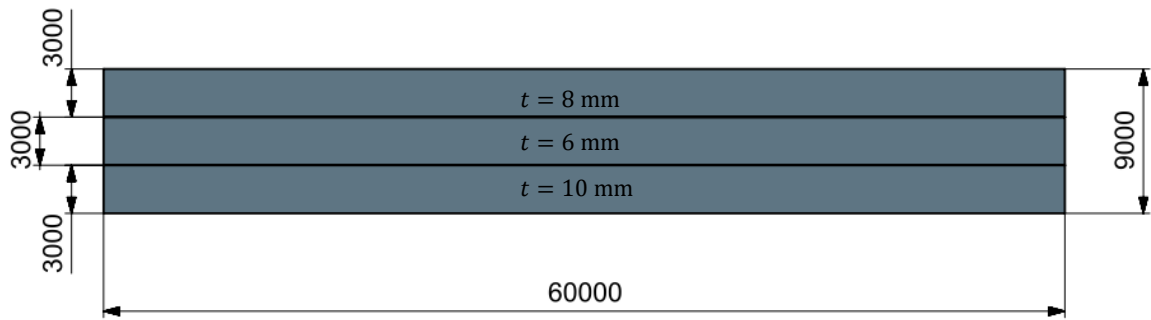


Figure 4-1 Case A FE plate model

Case B model consists of three vertically adjacent plate sections with varying dimensions. FE-model consists of 4000 plate elements with dimensions of 300x300 mm. An elastic foundation is used as boundary conditions. See Figure 4-2 for Case B model.

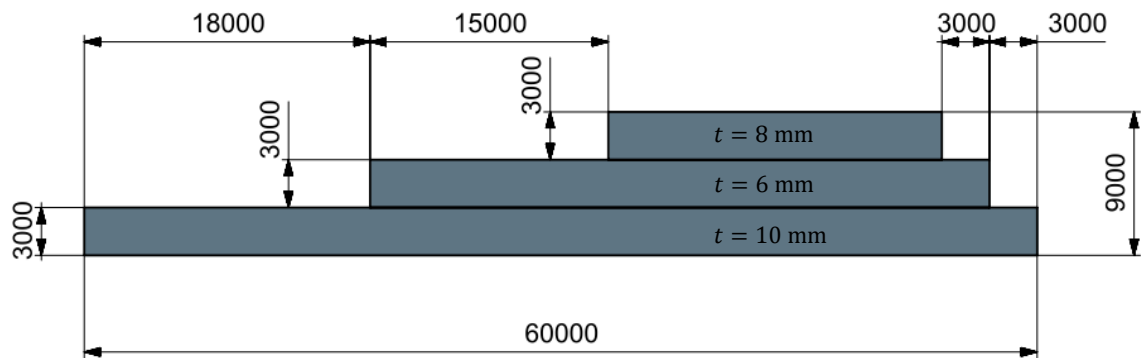


Figure 4-2 Case B FE plate model

Beam element models for higher-order shear deformation calculations use identical global models to FE-models, where the total length of the ship is divided into 60 beam elements. Case A beam element model has equal 60 elements in all three beam sections with identical thicknesses to FE model, see Figure 4-3. Case B beam element model has 60 elements in the bottom section, 39 elements in the middle section and 21 elements in the top section, see Figure 4-4, where longitudinally shown boxes identify a set of three beam elements. Beam elements are coupled using vertical and horizontal coupling schemes shown in Figure 3-6 and Figure 3-18.

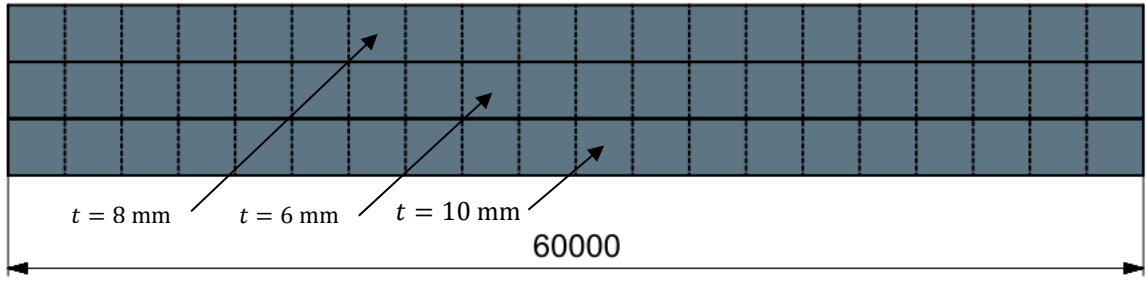


Figure 4-3 Case A HOSDT model

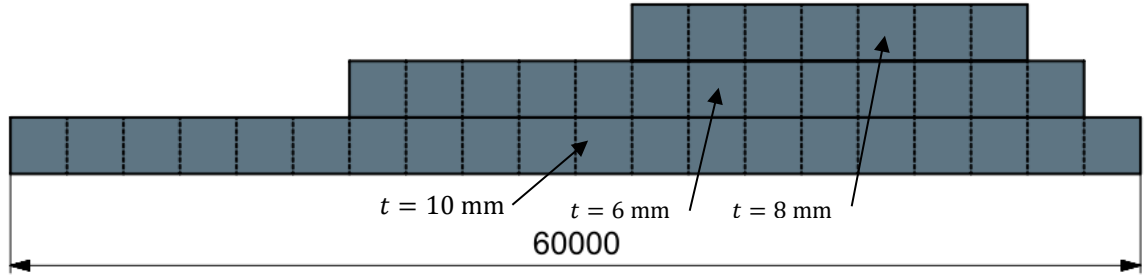


Figure 4-4 Case B HOSDT model

Identical material properties for Young's modulus and Poisson's ratio are used for HOSDT calculations and FE-modelling respectively as:

$$E = 210 \text{ GPa,}$$

$$\nu = 0.3.$$

4.2.2 Loading

Identical sinusoidal loading is used for both calculation models. The longitudinally distributed vertical loading is applied on the bottom surface of the models and is calculated as:

$$p(x) = p_0 * \cos\left(\frac{2\pi x}{L}\right), \quad (104)$$

where

p_0 – load amplitude, $p_0 = 60 \text{ N/mm}$,

L – total length of the model

Loading curve is seen in Figure 4-5.

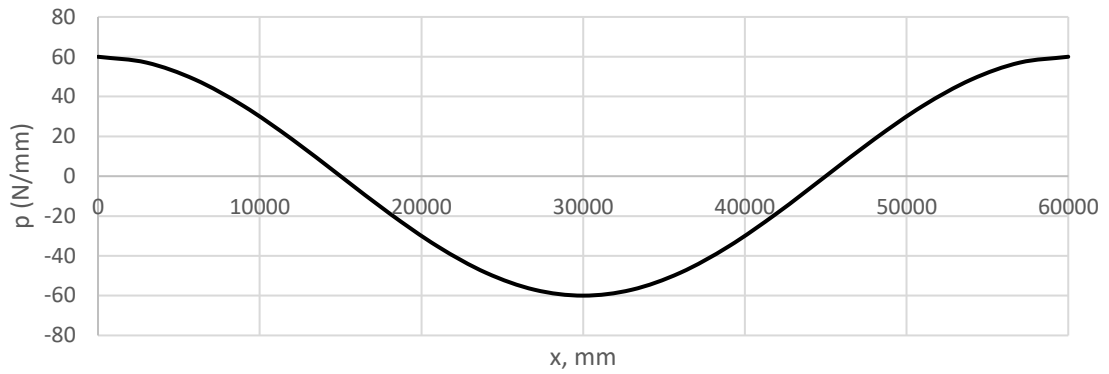


Figure 4-5 Distributed loading curve

4.2.3 Calculation cases

Two separate cross-sections are analysed for case A and case B model, which provides a wider look into beam model behaviour. In case A the global model consists of identical vertical beam sections and cross-section discontinuities do not occur. Thus, axial displacements, normal stresses and shear stresses are evaluated close to quarter-length and half-length of the ship, more specifically at locations $x = 0.225 * L$; $x = 0.475 * L$. In case B structural discontinuities are defined. Calculations at cross-sections $x = 0.575 * L$, $x = 0.625 * L$ and $x = 0.725 * L$ illustrate the effect of nonhomogeneous horizontal beam sections on displacements and stresses. See Figure 4-6 for calculation cross-sections.

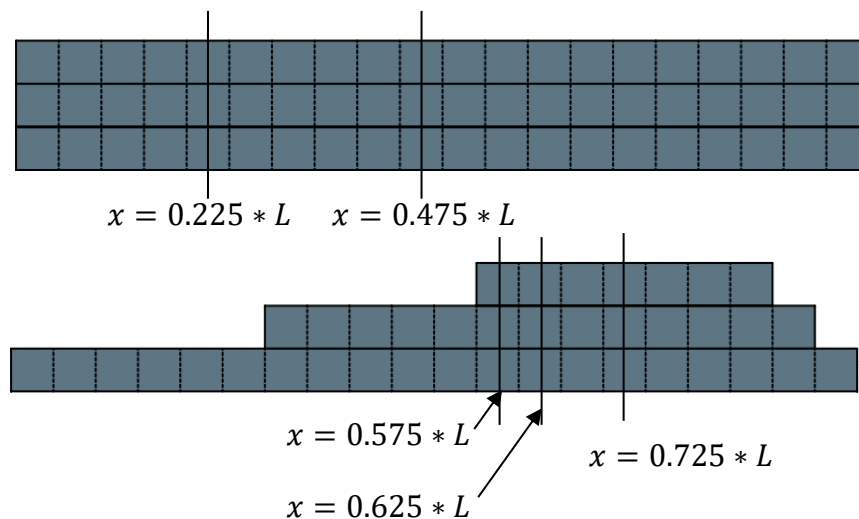


Figure 4-6 Calculation cross-section for beam models

5 Higher-order shear deformation theory calculation results and discussion

This chapter presents the results of comparative analyses for case A and case B beam models. A selection of displacement and stress variables are plotted for HOSDT and FEM calculations in the model cross-sections shown in Figure 4-6. The coincidence between the two methods is discussed to reflect the range of real-life practical use of the developed beam theory. Further work with the beam theory is also discussed.

5.1 Case A results

Comparative results for deflection is presented in Figure 5-1. The figure shows a good coincidence of deflection between two methods.

The difference between analytical and numerical deflection results in the ends of the beam make up 2% at $x = 0$ mm, about 4% at $x = 60000$ mm and about 0.4% at $x = 30000$ mm of the deflection amplitude calculated with numerical methods.

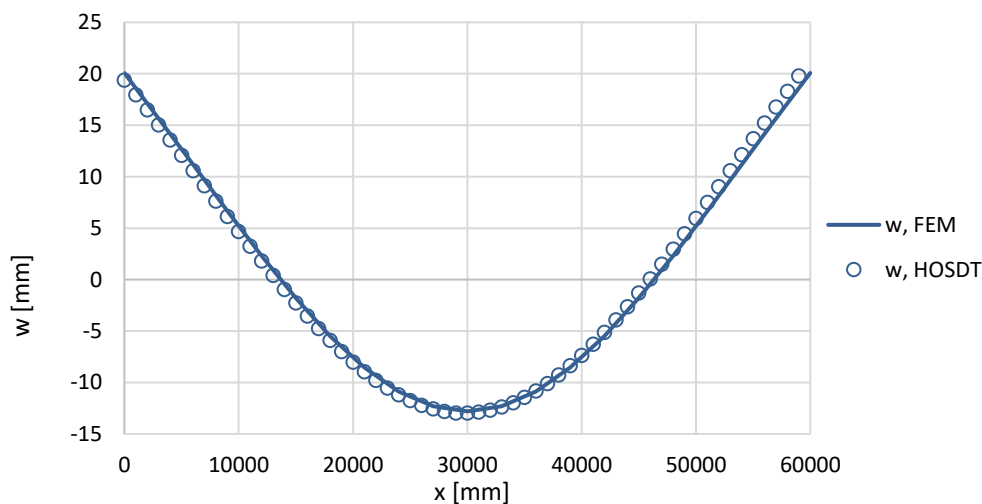


Figure 5-1 Case A deflection comparison

Comparative results for axial displacement vertical distribution is presented in Figure 5-2. The figure shows good coincidence of axial displacement between two methods in both calculation cross-sections.

The difference between analytical and numerical axial displacements results in the top and bottom surfaces of the beam make up 0.3% and 0.5% respectively at $x = 0.225L$ and about

10.9% and 9% respectively at $x = 0.475L$ of the axial displacement amplitude calculated with numerical methods for the cross-section.

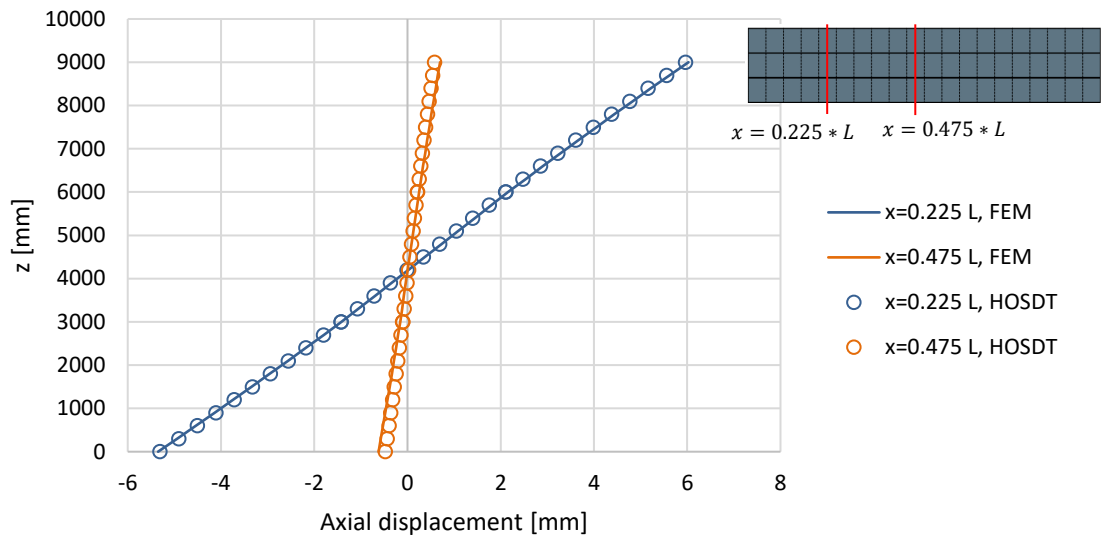


Figure 5-2 Case A axial displacement comparison

Comparative calculation results for normal stress vertical distribution is presented in Figure 5-3. The figure shows good coincidence of normal stress between two methods in both calculation cross-sections.

The difference between analytical and numerical normal stress results in the top and bottom surfaces of the beam makes up 1.2% and 1.3% respectively at $x = 0.225L$ and about 0.5% and 0.7% respectively at $x = 0.475L$ of the normal stress amplitude calculated with numerical methods for the cross-sections.

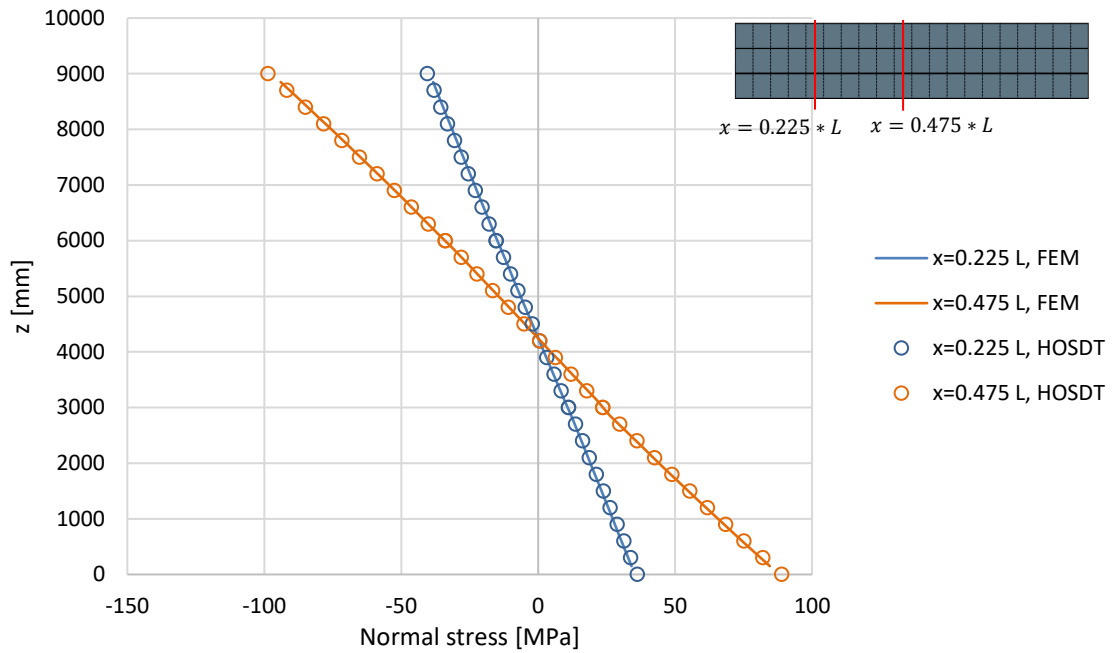


Figure 5-3 Case A normal stress comparison

Comparative calculation results for shear stress vertical distribution is presented in Figure 5-4. The figure shows good coincidence of shear stress between two methods in both calculation cross-sections.

The difference between analytical and numerical shear stress results in the middle layer, at $z = 4500$ mm makes up 0.8% at $x = 0.225L$ and about 9.0% at $x = 0.475L$ of the shear stress amplitude calculated with numerical methods for the cross-sections.

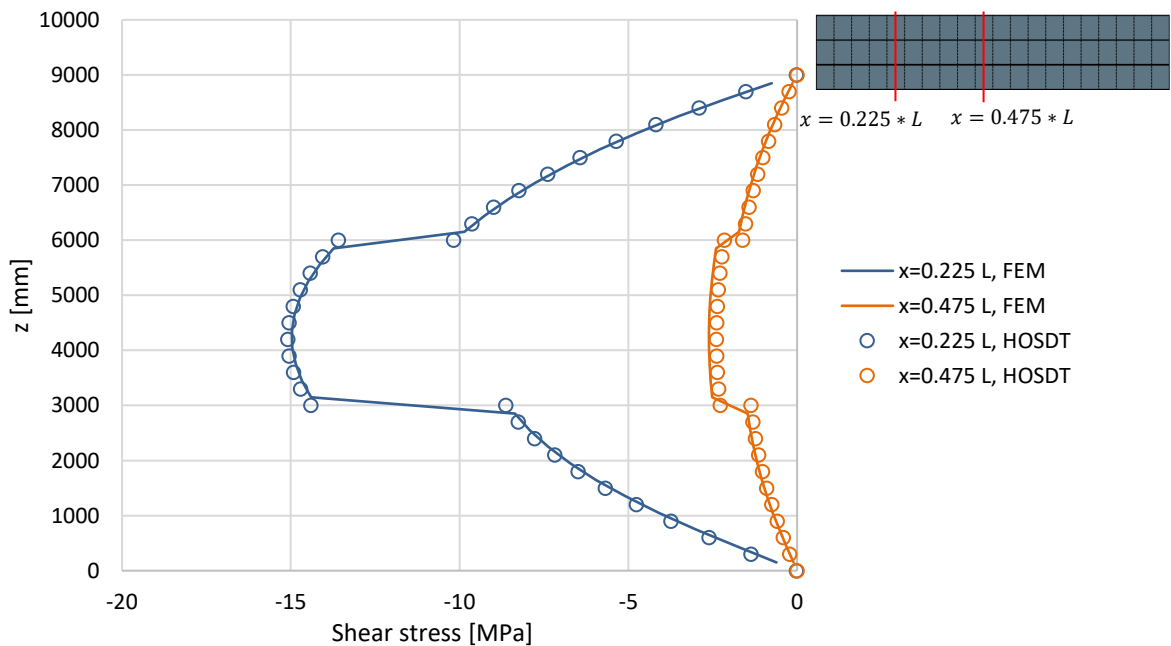


Figure 5-4 Case A shear stress comparison

5.2 Case B results

Comparative results for deflection is presented in Figure 5-5. The figure shows good coincidence between FEM and analytical results.

The difference between analytical and numerical deflection results in the ends of the beam make up 5.2% at $x = 0$ mm, about 0.1% at $x = 60000$ mm and about 0.2% at $x = 24000$ mm of the deflection amplitude calculated with numerical methods.

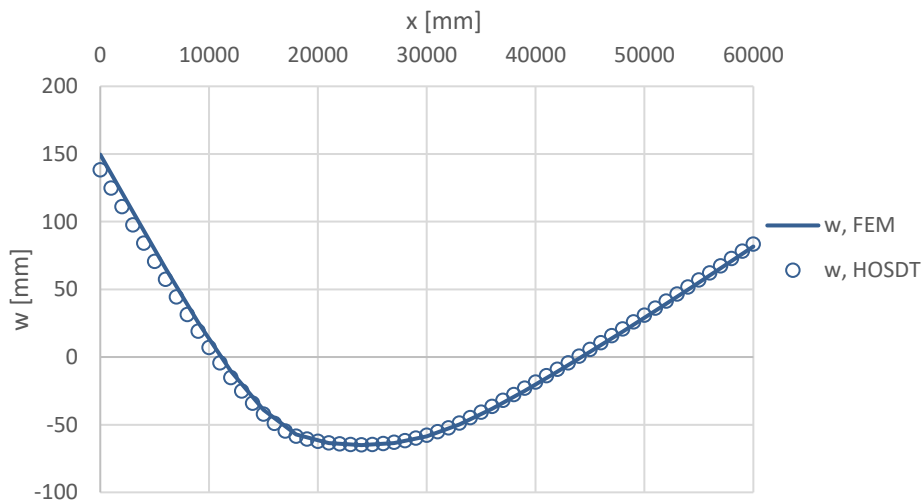


Figure 5-5 Case B deflection comparison

Comparative results for axial displacement vertical distribution is presented in Figure 5-6. The figure shows a good coincidence of axial displacement in all calculation cross-sections. The difference between analytical and numerical axial displacements results in the top and bottom surfaces of the beam make up 0.1% and 0.5% respectively at $x = 0.575L$, about 0.3% and 0.5% respectively at $x = 0.625L$ and about 0.4% and 0.7% respectively at $x = 0.725L$ of the axial displacement amplitude calculated with numerical methods for the cross-sections.

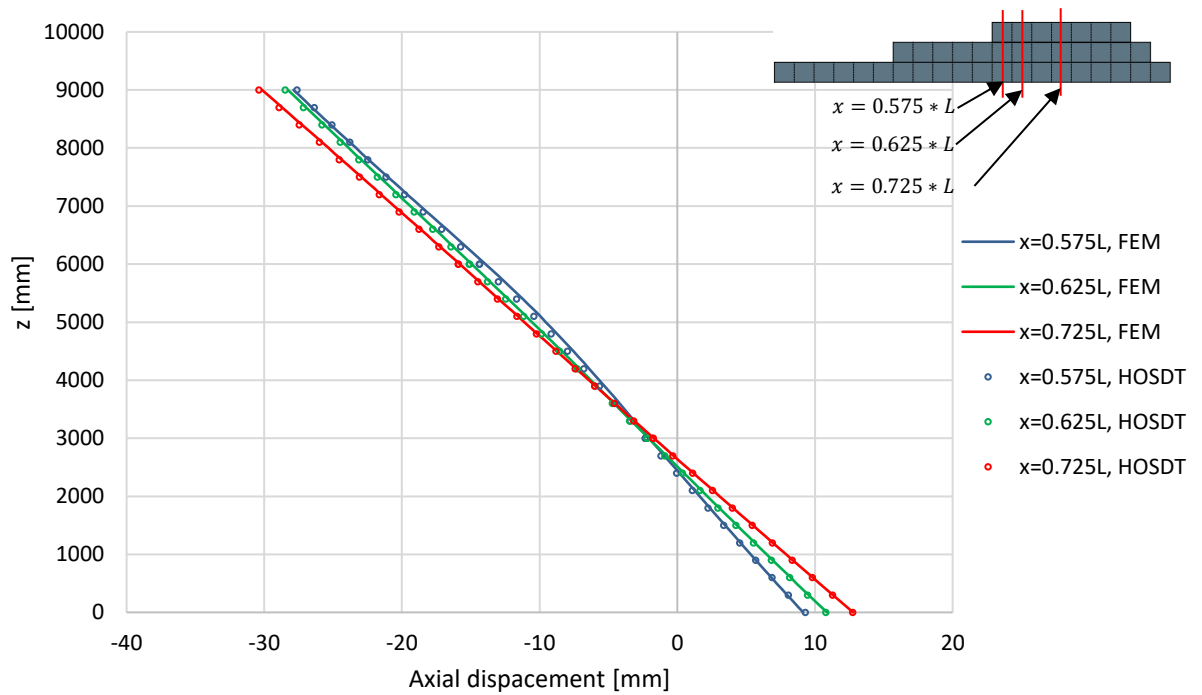


Figure 5-6 Case B axial displacement comparison

Comparative calculation results for normal stress vertical distribution is presented in Figure 5-7. The figure shows good coincidence of normal stress in two calculation cross-sections furthest away from discontinuities. In cross-section at $x = 0.575L$, where structural discontinuities have a significant effect, the HOSDT shows good ability to assess the overall vertical distribution of normal stresses but underestimates peak stress values. Also, the calculation cannot assess stresses in the top layer of the global mode close to discontinuities. It can be seen that for $x = 0.575L$ cross-section, numerical normal stresses are close to 0 at the top layer. This is due to free corners not being subjected to compression.

The difference between analytical and numerical normal stress results in the top and bottom surfaces of the beam makes up 3.3% and 1.6% respectively at $x = 0.725L$, about 3.8% and 7.2% respectively at $x = 0.625L$ of the normal stress amplitude calculated with numerical methods for the cross-sections.

In the cross-section closest to discontinuities at $x = 0.575L$ difference between analytical and numerical results makes up 8.6% in the bottom surface, 10.2% at $z = 5400$ mm and 19.6% in the top surface, of the numerically calculated normal stress amplitude for these cross-sections. These large differences show that the HOSDT is not able to assess vertical stress distribution in regions close to discontinuities.

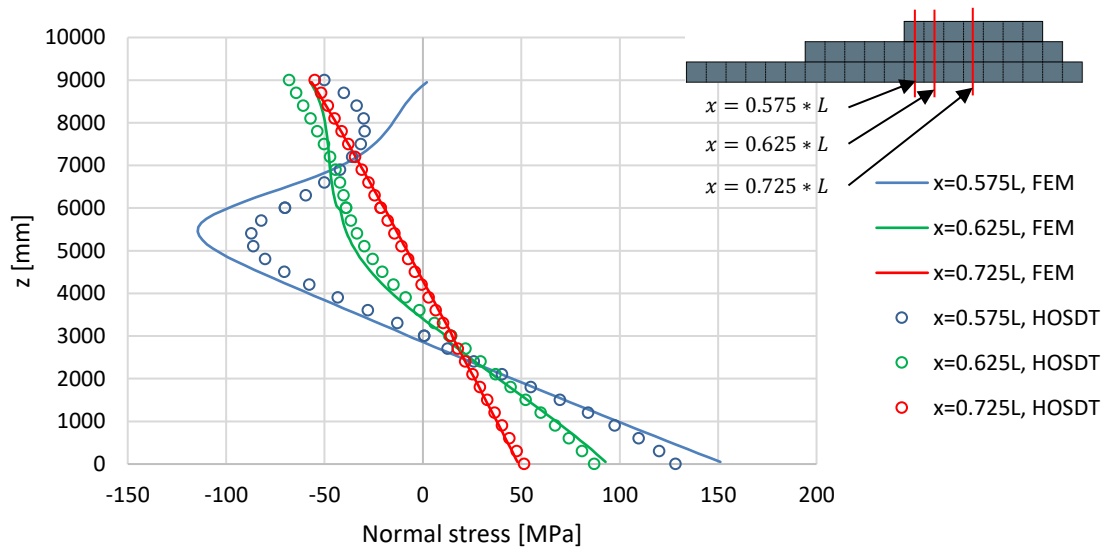


Figure 5-7 Case B normal stress comparison

Comparative calculation results for shear stress vertical distribution is presented in Figure 5-4. The figure shows good coincidence on shear stress overall, however small discrepancies occur due to the varying beam thicknesses. In cross-section at $x = 0.725L$, where the effects of noncontinuous beam section are negligible, shear stress vertical distribution shows good coincidence. In cross-section at $x = 0.575L, x = 0.625L$ where discontinuities have greater effect, the figure shows good coincidence in the vertical distribution of shear stress.

In the cross-section at $x = 0.725L$ the difference between analytical and numerical shear stress results in the middle layer, at $z = 4500$ mm makes up 0.1% of the shear stress amplitude calculated with numerical methods for the cross-section.

In cross-section at $x = 0.625L$, the maximum difference between analytical and numerical shear stress makes up 14.4% at $z = 1500$ mm and 20,7% at $z = 7500$ mm of the shear stress amplitude.

In cross-section at $x = 0.527L$, the maximum difference between analytical and numerical shear stress makes up 5.7% at $z = 2100$ mm and 9% at $z = 6500$ mm of the shear stress amplitude.

m

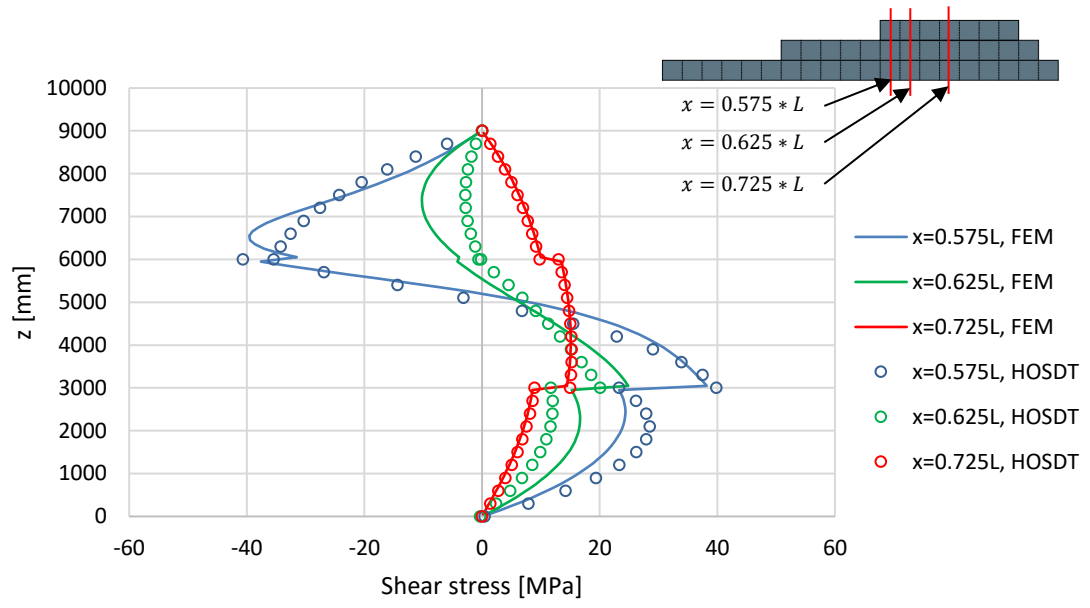


Figure 5-8 Case B shear stress comparison

6 Further work on the topic

In this thesis, comparative calculations included simple beam models, which roughly describe ships longitudinal structural unit. The models used solely vertical loading, which in most cases is not realistic when it comes to assessing loads acting on a ship at sea. This raises the need for further work to be done in this field. The higher-order shear deformation theory provides the ability to apply different loading cases, as the external work matrix presented in chapter 3.3 contains not only vertical loading components but also components to describe shear loads and load-induced moments. During the development, shear loading was investigated to ensure the holistic behaviour of the beam theory, but no results are presented to express that. Further work on the topic would likely include a more complex external loading on the beams, where distributed vertical and horizontal forces are combined.

In terms of ship structural strength analysis, more realistic models could be used. For example, ship sections, where vertical structures are coupled with horizontal deck structures using coupling schemes provided in this thesis could be investigated. This would provide feedback on whether this method is sufficiently time-saving to prefer it to for example FE-modelling.

It would also be beneficial to explore additional boundary conditions for defined parameters and the capabilities of finer meshing in the areas of discontinuous structures. Shear stress and normal stress analysis results presented in chapter 5.2 showed discrepancies due to local discontinuities. In the case of smaller HOSDT beam element dimensions and more accurate definition of boundary conditions, these deficiencies in global models could be neglected. Finer meshing would also be beneficial in models where openings in structures are investigated.

7 Conclusions

This thesis aimed to define a beam theory which would improve the coupled beam method introduced by Naar et al [1] by further developing the description of displacement and stress distributions in an arbitrary cross-section of a beam model. In addition to the single element definition, the coupling of elements was necessary to the holistic behaviour of this theory, as it aimed to define variables as continuous functions over the whole cross-section of a global model. This was achieved by defining 6 degrees of freedom for both beam element nodes:

- deflection at reference line,
- rotation of cross-section at reference line,
- axial displacement due to shear at a beam bottom surface,
- axial displacement due to shear at a beam top surface,
- shear deformation at a beam bottom surface,
- shear deformation at a beam top surface.

Vertical continuity of displacements and stresses was achieved by defining a coupling element, which rigidly connected deflection of vertically adjacent nodes as well as total axial displacement of adjacent beam surfaces.

The developed theory was tested on a selection of two simple beam models. Case A represented a vertically segmented beam with homogenous beam element configuration. Case B represented a beam model where the vertical beam segments varied in length providing an opportunity to assess the capabilities of the developed theory in regions, where structural discontinuities have a local effect on global displacements and stresses.

Beam models were subjected to sinusoidal vertical distributed loading. An elastic foundation was used as boundaries for the models.

Comparative calculations were performed using FE-modelling and analytical results. Selection of parameters was described:

- deflection in the bottom surface over the length of the beam model,
- axial displacement in a cross-section over the vertical span of the beam model,
- normal stress in a cross-section over the vertical span of the beam model,
- shear stress in a cross-section over the vertical span of the beam model.

Calculation cross-sections were chosen so that in case A, results close to half-length and quarter-length of the beam model were described. In case B calculation cross-sections were chosen so that local effects could be described in a cross-section close to structural discontinuity and further away.

The developed beam theory proved to have highly coincident results to FE-modelling in case A for a homogenous structure. For case B the results were highly coincident in the cross-section further away from discontinuities. In the region closer to the discontinuities the theory proved to provide overall good coincidence of results, however, due to local effects, normal stress and shear stress results had discrepancies.

Peak normal stress values were underestimated by up to 10.2% and in the top surface up to 19.6% of the normal stress amplitude in the cross-section. In the region, where discontinuities do not have an effect, differences in normal stress values stay below 4% of the normal stress amplitude.

Peak shear stress values in the cross-sections closer to the discontinuities showed a maximum difference between numerical and analytical results up to 20% of the shear stress amplitude. In the region, where discontinuities do not have an effect, differences in shear stress values stay below 9% of the shear stress amplitude.

Figure 7-1 and Figure 7-2 show the deficiency of the coupled beam theory on a vertical normal stress distribution graph presented by Toming et al [28]. Black projection lines have been added to the graph to illustrate discontinuous calculation results. Figure 7-3 and Figure 7-4 show corresponding results for the HOSDT.

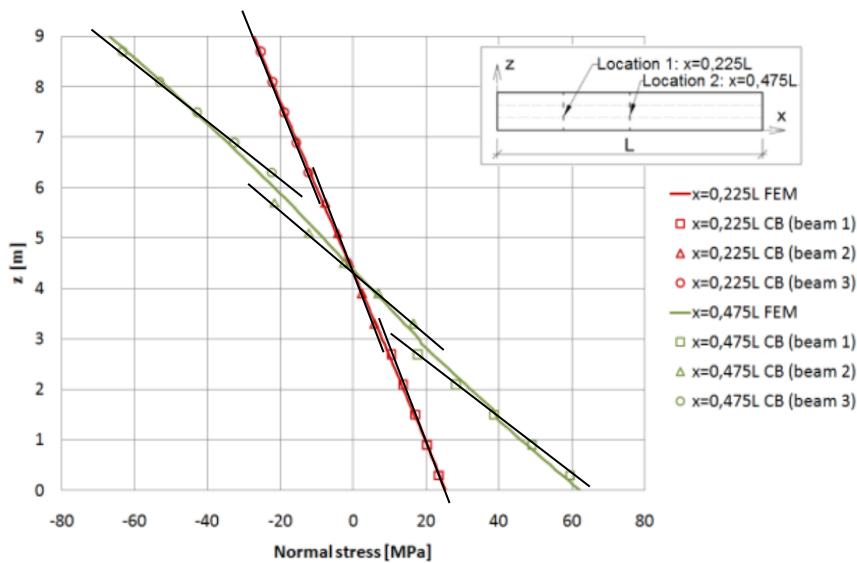


Figure 7-1 Vertical normal stress distribution in case A beam model [28]

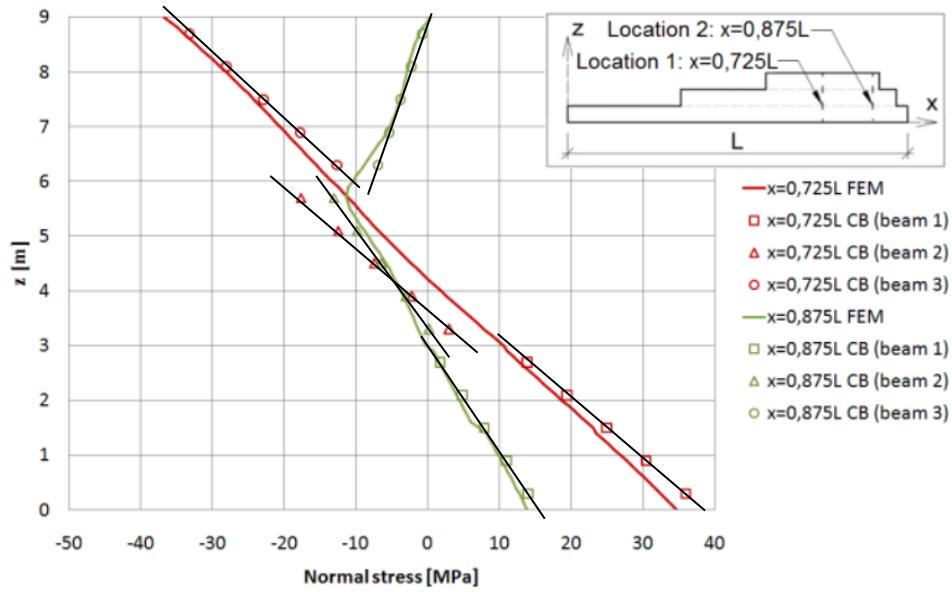


Figure 7-2 Vertical normal stress distribution in case B beam model [28]

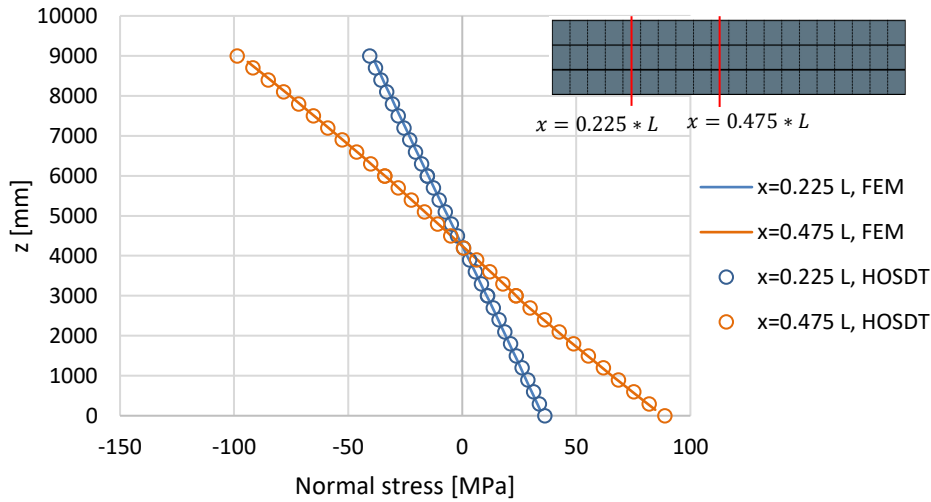


Figure 7-3 Case A normal stress distribution

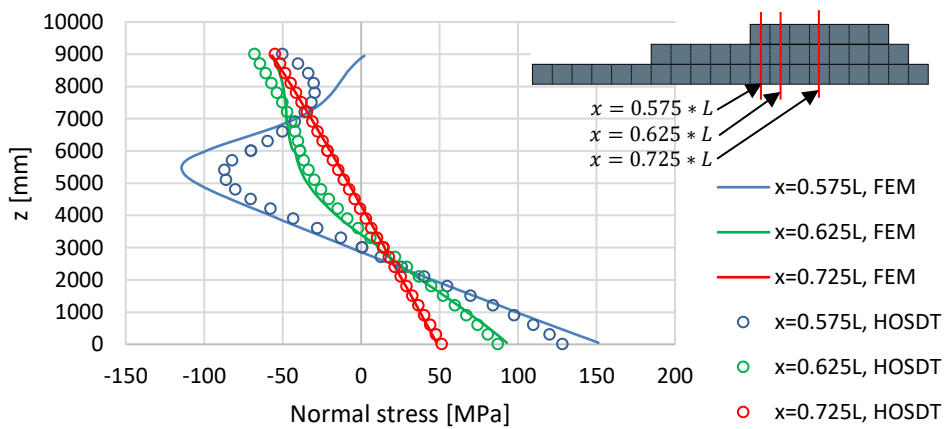


Figure 7-4 Case B normal stress distribution

Broadly the theory proved to be a good tool to assess thick beam behaviour in simple models. The quality of results for analyses with more complicated models is dependant on the beam element size and boundary conditions for defined parameters. Further work is needed to be done to ensure the effectiveness of the presented theory when assessing more complex structures and loadings.

8 Kokkuvõte (conclusions in Estonian)

Käesoleva lõputöö eesmärgiks on talateooria defineerimine, mis arendaks edasi P. Sc. Hendrik Naari poolt esitatud seotud talade meetodit [1]. Töö defineerib uut tüüpi talaelemendi, millega on võimalik hinnata kirjeldatavaid parameetreid vabalt valitud talaelemendi läbilõikes ning esitada tulemused pidevate jaotustena. Lõputöö keskendub lisaks talaelemendi ka elementide siduvuse defineerimisele, mis on vajalik mitmest elemendireast koosnevate talamudelite analüüsimisel. Uudset tüüpi 2D talaelemendil on defineeritud järgmised vabadusastmed:

- Läbipaine referentsjoonel
- Rislõike pööre referentsjoonel
- Lõikest tingitud pikisiire alumisel pinnal
- Lõikest tingitud pikisiire ülemisel pinnal
- Lõike deformatsioon alumisel pinnal
- Lõike deformatsioon ülemisel pinnal

Siirete ning pingete kõrgussuunaline jätkuvuse võimaldamiseks talamudeli ristlõikes on defineeritud siduvuselement, kasutades eeldusi, et kogu pikisiire kõrvuti asuvates pindades ning läbipaine vertikaalselt kõrvuti paiknevates sõlmedes on võrdsed.

Võrdlusanalüüsiks on esitatud kaks lihtsat talamudelit. Mudel A kasutab kolme identset talaelementide kihti, mis on ühendatud, kasutades siduvuselemente. Mudel B kasutab kolme talaelementide kihti, mis on ebaühtlase elementide paigutusega, võimaldades uurida teooria rakenduslikku võimet piirkondades, kus struktuuri ebaühtlustel on suur mõju globaalsetele pingetele.

Talamudelitele on võrdlusanalüüsis rakendatud identset sinusoidaalset vertikaalset jaotatud koormust. Rajatingimustena on mõlema mudeli puhul kasutatud elastset vundamenti.

Lõplike elementide meetodi ja talateooria tulemuste võrdlusanalüüsis on esitatud tulemused järgmistele parameetritele:

- Läbipainde tala pikkusesuunaline jaotus globaalse mudeli alumisel pinnal
- Kogu pikisiirde jaotus valitud ristlõigetes
- Normaalpinge jaotus valitud ristlõikes
- Lõikepinge jaotus valitud ristlõikes

Analüüsitavad ristlõiked mudelis A valiti kõige optimaalselt iseloomustama käitumisi kogu tala ulatuses. Esimene ristlõige asetseb talamudeli esimese veerandi lähistel ning teine ristlõige talamudeli poole pikkuse lähistel. Ristlõiked mudelis B valiti iseloomustama ebaühtluste lokaalseid mõjusid.

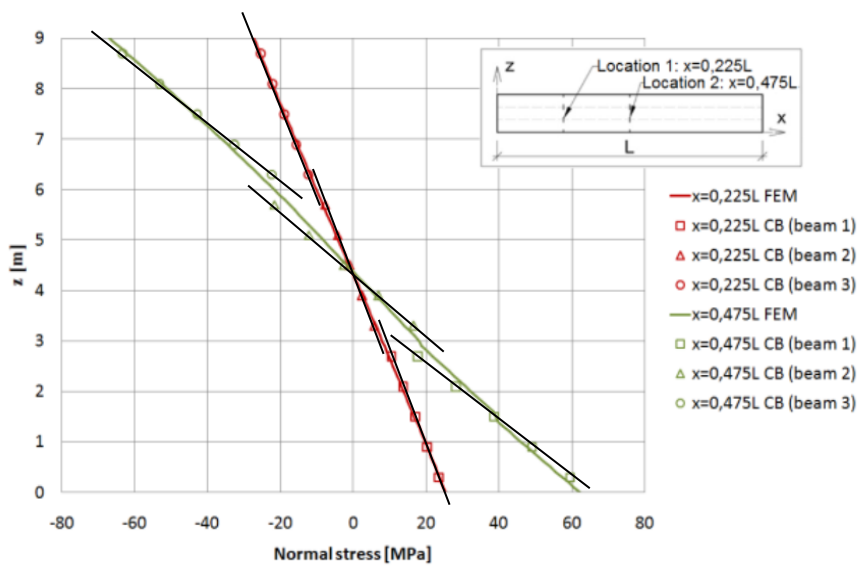
Võrdlusanalüüsi tulemused näitavad, et mudeli A puhul analüütiliselt iseloomustatud parameetrid langevad kokku lõplike elementide meetodi tulemustega. Mudeli B puhul olid tulemused kokkulangevad ristlõikes, kus lokaalsed mõjud puuduvad. Ristlõigetes, mis asusid lokaalsete mõjude piirkonnas on siirde jaotused kõrge kokkulangevusega, kuid pingeaotustes esines erinevusi. Talateooriaga arvatud maksimaalsed pingeväärtused osutusid lõplike elementide meetodi tulemustest väiksemateks ning normaalpingeväärtused vabadel pindadel erinesid lõplike elementide meetodi tulemustest.

Arvutuste tulemustest selgus, et maksimaalsed normaalpinge väärtuste erinevused moodustasid kuni 10.2% ja normaalpinge väärtuste erinevused tala ülemises pinnas moodustasid kuni 19.6% kogu normaalpinge amplituudist vaadeldavas ristlõikes. Ristlõigetes, kus geomeetria katkevused lokaalseid mõjusid pingetele ei tekita, erinesid normaalpinge väärtused maksimaalselt kuni 4% kogu normaalpinge amplituudist ristlõikes.

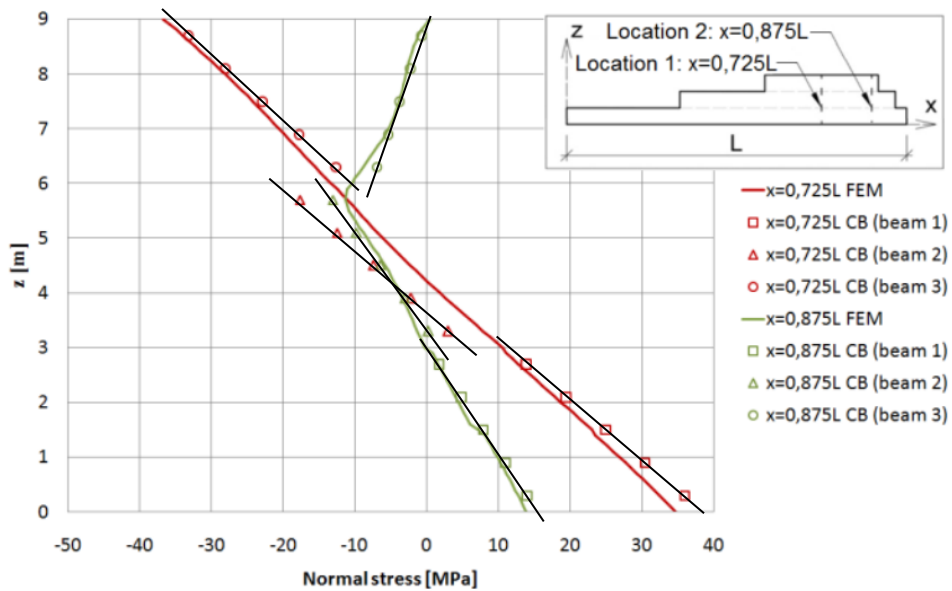
Piirkonnas, kus geomeetria katkevustel on suur mõju moodustasid maksimaalsed lõikepinge väärtuste erinevused kuni 20% lõikepinge amplituudist vaadeldavas ristlõikes. Piirkondades, kus lokaalseid mõjusid ei esine jäid lõikepingete erinevused alla 9% kogu lõikepinge amplituudist vaadeldavas ristlõikes.

Joonis 8-1 ja Joonis 8-2, mille esitas Toming [28], illustreerivad seotud talade meetodi puudujääke, mille puhul pingete vertikaalset jaotust ei ole võimalik kirjeldada ühtlaselt. Joonistele on lisatud mustad projektsioonjooned, et rõhutada pingeväärtuste katkevusi.

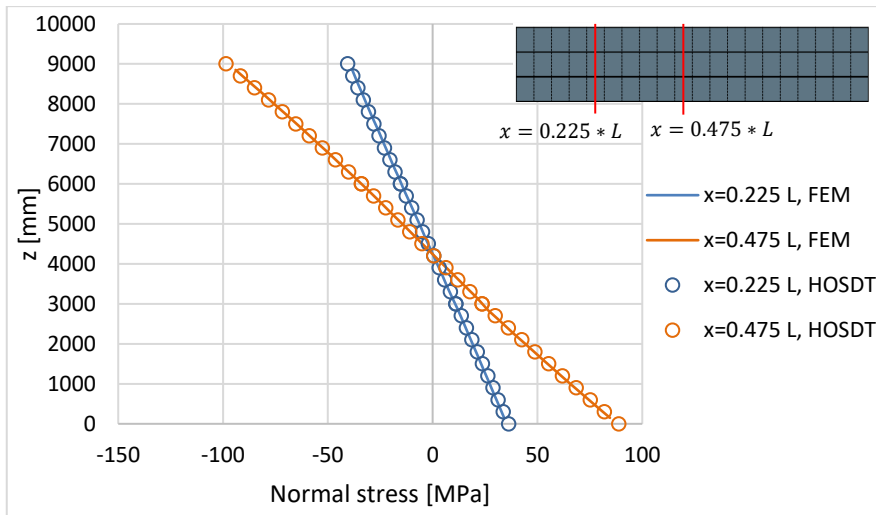
Joonis 8-3 ja Joonis 8-4 näitavad vastavaid tulemusi kõrgemat järku lõike deformatsiooniga teooria kohta.



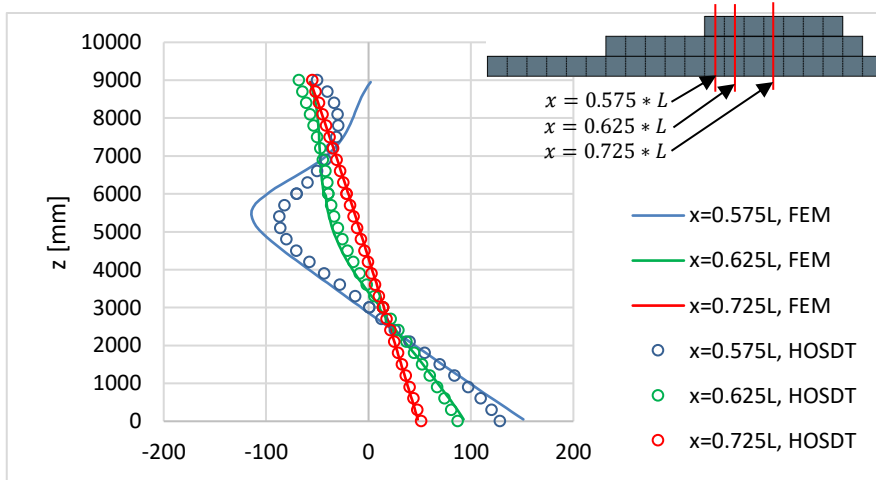
Joonis 8-1 Mudeli A normaalpinge jaotus ritlõigetes[28]



Joonis 8-2 Mudeli B normaalpinge jaotus ristlõigetes [28]



Joonis 8-3 Mudeli A normaalpinge jaotus ristlõikes



Joonis 8-4 Mudeli B normaalpinge jaotus ristlõikes

Kokkuvõtvalt osutus esitatud teooria hästi töötavaks meetodiks kõrgete talade hindamiseks lihtsates mudelites. Tulemuste kvaliteet keerulisemates mudelites sõltub kasutatava tala elemendi suuruselt ning rajatingimuste definitsioonist. Teooria nõuab edasist tööd, et tagada usaldusväärsed tulemused keerulisemate talamudelite ja koormuste rakendamisel.

Appendix A

Shear deformation theory potential energy partial derivative equations:

$$\begin{aligned} \frac{\partial \Pi}{\partial w_1} = \int_0^L \int_A E \left(-z \frac{\partial^2 \xi_1}{\partial x^2} w_1 - z \frac{\partial^2 \xi_2}{\partial x^2} \theta_1 - z \frac{\partial^2 \xi_3}{\partial x^2} w_2 - z \frac{\partial^2 \xi_4}{\partial x^2} \theta_2 + \right. \\ \left. \psi_1 \frac{\partial \phi_1}{\partial x} u_{bot,1} + \psi_2 \frac{\partial \phi_1}{\partial x} u_{top,1} + \psi_3 \frac{\partial \phi_1}{\partial x} \gamma_{bot,1} + \psi_4 \frac{\partial \phi_1}{\partial x} \gamma_{top,1} + \right. \\ \left. \psi_1 \frac{\partial \phi_2}{\partial x} u_{bot,2} + \psi_2 \frac{\partial \phi_2}{\partial x} u_{top,2} + \psi_3 \frac{\partial \phi_2}{\partial x} \gamma_{bot,2} + \psi_4 \frac{\partial \phi_2}{\partial x} \gamma_{top,2} \right) * \\ \left(-z \frac{\partial^2 \xi_1}{\partial x^2} \right) dAdx - \int_0^L p_z \xi_1 dx = 0 \end{aligned} \quad (105)$$

$$\begin{aligned} \frac{\partial \Pi}{\partial \theta_1} = \int_0^L \int_A E \left(-z \frac{\partial^2 \xi_1}{\partial x^2} w_1 - z \frac{\partial^2 \xi_2}{\partial x^2} \theta_1 - z \frac{\partial^2 \xi_3}{\partial x^2} w_2 - z \frac{\partial^2 \xi_4}{\partial x^2} \theta_2 + \right. \\ \left. \psi_1 \frac{\partial \phi_1}{\partial x} u_{bot,1} + \psi_2 \frac{\partial \phi_1}{\partial x} u_{top,1} + \psi_3 \frac{\partial \phi_1}{\partial x} \gamma_{bot,1} + \psi_4 \frac{\partial \phi_1}{\partial x} \gamma_{top,1} + \right. \\ \left. \psi_1 \frac{\partial \phi_2}{\partial x} u_{bot,2} + \psi_2 \frac{\partial \phi_2}{\partial x} u_{top,2} + \psi_3 \frac{\partial \phi_2}{\partial x} \gamma_{bot,2} + \psi_4 \frac{\partial \phi_2}{\partial x} \gamma_{top,2} \right) * \\ \left(-z \frac{\partial^2 \xi_2}{\partial x^2} \right) dAdx - \int_0^L p_z \xi_2 dx - \int_0^L s_{bot} z_r d\xi_2 dx + \int_0^L s_{top} (h - \\ z_r) d\xi_2 dx = 0 \end{aligned} \quad (106)$$

$$\begin{aligned} \frac{\partial \Pi}{\partial w_2} = \int_0^L \int_A E \left(-z \frac{\partial^2 \xi_1}{\partial x^2} w_1 - z \frac{\partial^2 \xi_2}{\partial x^2} \theta_1 - z \frac{\partial^2 \xi_3}{\partial x^2} w_2 - z \frac{\partial^2 \xi_4}{\partial x^2} \theta_2 + \right. \\ \left. \psi_1 \frac{\partial \phi_1}{\partial x} u_{bot,1} + \psi_2 \frac{\partial \phi_1}{\partial x} u_{top,1} + \psi_3 \frac{\partial \phi_1}{\partial x} \gamma_{bot,1} + \psi_4 \frac{\partial \phi_1}{\partial x} \gamma_{top,1} + \right. \\ \left. \psi_1 \frac{\partial \phi_2}{\partial x} u_{bot,2} + \psi_2 \frac{\partial \phi_2}{\partial x} u_{top,2} + \psi_3 \frac{\partial \phi_2}{\partial x} \gamma_{bot,2} + \right. \\ \left. \psi_4 \frac{\partial \phi_2}{\partial x} \gamma_{top,2} \right) \left(-z \frac{\partial^2 \xi_3}{\partial x^2} \right) dAdx - \int_0^L p_z \xi_3 dx = 0 \end{aligned} \quad (107)$$

$$\begin{aligned} \frac{\partial \Pi}{\partial \theta_2} = \int_0^L \int_A E \left(-z \frac{\partial^2 \xi_1}{\partial x^2} w_1 - z \frac{\partial^2 \xi_2}{\partial x^2} \theta_1 - z \frac{\partial^2 \xi_3}{\partial x^2} w_2 - z \frac{\partial^2 \xi_4}{\partial x^2} \theta_2 + \right. \\ \left. \psi_1 \frac{\partial \phi_1}{\partial x} u_{bot,1} + \psi_2 \frac{\partial \phi_1}{\partial x} u_{top,1} + \psi_3 \frac{\partial \phi_1}{\partial x} \gamma_{bot,1} + \psi_4 \frac{\partial \phi_1}{\partial x} \gamma_{top,1} + \right. \\ \left. \psi_1 \frac{\partial \phi_2}{\partial x} u_{bot,2} + \psi_2 \frac{\partial \phi_2}{\partial x} u_{top,2} + \psi_3 \frac{\partial \phi_2}{\partial x} \gamma_{bot,2} + \right. \\ \left. \psi_4 \frac{\partial \phi_2}{\partial x} \gamma_{top,2} \right) \left(-z \frac{\partial^2 \xi_4}{\partial x^2} \right) dAdx - \int_0^L p_z \xi_4 dx - \int_0^L s_{bot} z_r d\xi_4 dx + \\ \int_0^L s_{top} (h - z_r) d\xi_4 dx = 0 \end{aligned} \quad (108)$$

$$\begin{aligned} \frac{\partial \Pi}{\partial u_{bot,1}} = \int_0^L \int_A E \left(-z \frac{\partial^2 \xi_1}{\partial x^2} w_1 - z \frac{\partial^2 \xi_2}{\partial x^2} \theta_1 - z \frac{\partial^2 \xi_3}{\partial x^2} w_2 - z \frac{\partial^2 \xi_4}{\partial x^2} \theta_2 + \right. \\ \left. \psi_1 \frac{\partial \phi_1}{\partial x} u_{bot,1} + \psi_2 \frac{\partial \phi_1}{\partial x} u_{top,1} + \psi_3 \frac{\partial \phi_1}{\partial x} \gamma_{bot,1} + \psi_4 \frac{\partial \phi_1}{\partial x} \gamma_{top,1} + \right. \\ \left. \psi_1 \frac{\partial \phi_2}{\partial x} u_{bot,2} + \psi_2 \frac{\partial \phi_2}{\partial x} u_{top,2} + \psi_3 \frac{\partial \phi_2}{\partial x} \gamma_{bot,2} + \right. \\ \left. \psi_4 \frac{\partial \phi_2}{\partial x} \gamma_{top,2} \right) \left(-z \frac{\partial^2 \xi_1}{\partial x^2} \right) dAdx - \int_0^L p_z \xi_1 dx = 0 \end{aligned} \quad (109)$$

$$\begin{aligned}
\frac{\partial \Pi}{\partial \gamma_{top,2}} &= \int_0^L \int_A E \left(-z \frac{\partial^2 \xi_1}{\partial x^2} w_1 - z \frac{\partial^2 \xi_2}{\partial x^2} \theta_1 - z \frac{\partial^2 \xi_3}{\partial x^2} w_2 - z \frac{\partial^2 \xi_4}{\partial x^2} \theta_2 + \right. \\
&\psi_1 \frac{\partial \phi_1}{\partial x} u_{bot,1} + \psi_2 \frac{\partial \phi_1}{\partial x} u_{top,1} + \psi_3 \frac{\partial \phi_1}{\partial x} \gamma_{bot,1} + \psi_4 \frac{\partial \phi_1}{\partial x} \gamma_{top,1} + \\
&\psi_1 \frac{\partial \phi_2}{\partial x} u_{bot,2} + \psi_2 \frac{\partial \phi_2}{\partial x} u_{top,2} + \psi_3 \frac{\partial \phi_2}{\partial x} \gamma_{bot,2} + \\
&\left. \psi_4 \frac{\partial \phi_2}{\partial x} \gamma_{top,2} \right) \left(\psi_4 \frac{\partial \phi_2}{\partial x} \right) dAdx + \int_0^L \int_A G \left(\frac{\partial \psi_1}{\partial z} \phi_1 u_{bot,1} + \frac{\partial \psi_2}{\partial z} \phi_1 u_{top,1} + \right. \\
&\frac{\partial \psi_3}{\partial z} \phi_1 \gamma_{bot,1} + \frac{\partial \psi_4}{\partial z} \phi_1 \gamma_{top,1} + \frac{\partial \psi_1}{\partial z} \phi_2 u_{bot,2} + \frac{\partial \psi_2}{\partial z} \phi_2 u_{top,2} + \\
&\left. \frac{\partial \psi_3}{\partial z} \phi_2 \gamma_{bot,2} + \frac{\partial \psi_4}{\partial z} \phi_2 \gamma_{top,2} \right) \left(\frac{\partial \psi_4}{\partial z} \phi_2 \right) dAdx - \int_0^L s_1 \psi_4 \phi_2 dx - \\
&\int_0^L s_2 \psi_4 \phi_2 dx = 0
\end{aligned} \tag{116}$$

Appendix B

Shear deformation theory variational multipliers used in the stiffness matrix:

$$k_1 = -z \frac{\partial^2 \xi_1}{\partial x^2} \quad (117)$$

$$k_2 = -z \frac{\partial^2 \xi_2}{\partial x^2} \quad (118)$$

$$k_3 = \psi_1 \frac{\partial \phi_1}{\partial x} \quad (119)$$

$$k_4 = \psi_2 \frac{\partial \phi_1}{\partial x} \quad (120)$$

$$k_5 = \psi_3 \frac{\partial \phi_1}{\partial x} \quad (121)$$

$$k_6 = \psi_4 \frac{\partial \phi_1}{\partial x} \quad (122)$$

$$k_7 = -z \frac{\partial^2 \xi_3}{\partial x^2} \quad (123)$$

$$k_8 = -z \frac{\partial^2 \xi_4}{\partial x^2} \quad (124)$$

$$k_9 = \psi_1 \frac{\partial \phi_2}{\partial x} \quad (125)$$

$$k_{10} = \psi_2 \frac{\partial \phi_2}{\partial x} \quad (126)$$

$$k_{11} = \psi_3 \frac{\partial \phi_2}{\partial x} \quad (127)$$

$$k_{12} = \psi_4 \frac{\partial \phi_2}{\partial x} \quad (128)$$

$$k_{13} = \frac{\partial \psi_1}{\partial z} \phi_1 \quad (129)$$

$$k_{14} = \frac{\partial \psi_2}{\partial z} \phi_1 \quad (130)$$

$$k_{15} = \frac{\partial \psi_3}{\partial z} \phi_1 \quad (131)$$

$$k_{16} = \frac{\partial \psi_4}{\partial z} \phi_1 \quad (132)$$

$$k_{17} = \frac{\partial \psi_1}{\partial z} \phi_2 \quad (133)$$

$$k_{18} = \frac{\partial \psi_2}{\partial z} \phi_2 \quad (134)$$

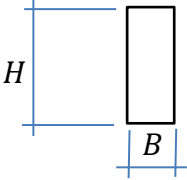
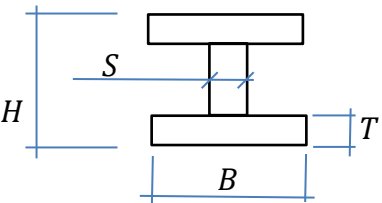
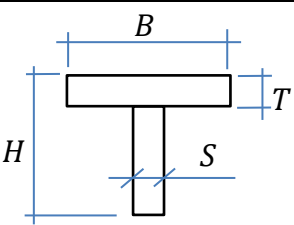
$$k_{19} = \frac{\partial \psi_3}{\partial z} \phi_2 \quad (135)$$

$$k_{20} = \frac{\partial \psi_4}{\partial z} \phi_2 \quad (136)$$

Appendix C

Selection of cross-sections used for calculations using refined shear deformation theory:

Table 0-1 Cross-sections used for comparative analysis

		Cross-section 1	Cross-section 2	Cross-section 3	Cross-section 4	Cross-section 5	Cross-section 6	Cross-section 7
Overall height	h (mm)	300	300	300	300	300	300	300
Overall width	b (mm)	2	5	10	10	10	20	40
Flange thickness	t (mm)	-	-	-	20	20	20	20
Web thickness	s (mm)	-	-	-	2	5	2	2
Cross-section								
		Cross-section 8	Cross-section 9	Cross-section 10				
Overall height	h (mm)	300	300	300				
Overall width	b (mm)	40	40	40				
Flange thickness	t (mm)	20	20	20				
Web thickness	s (mm)	2	10	20				
Cross-section								

Appendix D

For all graphs, FE-calculations results are presented in black lines and analytical results according to refined shear deformation theory are presented in red lines.

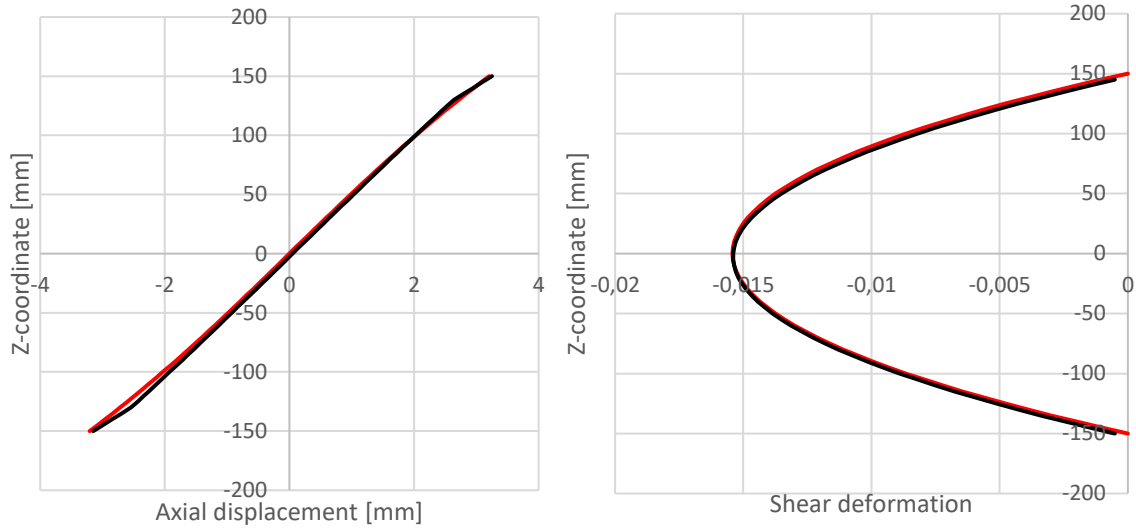


Figure 0-1 Axial displacement and shear deformation comparison for cross-section 1

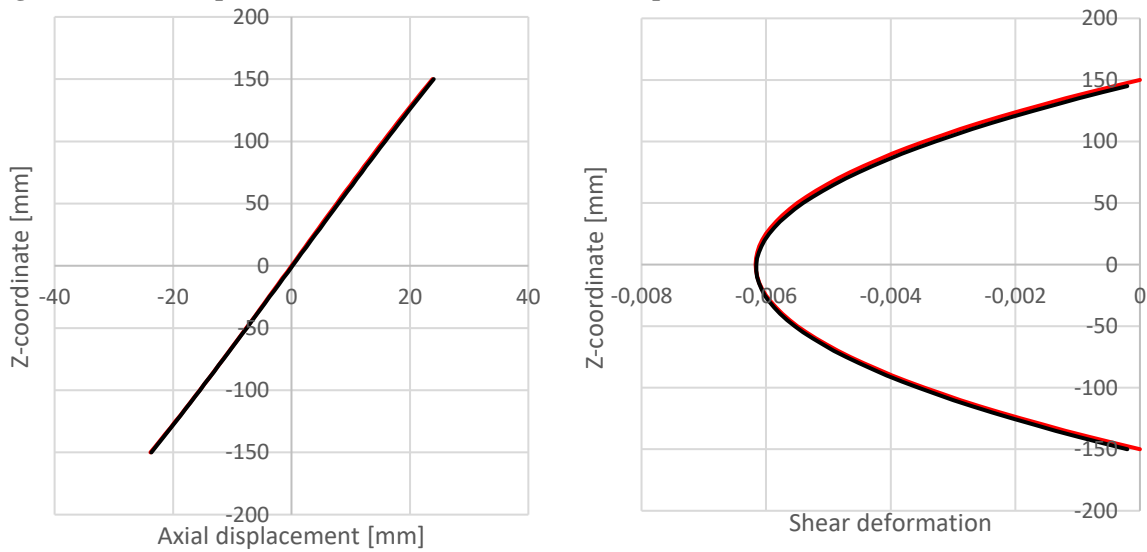


Figure 0-2 Axial displacement and shear deformation comparison for cross-section 2

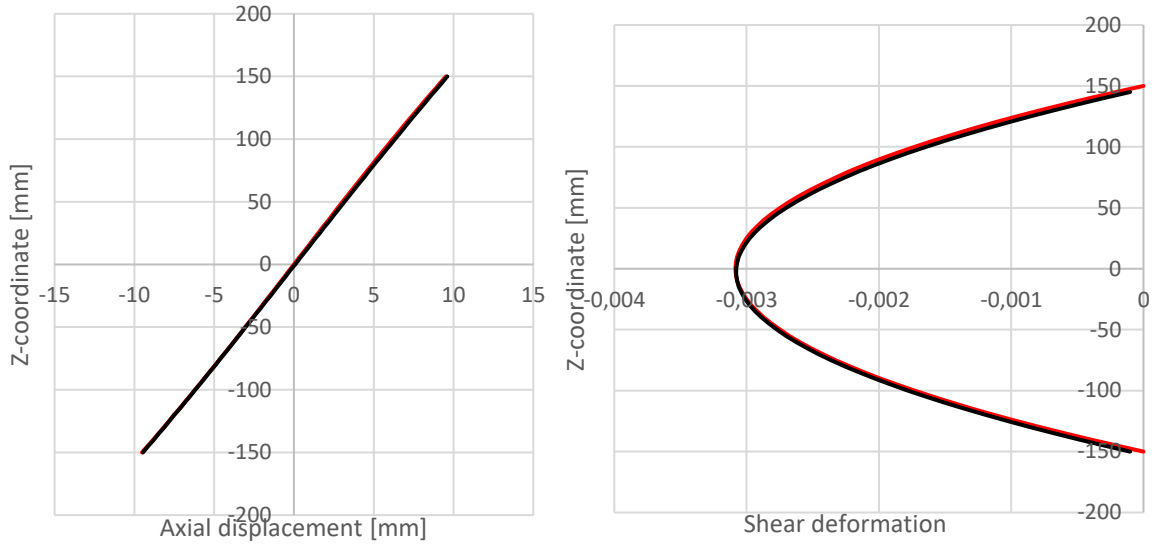


Figure 0-4 Axial displacement and shear deformation comparison for cross-section 3

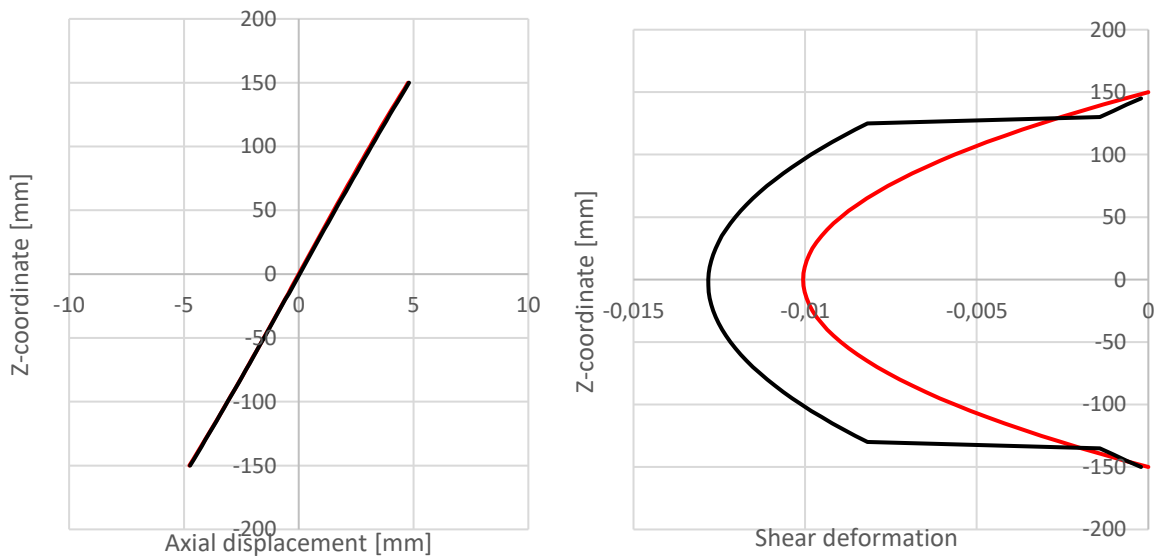


Figure 0-3 Axial displacement and shear deformation comparison for cross-section 4

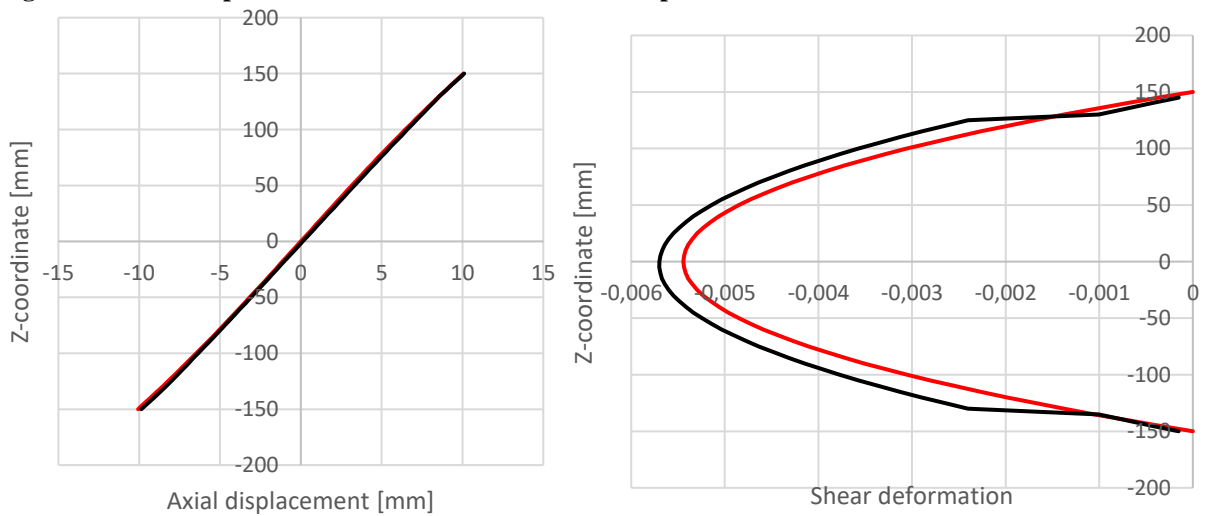


Figure 0-5 Axial displacement and shear deformation comparison for cross-section 5

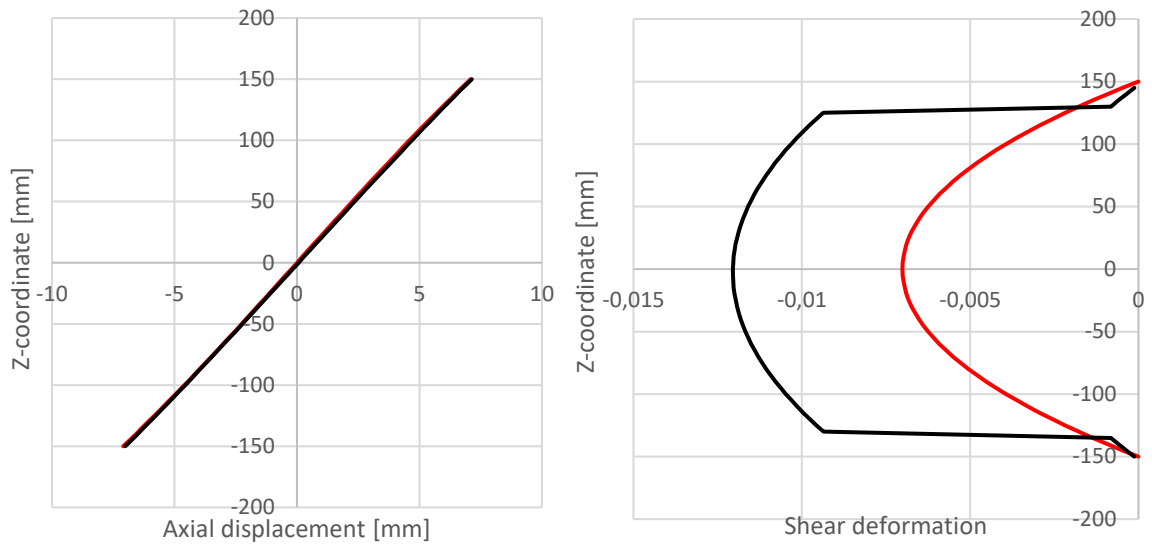


Figure 0-6 Axial displacement and shear deformation comparison for cross-section 6

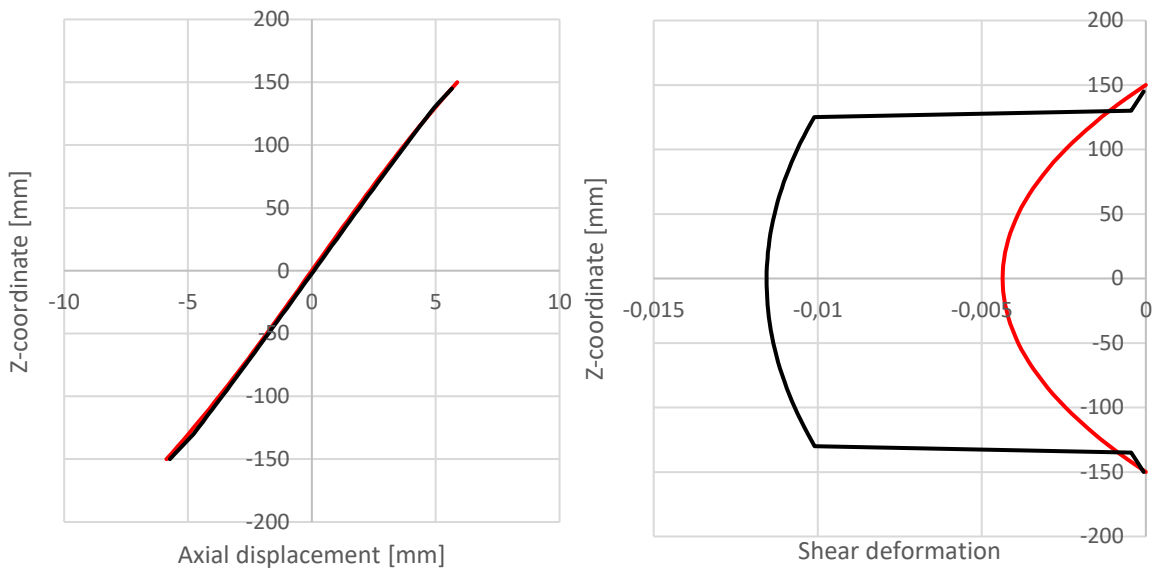


Figure 0-7 Axial displacement and shear deformation comparison for cross-section 7

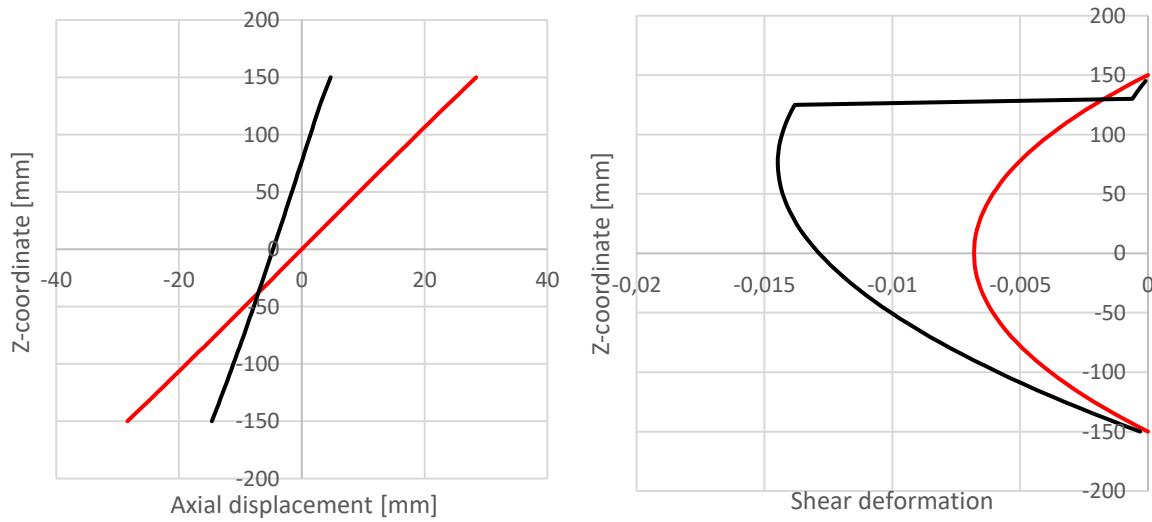


Figure 0-8 Axial displacement and shear deformation comparison for cross-section 8

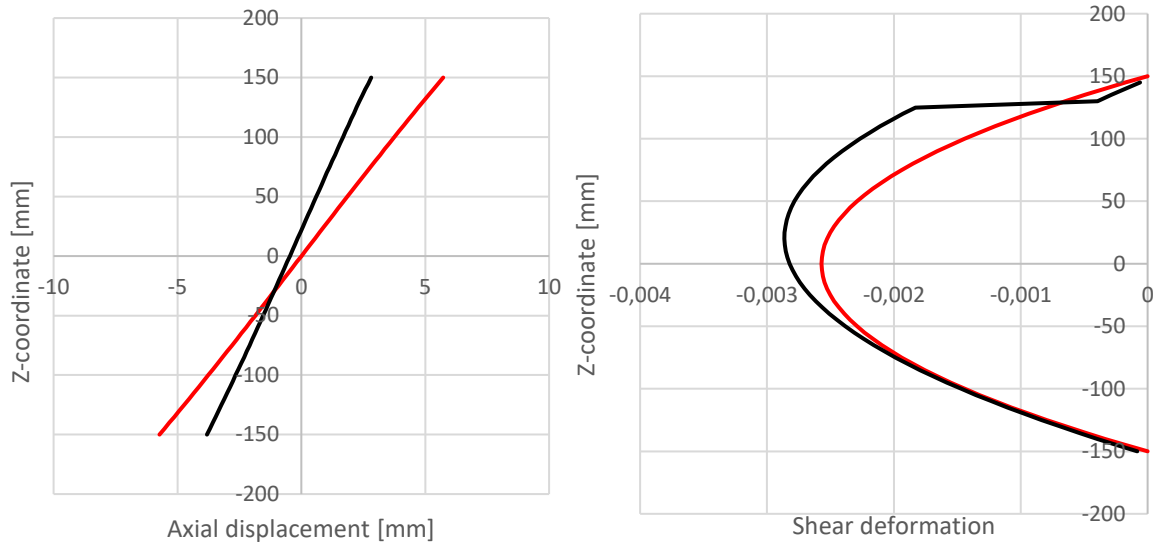


Figure 0-9 Axial displacement and shear deformation comparison for cross-section 9

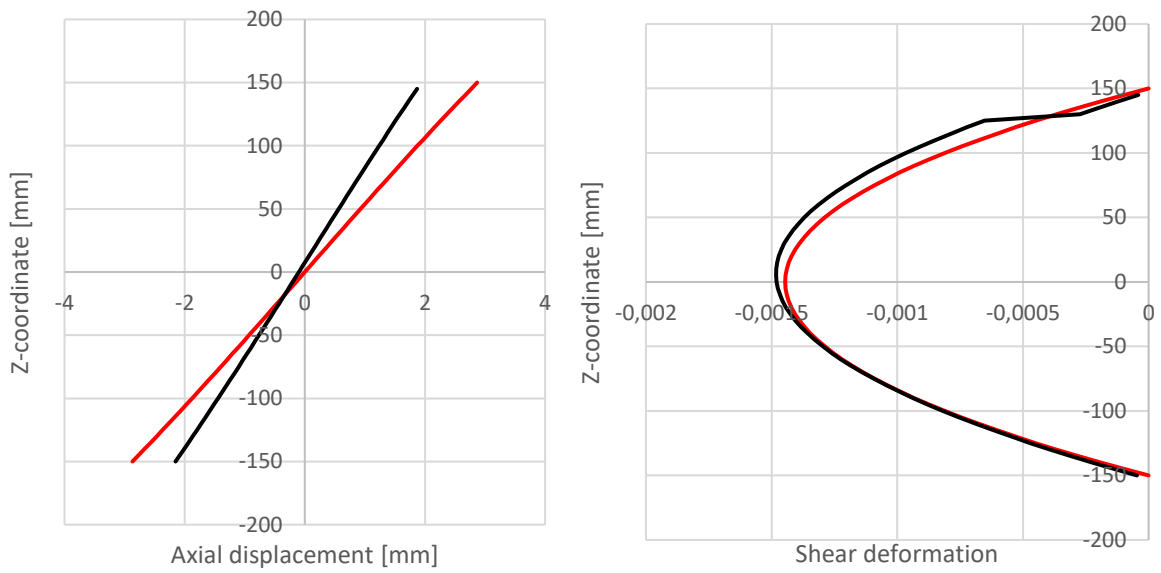


Figure 0-10 Axial displacement and shear deformation comparison for cross-section 10

Bibliography

- [1] Naar H., Varsta P., Kujala P. A theory of coupled beams for strength assessment of passenger ships. *Marine Structures*, Vol. 17, 2004, pp. 590-611.
- [2] Hughes, O. F., Paik, J. K., *Structural Analysis and Design*. Jersey City: The Society of Naval Architects and Marine Engineers, 2010, no. 1072.
- [3] Matusiak, J., *Dynamics of a Rigid Ship*, 2nd corrected ed. Aalto University publication series Science + Technology, 2017.
- [4] K. Rawson and E. Tupper, *Basic Ship Theory*, 5th ed. Oxford: ButterworthHeinemann, 2001.
- [5] DNV GL, "Class guideline: Direct strength analysis of hull structures in passenger ships," Tech. Rep., 2016
- [6] Crawford L. Theory of long ships' superstructure. *Trans RINA*, 1965;107:411-430.
- [7] Bleich HH. Nonlinear distribution of bending stresses due to distortion of the cross section. *Journal of Applied Mechanics*, Vol. 20, 1952, p. 95.
- [8] Terazawa, K., Yagi, J. Stress distribution in deckhouse and superstructure. *The Society of Naval Architects of Japan, 60th Anniversary Series*, 1964;9:51-150.
- [9] Romanoff, J., Remes, H., Varsta, P. Hull-superstructure interaction in optimised passenger ships. *Journal of Ships and Offshore Structures*, Vol. 8, 2013, p. 612-620.
- [10] Andri, J., Ani, V. The global structural response model for multi-deck ships in concept design phase. *Journal of Ocean Engineering*, Vol. 37, Issues 8-9, 2010, p. 688-704.
- [11] Chen, Q. The effectiveness Research of Aluminum Superstructure in the Longitudinal Strength. MS Thesis. Shanghai Jiao Tong University.

- [12] Zhiyong, P., Zhongyuan, M., Bo, Z., Weiguo, W. Research on the bending efficiency of superstructure to hull girder strength on inland passenger ship. *Journal of Ocean Engineering*, Vol. 195, 2020
- [13] Zanic, V., Andric, J., Predeg, P., Stipcevic, M., Piric, K. Ropax structural design-multi-level decision support methodology. 11th Symposium on Practical Design of Ships and Other Floating Structures, PRADS 2010.
- [14] Andric, J. Decision Support Methodology for Concept Design of the Ship Structures with Hull-Superstructure Interaction. PhD thesis. Faculty of Mechanical Engineering and Shipbuilding, Zagreb, 2007.
- [15] Zou, J. Investigation of the hull-superstructure interaction in order to predict the contribution of superstructure to hull girder strength. MS Thesis. University of Liege, 2013.
- [16] Fricke, W., Gerlach, B. Effect of large openings without and with windows on the shear stiffness of side walls in passenger ships. *Ships and Offshore Structures*, Vol. 10, 2015, Issue 3, p. 256-271.
- [17] Caldwell, J. The effect of superstructure on the longitudinal strength of ships. *Trans RINA* 1957:664-81.
- [18] Fransman, J. The influence of passenger ship superstructures on the response of the hull girder. *Trans RINA* 1988.
- [19] Timoshenko S.P. On the correction for shear of the differential equation for transverse vibrations of prismatic bars. *Philosophical Magazine Series*, 6:742-746, 1921.
- [20] Levinson, M., 1981. A new rectangular beam theory. *Journal of Sound and Vibration*, 74(1), 81-87.
- [21] Bickford, W. B., 1982. A consistent higher order beam theory. *Development in Theoretical and Applied Mechanics, SECTAM 11*, 137-150.
- [22] Rehfield L. W., Murthi P. L. N. Toward a new engineering theory of bending: Fundamentals *AIAA J.*, 20(5):693-699, 1982.
- [23] Krishna Murthy A. V. Towards a consistent beam theory. *AIAA J.* 22(6), 811-816, 1984

- [24] Bhimaraddi A., Chandrashekhara K. Observations on higher order beam theory. ASCE, Journal of Aerospace Engineering, 6(4), 408-413, 1993
- [25] Baluch M. H., Azad A. K., Khidir M. A. Technical theory of beams with normal strain. ASCE Journal of Engineering Mechanics, 110(8), 1233-1237, 1984.
- [26] Ghugal Y. M., Sharma R. A Hyperbolic shear deformation theory for flexure and vibration of thick isotropic beams. International Journal of Computational Methods, 6(4), 585-604, 2009
- [27] Ghugal Y. M., Sharma R. A refined shear deformation theory for flexure of thick beams. Latin American Journal of Solids and Structures, 8(2), 183-195, 2011
- [28] Toming, R., Kerge, E. H., Naar, H., Tabri, K., Romanoff, J., Remes, H. Hull and superstructure interaction using coupled beam method. Proceedins of PRADS2016, 4th-8th September, 2016, Copenhagen, Denmark.